2015

Nanoscale GUMBOS: Size-Control, Characterization, and Applications as Enantioselective Molecularly Imprinted Polymers and Fluorescent Materials

Suzana Hamdan
Louisiana State University and Agricultural and Mechanical College, suzanahamdan2@gmail.com

NANOSCALE GUMBOS: SIZE-CONTROL, CHARACTERIZATION, AND APPLICATIONS AS ENANTIOSELECTIVE MOLECULARLY IMPRINTED POLYMERS AND FLUORESCENT MATERIALS

A Dissertation

Submitted to the Graduate Faculty of the
Louisiana State University and
Agriculture and Mechanical College
in partial fulfillment of the
requirements for the degree of
Doctor of Philosophy

in

The Department of Chemistry

by
Suzana Hamdan
B.S., Lebanese University, 2006
M.S., East Tennessee State University, 2009
May 2015

“I dedicate this dissertation to my parents Drs. Wahibe Abi Chahine and Hamdan Hamdan who supported and encouraged me throughout my studies. My dedications are also to my sister Mireille and her husband Dr. Lucien Abboud who helped and guided me from first entrance into graduate school. My final dedications are to my nephew Jason and niece Cassandra for bringing total joy into my life.”

ACKNOWLEDGMENTS

Prof. Isiah M. Warner for being such a great mentor, teaching me how to be a better scientist, and believing in my capabilities. Thank you for all the support that you have shown and all the knowledge that you have provided. You will always be an inspiration for me.

Prof. David A. Spivak for teaching me about molecular imprinting and for all the time and effort you afforded for the imprinting research project.

Doctoral Committee Members: Prof. Samuel D. Gilman, Prof. Kermit K. Murray, Prof. Megan A. Macnaughtan, and Prof. Wayne D. Newhauser for all the help and advice provided to improve my work.

Prof. Chu-Ngi Ho for enriching my background in analytical chemistry and guiding me through my Master's degree.

Dr. Bilal El-Zahab, Dr. Noureen Siraj, Dr. Farhana Hasan, and Dr. Susmita Das for all your suggestions and proofing of documents during my graduate studies.

Dr. Leonard Moore Jr. and Dr. Jonathan Dumke for all the support that you have provided in challenging situations.

The Warner Research Group for sharing your scientific knowledge and discussing ideas in group meetings.

TABLE OF CONTENTS

LIST OF TABLES

LIST OF FIGURES

LIST OF SCHEMES

LIST OF ABBREVIATIONS

0D	Zero-dimensional
1D	One-dimensional
2D	Two-dimensional
2HP-β-CD	2-Hydroxypropyl-β-cyclodextrin
2HP-α-CD	2-Hydroxypropyl-α-cyclodextrin
3D	Three-dimensional
AAPH	2,2′-Azobis(2-methylpropionamidine) dihydrochloride
AIBN	2,2′-Azobis(2-methylpropionitrile)
AF_4	Asymmetric-flow field flow fractionation
AOT	Sodium (bis 2-ethylhexyl)sulfosuccinate
$BETI^-$	Bis(pentafluoroethylsulfonyl)imide
BF_4^-	Tetrafluoroborate
CI	Carbazoleimidazole
CMC	Critical micellar concentration
D-Trp	D-Tryptophan
DIC	Differential interference contrast
DLS	Dynamic light scattering
EML	Emissive layer
ETL	Electron transport layer
FEG	Field emission gun
FL^{2-}	Fluorescein (Dianionic)
FONs	Fluorescent organic nanoparticles
FTIR	Fourier transform infrared spectroscopy
GUMBOS	Group of uniform materials based on organic salts
HIL	Hole injection layer
$Hmim^+$	1-Hexyl-3-methylimidazolium
HTL	Hole transport layer

I^-	Iodide
ILs	Ionic liquids
L-Trp	L-Tryptophan
LDE	Laser Doppler electrophoresis
LDV	Laser Doppler velocimetry
LEDs	Light emitting diodes
MIPs	Molecularly imprinted polymers
MS	Molar substitution
NanoGUMBOS	Nanoparticles derived from GUMBOS
NGMIPs	NanoGUMBOS molecularly imprinted polymers
NGNIPs	NanoGUMBOS non-imprinted polymers
NMR	Nuclear magnetic resonance
NTf_2^-	bis(trifluoromethylsulfonyl)amide
OLEDs	Organic light emitting diodes
OTf^-	Trifluoromethanesulfonate
OVP	Oligophenylenevinylenes
PILs	Polymeric ionic liquids
PPV	Polyphenylenevinylenes
QDs	Quantum dots
RTILs	Room temperature ionic liquids
Tan δ	Loss tangent
TEM	Transmission electron microscopy
TGA	Thermogravimetric analysis
TPB^-	1,1,4,4-Tetraphenyl-1,3-butadiene Tetraphenylborate
TSILs	Task-specific ionic liquids
TTP^+	Trihexyltetradecylphosphonium
TX-100	Triton X-100

ABSTRACT

Nanomaterials derived from a group of uniform materials based on organic salts (GUMBOS) have been introduced into the scientific literature through many analytical, biological, and technological applications. These nanomaterials, referred to as nanoGUMBOS, have been shown to display a number of interesting properties including fluorescence, magnetism, tumor targeting, and optoelectronic properties. Herein, we present major studies on nanoGUMBOS including synthesis and size-control, chiral molecular imprinting in polymers, as well as investigation of optical properties and quantum yield of fluorescent semiconductor-based nanoGUMBOS. Various strategies were introduced for production of well-defined nanoGUMBOS. Specifically, several methods based on sonochemistry, microwave, cyclodextrin, and surfactant-assisted syntheses of nanoGUMBOS are described while evaluating the efficiency of each technique in controlling size, morphology, and uniformity of nanoparticles. The systematic variations in experimental parameters such as concentration, cation-to-anion ratio, as well as presence and type of templates introduced for the formation of nanoGUMBOS were also investigated. Moreover, imidazolium-based ionic liquid crosslinkers were tested as platforms for chiral imprinting under aqueous conditions. Using photoinitiated dispersion polymerization, molecularly imprinted polymeric nanoGUMBOS were designed with recognition properties for L-tryptophan. Rebinding studies were performed in batch mode analysis using fluorescence spectroscopy. Strong interactions between GUMBOS and L-tryptophan made imprinting possible in aqueous media. Various spacers between the imidazolium rings of the cation afforded the presence of secondary interactions responsible for distinctive enantiorecognition behavior of these polymeric nanoparticles.

In this regard, these vinylimidazolium ionic liquids were polymerized using gamma irradiation, for potential application in drug loading. Furthermore, carbazole-based nanoGUMBOS were investigated as fluorescent materials for potential applications in blue organic light emitting devices. These nanoGUMBOS were synthesized using a reprecipitation method in the absence or presence of 2-hydroxypropyl-β-cyclodextrin, in order to tune the size and optical properties of the nanoparticles. The carbazoleimidazole-based cation was coupled with different couteranions: iodide ([I]), trifluoromethanesulfonate ([OTf]), and bis(pentafluoroethylsulfonyl)imide ([BETI]). Absolute quantum yields were compared for each type of nanoGUMBOS synthesized under different experimental conditions. Doping with the transition metal Cu^{2+} was also explored as an alternative strategy for tuning the quantum yield of nanoGUMBOS, which was enhanced by optimizing the molar percentage of dopant to host.

CHAPTER ONE
INTRODUCTION

1.1. Nanotechnology Concept

Nanotechnology is a term that describes production and applications of systems at the nanometer scale, *i.e.*, one billionth of a meter. The vast diversity in the nanotechnology field is based on investigating unusual properties of nanoscale materials.[1] Depending on the definition used, the nanometer regime can be categorized as being “below 100 nm” or “between 0.1-100 nm”; [2] however, many scientists believe that the size-dependent properties related to nanotechnology may also exist above 100 nm size.[2] Therefore, it is reasoned that, in defining nanotechnology, one should also focus on the properties observed in nanotechnology-based systems rather than being limited to the size definition.[2]

Production of natural materials and biological systems that function at small scales are mimicked within the nanotechnology field (Figure 1.1).[1] Most of the interactions

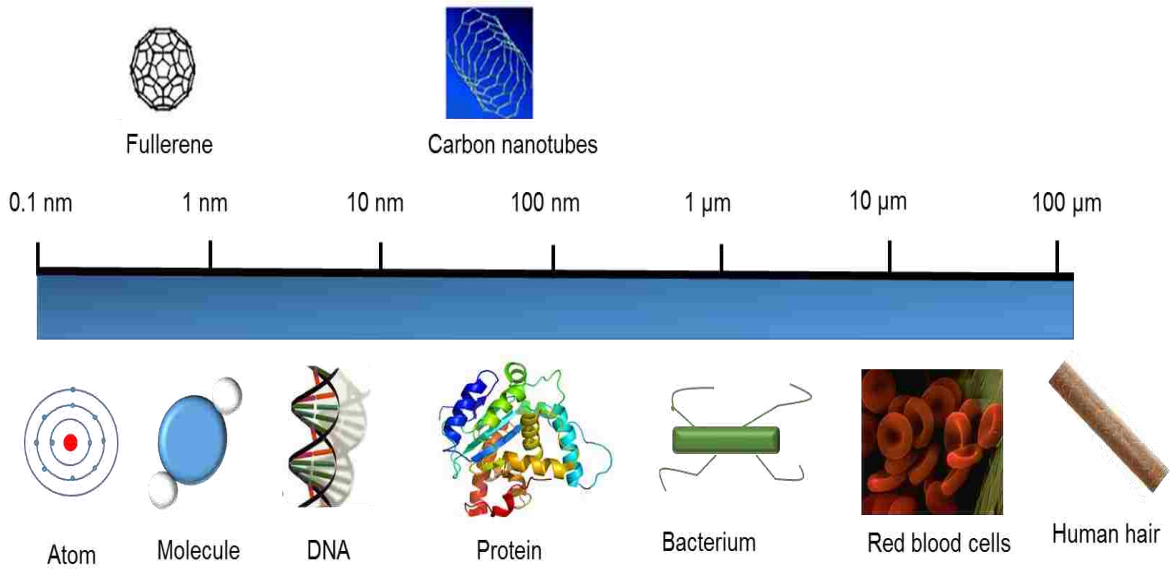

Figure 1.1. Several biological and natural structures exist in nanometer and micrometer regimes. Adapted from Reference 3.

in nature and biological systems that range from molecular assembly of viruses to the molecular building blocks of enzymes and proteins are similar in concept to the self-assembly mechanism exploited during the formation of nanostructures.[4]

1.2. Nanotechnology in Chemistry: Nanomaterials

1.2.1. Historical View

The concept of nanotechnology was first introduced by Richard Feynman in his famous lecture “There’s Plenty of Room at the Bottom” in 1959, wherein he spoke on the importance of manufacturing objects at the nanoscale level and the large number of associated potential applications.[5] Although the nanotechnology theme did not arise until that year, the concept of working with colloids dates back to many decades earlier. The idea of preparing particles from assembled molecules was initiated by Francesco Selmi (1845) and Michael Faraday (1857). Selmi and Faraday’s research involved silver chloride and gold colloids, respectively. Michael Faraday’s studies led to the discovery that optical properties of gold nanoparticles are dependent on the particle size, which was a major breakthrough within the history of nanotechnology.[6] Thomas Graham, the father of colloid chemistry, revealed the presence of colloids from the nanometer to micrometer range, which present low diffusivity in comparison to molecules.[7] At the onset of the twentieth century, Gustav Mie clarified the relationship between particle size and optical properties in colloidal solution leading up to what is now known as Mie Theory.[7] Later, Richard Zsigmondy, a Nobel Laureate, studied more deeply the chemistry of colloids, especially gold sols.[8]

Recently, various nanomaterials have been extensively reported in the scientific literature.[9-11] For example, carbon nanotubes have become a popular form of

nanomaterials due to the light weight and high strength characteristics of such materials.[9-10] Metal-based nanoparticles such as aluminum oxide nanopowders are of great interest due to the measured high surface area to volume ratio. These materials, with high chemical activity, have been successfully employed as chemical catalysts and sorbents.[10] From the 1980s to present, quantum dots (QDs) have remained the primary example of inorganic semiconductors nanoparticles that have attracted substantial attention from material scientists. The dependence of electronic and optical properties on the spatial confinement of electrons in these nanostructures allow tunability of the properties through size, shape, and composition.[11]

1.2.2. Nanomaterials in the Service of Chemistry

The breakthrough of nanotechnology in the chemical sciences has greatly benefited numerous analytical applications. Metallic nanoparticles have been used in fluorescence techniques to enhance fluorescence lifetime and quantum yields.[12] One example of these types of nanoparticles (*i.e.,* gold nanoparticles) has been extensively applied as biological and chemical sensors.[13] Carbon-based nanomaterials such as single walled and multiple walled nanotubes have been employed in applications such as the sorption of heavy metals and organic molecules for preconcentration purposes and subsequent detection.[12] In addition, the use of nanoparticles has been highlighted in organic synthesis for separation of product from reaction medium,[14] and performance of catalytic reactions.[15] In the field of chemistry, nanomaterials can be directly applied in a raw state or alternatively functionalized to enhance a desired function. The formation of nanomaterials is based on chemical routes that have been studied and discussed in a

large number of publications.[16-17] In addition, several chemical analysis methods have been designated for study of the size, shape, surface, structure, and chemical composition of nanomaterials.[18-19]

1.2.3. Dimensionality of Nanomaterials

Nanomaterials are low-dimensional materials presenting at least one dimension at the nanoscale level. Various types of nanomaterials are distinguished by classifying the geometries according to 0D, 1D, 2D, or 3D dimensionality (Figure 1.2). Zero-dimensional

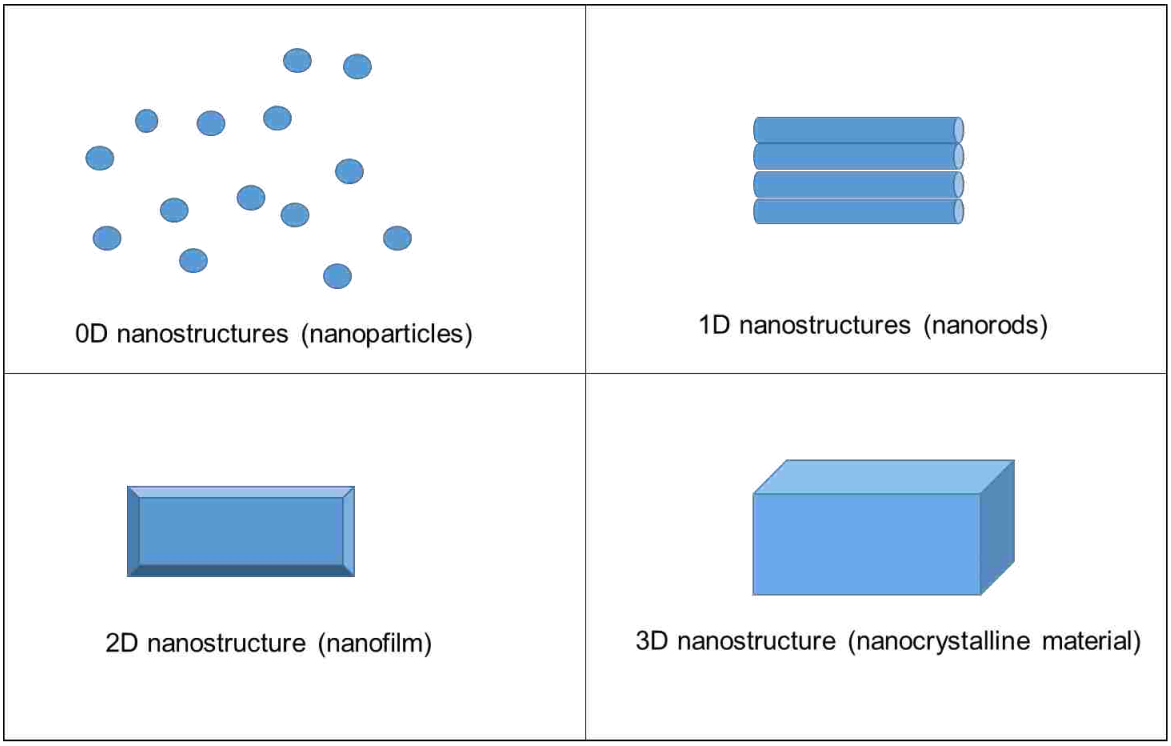

Figure 1.2. Nanostructures are low-dimensional materials with at least one dimension at nanoscale.

nanostructures have all three dimensions at nanoscale, and this category includes spherical nanoparticles, quantum dots, and hollow nanospheres.[20] The zero-dimensionality offers flexibility in the design, which permits the application of nanomaterials in a variety of research areas. More specifically, engineering

functionalized/surface-modified zero-dimensional nanoparticles makes these nanostructures popular for medical imaging and drug delivery.[21] In contrast, the one-dimensional (1D) nanostructures such as nanotubes and nanorods, with one dimension at the nanoscale, have been widely used in optoelectronic devices. Two-dimensional (2D) nanostructures like nanosheets and nanowalls, emerged as potential substrates for sensors, photocatalysts, and nanoreactors.[20] Lastly, the three-dimensional (3D) nanostructures including nanoballs and nanoreactors, show unique properties compared to the bulk counterparts due to quantum effects.[20]

1.2.4. Synthesis Strategies of Nanomaterials: Top-down and Bottom-up Approaches

Fabrication of nanomaterials can be achieved using two approaches: bottom-up and top-down (Figure 1.3). The bottom-up technique starts at the molecular level, where the molecule interacts with surrounding molecules to aggregate and form the final particle size. Methods such as crystallization and polymerization belong to this type of nanoparticle fabrication. Furthermore, nucleation and growth mechanisms are the fundamental processes in the bottom-up approach.[22]

The top-down technique is based on several processes which reduce a bulk material to result in the colloidal structures formation. Top-down techniques are mainly for industrial purpose because the materials are massively produced and tend to be non-spherical as opposed to the bottom-up approaches.[22] Milling and grinding are two examples of top-down techniques lacking control of particle size and shape. However, other techniques such as hard-template synthesis, microfluidics-based methods, and photolithography are employed to deliver shape-specific nanoparticles.[22] The procedures

detailed in following sections are classified as bottom-up approaches where the manufacturing processes occur at atomic and molecular levels.

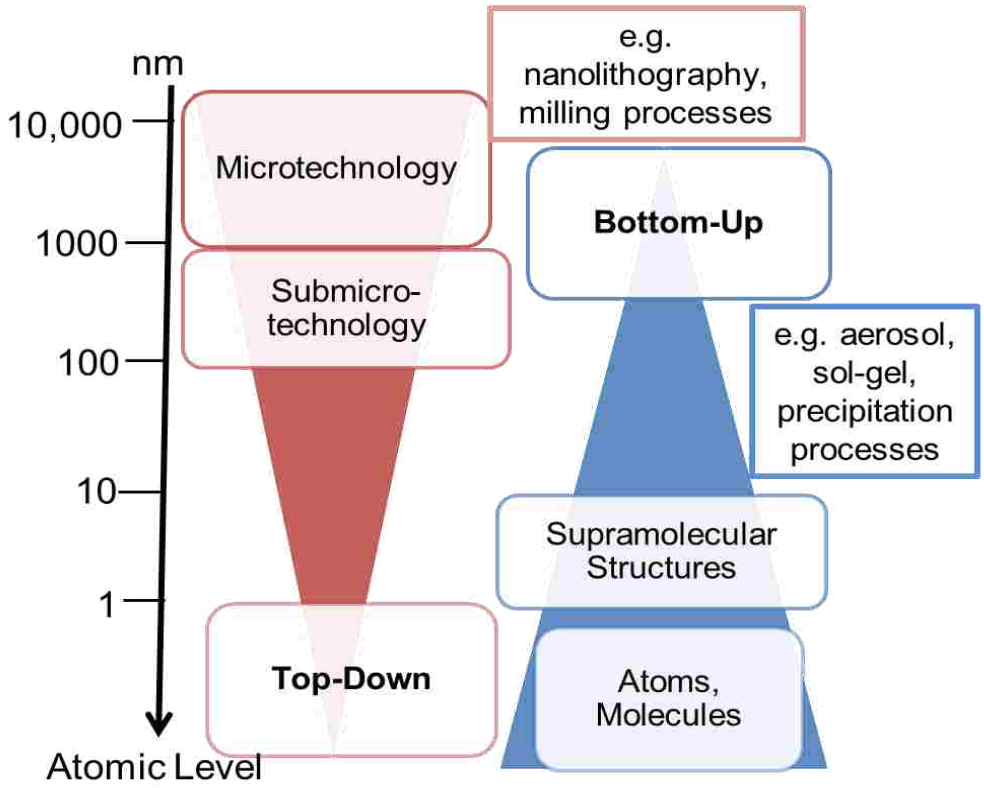

Figure 1.3. The top-down and bottom-up approaches used for synthesis of nanomaterials. Adapted from Reference 23.

1.3. Zero-Dimensional Nanomaterials (Nanoparticles)

1.3.1. Synthesis and Size-Control of Nanoparticles

The ability to control the size and polydispersity of nanoparticles is necessary to improve the performance of these nanomaterials in a specific application. Monodisperse nanomaterials are useful for a wide variety of applications including biological, technological, and analytical areas.[24] The size of nanoparticles in a system alters the characteristics and efficiency of the materials which are mainly employed in applications such as drug delivery and cells targeting.[25] Moreover, optical and electrical properties are

often size-dependent in nanomaterials and are affected by variations in size or change in the intramolecular arrangement.[26] Several limiting factors such as the reactants concentration and the type of solvent, determine the final size and polydispersity of nanoparticles by influencing the nucleation and growth of these nanostructures.[27] The classical nucleation theory is the most common model used to clarify the nucleation and growth mechanisms. LaMer and Dinegar explained the classical nucleation theory which is based on a model that describes the formation of monodisperse sulfur hydrosols (Figure 1.4).[28]

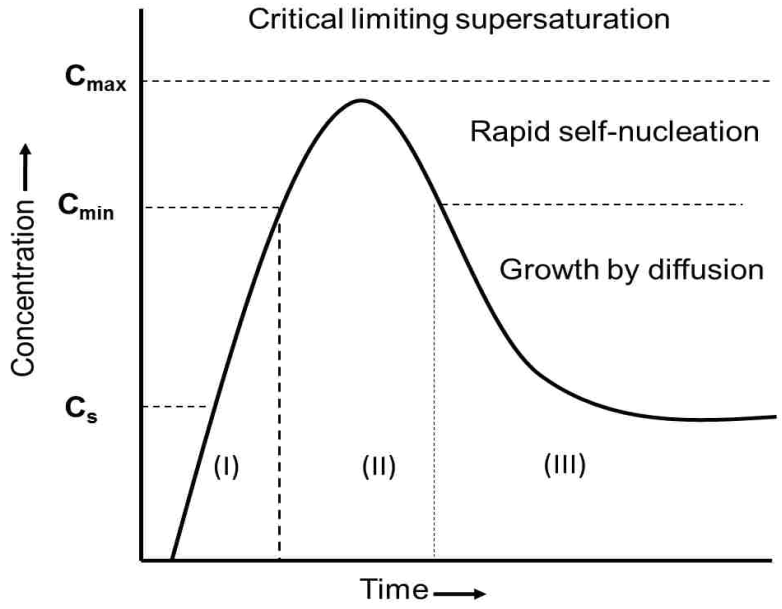

Figure 1.4. The classical nucleation theory as explained by LaMer. Adapted from Reference 28.

LaMer described in his diagram that at stage I, the concentration of the solute in the medium increases and nucleation initiates when this concentration attains a critical value (C_{min}). An equilibrium between the supply rate, and nucleation as well as growth rates of the formed cluster occurs when the concentration reaches a maximum value

(C_{max}). The cluster grow to a stable shape causing a decrease in solute concentration to C_{min}. The formation of stable nuclei is considered the end of nucleation. At this point, each critical nucleus has a radius r and appropriate energy level which is the combination of free energy per unit volume (negative value) and interfacial energy per unit area (positive value). In case of homogeneous nucleation, the cluster free energy (in Joules, J) can be calculated using Equation 1.[29]

$$\Delta G = -\frac{4}{3}\pi r^3|\Delta G_v|+4\pi r^2\gamma \quad (1)$$

In Equation 1, r is the radius of the cluster or nucleus (in meters), ΔG_v is the change in bulk free energy per volume ($J \cdot m^{-3}$), and γ is the surface free energy per unit area ($J \cdot m^{-2}$).

After nucleation, adsorption of species onto the nuclei occurs during the growth stage causing a subsequent decrease in solute concentration to its original level (stage III).[30] LaMer demonstrated the importance of tuning the experimental conditions to cause a rapid nucleation of sulfur and subsequent formation of monodisperse hydrosols. Three variables determine the final growth size of the sulfur particles: the number of nuclei present, the amount of diffusible species, and the diffusion coefficient of sulfur in the medium.[28] Two systems having the same concentration of species but different number of nuclei result in a dissimilar size of nanoparticles (Figure 1.5). The final size is related to the availability of species that can be adsorbed onto the surface.[31] The amount of diffusible species may also increase the rate of supersaturation during the nucleation stage, controlling the size and dispersity of the nanoparticles.[27, 30] In addition, the rate of supersaturation is related to the pH and temperature of the medium, affecting the final size of nanoparticles.

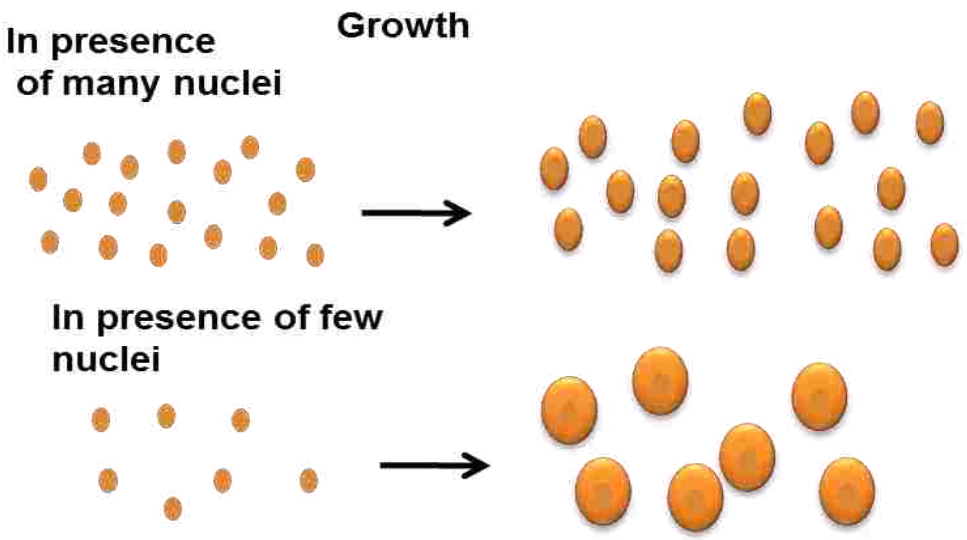

Figure 1.5. The number of nuclei affects the final size of nanoparticles in two systems with equal concentration of solute. The presence of larger number of nuclei causes the formation of smaller size nanoparticles as a result of fewer available species which adsorb onto the nuclei.

1.3.2. Synthesis of Organic Nanoparticles

Research related to organic nanomaterials has expanded in the past few years considering the applicability of these materials in electronic, optoelectronic, photonic, and sensing domains.[32] The reprecipitation method, also called a solvent displacement method, is the most commonly used technique for the synthesis of organic nanoparticles. This facile technique introduced by Nakanishi *et al.,* is based on adding a small amount of an organic compound, dissolved in a good solvent, to an excess of a poor solvent.[33] The reprecipitation method usually produces a broad size distribution of nanoparticles, which gave rise to the development of other organic nanoparticles syntheses such as laser ablation[34] and sol-gel methods.[35] These methods either require expensive instrumentation or tedious work to free the nanomaterials from the template. Therefore, current research focuses on the investigation of new techniques for simple, rapid, and efficient nanoparticles syntheses.

1.4. Synthesis of Nanoparticles Derived From GUMBOS (NanoGUMBOS) Using Ionic Liquid Chemistry

1.4.1. Ionic Liquids, Polymeric Ionic Liquids, and GUMBOS

The diversity in potential applications offered by organic nanomaterials was a major reason to direct the research to organic materials such as ionic liquids (ILs). ILs, or molten salts, are organic materials that are composed of large varieties of ions and possess a melting point below 100 °C.[36] The inefficient packing between the large organic cation and the small anion causes the low melting point of ILs, reaching as low as -96 °C.[37-38] ILs can exist in the liquid phase (*i.e.,* room temperature ionic liquids), or in the solid state like frozen ionic liquids. The former, glorified as “designer solvents”, have a melting point below 25 °C and can dissolve a wide range of organic as well as inorganic materials due to the particular combination of weakly coordinating ions.[39] The latter are solid organic salts having a melting point range between 25 °C and 100 °C.

The first reported observation of ILs was encountered in the 19th century when a red oil was formed during a Friedel-Crafts reaction.[40] The history of ILs was crafted in 1914 when Paul Walden studied the properties of the compound ethylammonium nitrate $[EtNH_3][NO_3]$.[41] Between the 1960s and 1970s, research on chloroaluminates molten salts had its breakthrough and was sponsored by the US Air Force Academy. ILs popularity increased with scientists like John S. Wilkes who worked on series of dialkylimidazolium based ionic liquids obtained as a result of the metathesis reaction.[42,43] Currently, the era of ILs is governed by names like Thomas Welton, Peter Wasserscheid, and Kenneth R. Seddon.[44]

In general, ILs can exhibit unique properties such as low volatility, non-flammability, high ionic conductivity, thermal stability, and tunability.[45] However, these

properties are not universal to all ionic liquids. For example, it has been shown that some ionic liquids have a measurable vapor pressure, or exhibit slow decomposition reactions at temperature below 100 °C.[46] The tunable combination of anion and cation in an IL theoretically allows for a million formulations of binary ionic liquids.[38] The most common cations in ILs are made of imidazolium, pyrrolidium, tetraalkylammonium, and phosphonium, while the most common anions are halides, tetrafluoroborate ($[BF_4]$) and hexafluorophosphate ($[PF_6]$) (Figure 1.6).[47] Nevertheless, ILs can also be composed of more complex anionic structures including perfluorated anions like bis(trifluoromethanesulfonyl)amide ($[NTf_2]$).[36] The variability of the ionic structure allows for the chemical and physical properties of these compounds to be easily tailored, depending on the type of anions and cations employed.[37] Previous reports show that physical properties such as vapor pressure, thermal stability, viscosity, hydrophobicity, and miscibility are dependent on the nature of anion/cation combinations.[48] The incorporation of functional groups into these ions can result in exhibition of unique chemical properties, permitting the use of ILs in specific applications.[49] Davis *et al*. were the first to present the concept of task-specific ILs;[49] in addition to being used as unique solvents, ILs can be used as catalysts, supports for synthesis, gas absorbents, stationary phases in chromatography, electrolytes in batteries, and many other functions.[50] For example, the alkyl in imidazolium-based cations of an IL can been functionalized with thioether, thiourea, or urea functional groups for extractions of heavy metals.[51] Along with becoming more popular in industrial applications,[52] ILs can be employed in several physical science areas including organic chemistry, separation science, and nanotechnology.[36]

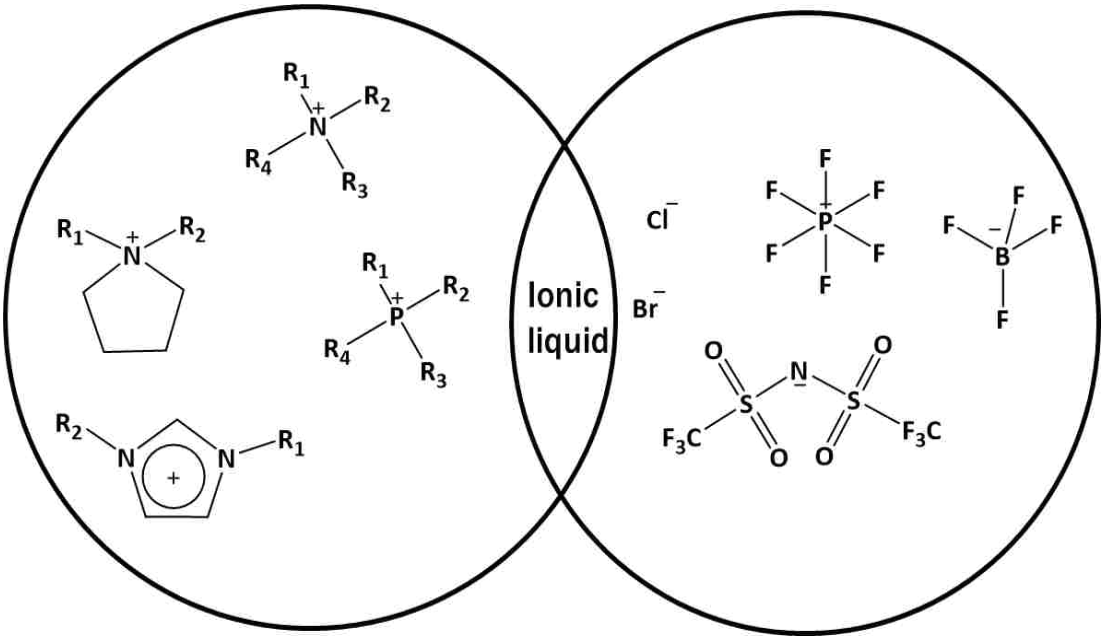

Figure 1.6. The most common cations and anions which constitute ionic liquids. The combination of these ions can result in the formation of immeasurable number of ILs structures. Adapted from Reference 47.

Many reports highlight the applications of ILs as solvent media in polymer science or for the preparation of polymer materials.[53] However, a major part of polymer science deals with polymeric ionic liquids (PILs) which are polyelectrolytes with the backbone structure comprising of an ionic liquid as a repeating unit. PILs usually result from polymerization of the alkene (*i.e.*, vinyl) or acrylate substituent group attached to the imidazolium or quartenary ammonium structure in the IL monomer.[54] These polymeric materials feature the properties of ionic liquids, as well as the chemical and physical stability of polymers depending on the choice of anion and cation.[55] PILs were used in a wide range of applications such as stationary phases in chromatography,[56] replacement for electrolytes in lithium-batteries,[57] and dye-synthesized solar cells.[58] Recently, PILs have been explored in molecular imprinting field where these polymers have been used

as sorbent for solid-phase extraction[59] and multi-phase dispersive extraction.[60] Polymeric nanostructures such as self-assembled liquid crystalline hydrogels[61] and polymer films with oriented nanochannels[62] were reported for sensing application and anisotropic ion conduction, respectively. For example, nanostructured PILs matrices have experienced a structure conversion upon swelling in the presence of alcohol and a change in the optical properties of the encapsulated gold nanoparticles.[63]

In 2008, the Warner Research Group introduced a group of uniform materials based on organic salts (GUMBOS) to designate organic salts with a melting point ranging from 25 °C to 250 °C. The concept of GUMBOS initiates from the incentive to drive the chemistry of ionic liquids into solid materials.[64] The novelty of GUMBOS stems from the concept of ionic liquids tunable properties allowing these advanced solid-phase materials to be used in a wide range of applications. Several studies support the significance of GUMBOS by affording the organic salts for anticancer[65] and antimicrobial targeting,[66] sensing applications,[67] and energy harvesting.[68] Nanoparticles derived from GUMBOS or nanoGUMBOS have also been investigated by the Warner Research Group.[69-72] The following document focuses on new procedures investigated for efficient production of nanoGUMBOS, the application of these nanomaterials in polymer and analytical chemistry, as well as possible applications in optoelectronic devices.

1.4.2. Size-Control of NanoGUMBOS

The significance of efficiently engineering nanoGUMBOS pertains to the fact that these nanomaterials present the unique properties of ionic liquids, mostly enhanced at the nanoscale. NanoGUMBOS can also be designed for scientific applications which

require solid state materials at small physical dimensions. The areas include biological studies mainly involving cellular uptake and technologies such as nanoparticle-integrated light emitting devices.

Melt-emulsion-quench was the technique reported by Tesfai *et al*. for the synthesis of nanoparticles composed of frozen ionic liquids.[73] In this procedure, $[bm_2Im][PF_6]$, an IL with a melting point of 42 °C, was melted at a high temperature and then quenched in an ice bath in presence of an emulsifier Brij 35. The use of a homogenizer or a probe sonicator was adopted prior to the rapid temperature quenching. Solvent evaporation from the oil-in-water emulsions causes the formation of nanoparticles with a uniform average size of 45 ± 7 nm. Some of the generated nanoparticles presented a less spherical shape compared to the spherical nanoparticles obtained from the same method in absence of a surfactant.[73] Tesfai *et al.* also reported the synthesis of magnetic nanoGUMBOS using organized systems where the formation of nanoparticles occurs inside the water pools of water-in-oil microemulsions, created by arranged surfactant monomeric units.[72] This procedure was used to generate $[bm_2Im][FeCl_4]$ nanoparticles in the presence of the surfactant sodium (bis 2-ethylhexyl)sulfosuccinate (AOT). Transmission electron micrographs displayed spherical nanoparticles with an average size below 100 nm that can be tunable upon changing the reagent concentration. Despite the simplicity and efficiency of this technique, a certain level of aggregation was still observed in the nanoparticles suspensions.

The choice of a suitable synthetic route for nanostructures such as nanoGUMBOS is critical considering the impact of the procedure on resulting physical properties exhibited by these structures.[74] Synthetic approaches are usually distinguished by the

presence or absence of a template, defined as any substrate onto which the species are deposited and grow into structures with specific morphologies and size.[75] In absence of a template, organization of nuclei into structures occurs based on self-assembly which results from molecular interactions.[75] Herein, a short background will be given for each technique (templated and non-templated) which was used and investigated to control the size and polydispersity of the synthesized nanoGUMBOS.

1.4.3. Free Template Syntheses of NanoGUMBOS

1.4.3.1. Ultrasonication-Assisted Synthesis

Ultrasonic irradiation is a form of energy used to monitor reaction conditions for nanomaterials formation.[74, 76] Ultrasound-assisted synthesis of nanoparticles is based on the formation and growth of nuclei around an acoustic cavitation (*i.e.,* bubble) created by the high intensity ultrasound. When ultrasound interacts with a liquid medium, it causes the formation of bubbles that grow and subsequently collapse to release accumulated ultrasonic energy. This phenomenon secures the optimal and favorable experimental conditions (high temperature and pressure) to promote formation of nuclei as shown in Figure 1.7.[74] The experimental setup (Figures 1.8a and 1.8b) for synthesis of nanoGUMBOS was designed using two different sources of ultrasound, which include the ultrasonication bath and ultrasonication probe. Both ultrasonication systems are based on the same acoustic theory;[77] however, the probe system delivers higher ultrasonication intensity compared to the bath system.[78] As shown in Figure 1.8, the formation of nanoparticles occurs via ion association (anion exchange between reactant 1 and 2) and subsequent precipitation of nanoGUMBOS in presence of ultrasonication.

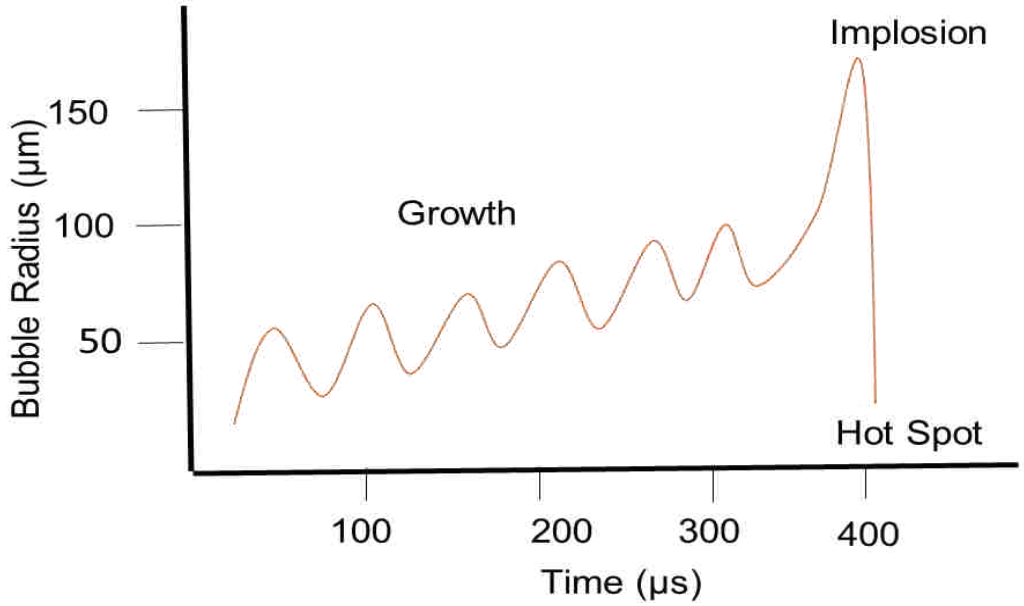

Figure 1.7. The presence of ultrasound forms acoustic cavitation. Adapted from Reference 74.

This method is simple and rapid, creating micro/nanoparticles depending on the concentration of reactants and the conditions of ultrasonication (*e.g.*, time of sonication, power of probe sonicator, and reaction temperature).

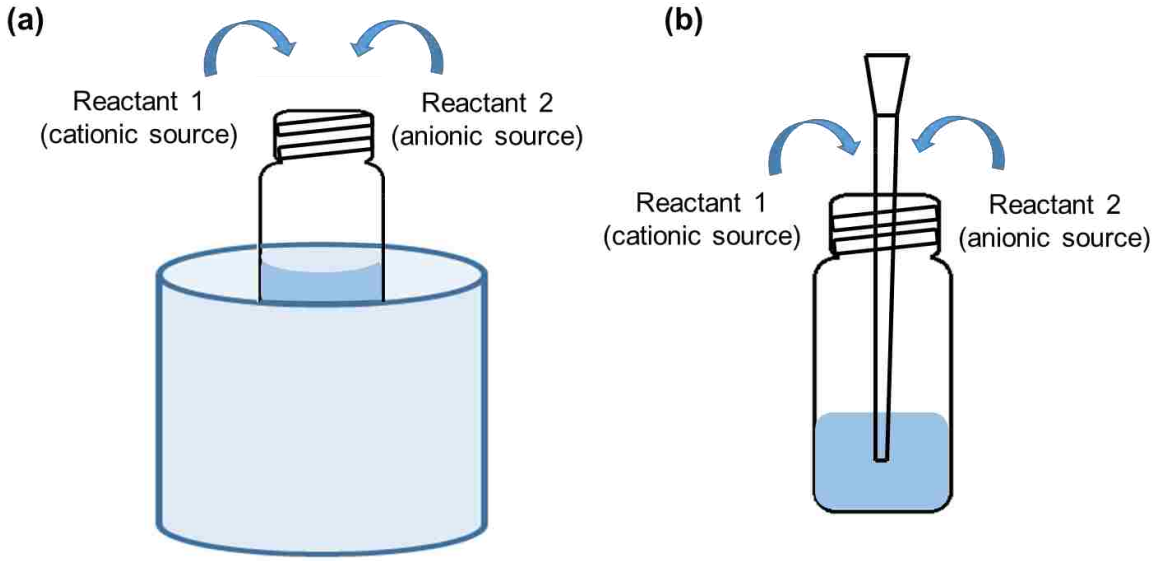

Figure 1.8. Two procedures based on ultrasonication: (a) bath and (b) probe are used for synthesis and size-control of nanoGUMBOS.

1.4.3.2. Microwave-Assisted Synthesis

Microwave heating is based on the use of microwaves with frequencies between 0.3 and 300 GHz, for a highly efficient method of heating.[79] Common industrial and domestic microwaves typically employ a frequency of 2.45 GHz. Microwave heating became popular in organic chemistry due to the short reaction time and compatibility of this pressurized system with a wide range of solvents that are used at temperatures above conventional boiling points.[79] Microwave irradiation targets individual molecules and provides homogeneous heating, which makes this technique useful for synthesis and enhancement of the nanoparticles polydispersity.[80] This type of heating offers more advantages in comparison to conventional heating devices such as oil baths, sand baths, and heating jackets. The microwaves in this technique target directly the reactants and the solvent, not the vessel or sample holder. The heating is uniformly produced inside the reactor as shown in Figure 1.9; therefore, fewer side reactions occur.[79] Microwave heating or dielectric heating, results from two mechanisms - dipolar polarization and ionic conduction. This technique has been previously employed for assisting the conventional reprecipitation method for synthesis of organic nanoparticles. The microwave-assisted reprecipitation delivered nearly monodisperse 1,1,4,4-tetraphenyl-1,3-butadiene (TPB) nanocrystals as reported by Baba *et al*.[81] Similarly, nanoGUMBOS were synthesized using the free-template ultrasonication bath method and then treated with microwave heating to achieve a decrease in size upon reorganization of the molecular assembly (Chapter Two).

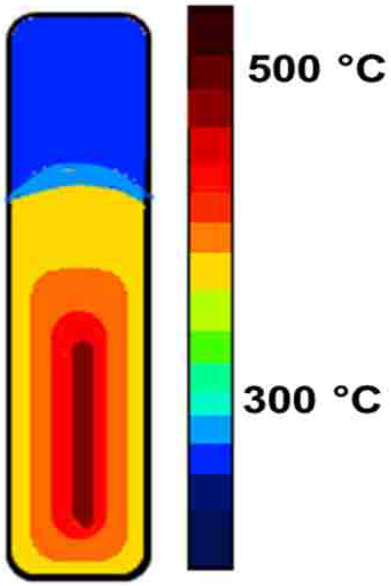

Figure 1.9. Microwave heating is homogeneous and uniformly produced inside the reactor. Adapted from Reference 82.

1.4.4. Templated Syntheses of NanoGUMBOS

1.4.4.1. Cyclodextrin-Directed Synthesis in the Presence of Ultrasonication

Cyclodextrins are cyclic oligosaccharides of which we distinguish parental cyclodextrins with six, seven, and eight glucose units known as α-, β-, and γ-cyclodextrins.[83] Cyclodextrins are considered successful complexation agents with hydrophobic molecules, as a result of the hydrophobicity of the interior cavity. The compound 2-hydroxypropyl-β-cyclodextrin (2HP-β-CD) is a highly water soluble cyclodextrin derivative which has been widely used in inclusion complexation (Figure 1.10).[84] Many recent papers show the use of cyclodextrins derivatives, especially 2HP-β-CD for the formation of nanoparticles such as C60 nanoparticles,[85] silver nanoparticles,[86] and copper sulfide CuS nanoparticles.[87] The molecule 2HP-β-CD takes part as a template in the synthesis of nanomaterials, which is essential to control the nanostructure dimensionality and provide monodisperse nanoparticles.[26]

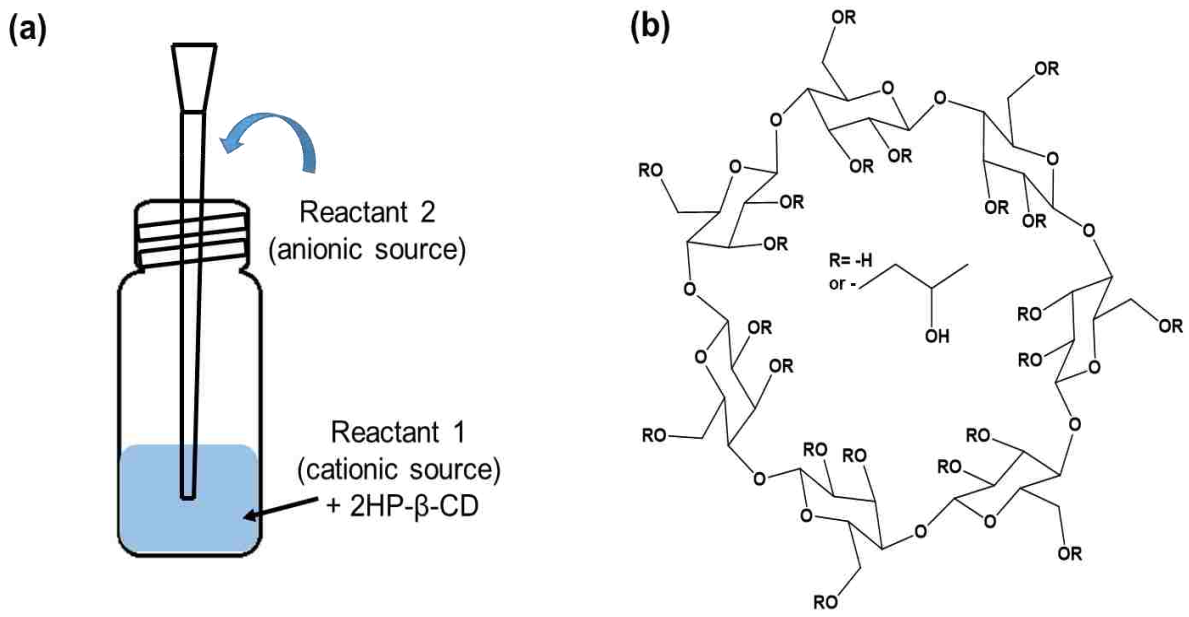

Figure 1.10. The (a) experimental procedure for synthesis of nanoGUMBOS under ultrasonication in assistance with (b) 2HP-β-CD.

Here, the template 2HP-β-CD was employed for the formation of nanoGUMBOS in the presence of ultrasonication. Scientists hypothesized that these structures cross-link under the effect of ultrasonication, which causes the formation of spherical assemblies.[87] Upon this crosslinking, nanoGUMBOS nuclei adsorb onto these assemblies and subsequently grow on the surface.

1.4.4.2. Micelle-assisted Synthesis

Normal micelles are organized structures formed as a result of self-assembly of surfactant monomeric units in a polar solvent.[88] This self-assembly occurs at a surfactant concentration beyond a critical value known as critical micellar concentration (CMC). In a polar solvent, the hydrophobic part of the amphiphilic monomer orients itself away from the solvent and the hydrophilic part is directed towards solvent molecules.[89] The opposite orientation for the organized structure is formed in nonpolar solvent and is called inverse

micelle.[89] Normal micelles are mainly used as carriers for poorly soluble drugs in drug delivery applications; however, inverse micelles are used for hydrophilic drugs.[89] Micelles, in regular or inverted orientation, have been recently used as “nanoreactors” for the formation of nanoparticles.[90] The size and shape of nanoparticles can be controlled by micellar colloidal templates. In the presence of micelles, different sizes and shapes can be produced depending on the type and concentration of surfactant, the volumes of oil and water used, as well as the amount of reactants.[90] For the normal micelle-assisted synthesis of nanoGUMBOS, the development of nanoparticles occurs within the hydrophobic core of normal micelles, which are important for steric stabilization and reduction of the agglomeration level (Figure 1.11).

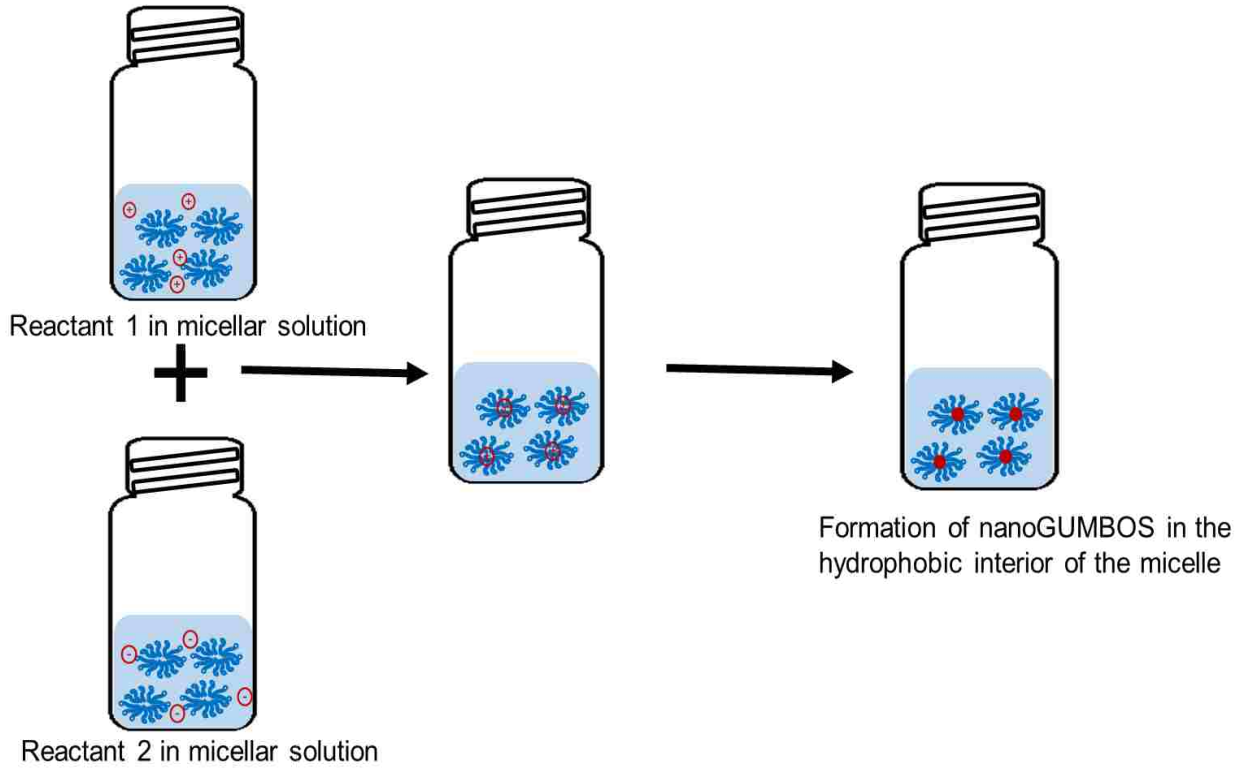

Figure 1.11. Normal micelle-based synthesis forms nanoGUMBOS within the hydrophobic interior of a micelle.

1.4.5. Doping NanoGUMBOS

Doping is a technique based on incorporating impurities into a host matrix, which can be at a bulk state or a nanoscale level. The purpose of doping is to introduce new physical and optical properties into the host material.[91] Generally, in case of doping, the electronic states of the dopant lie between the valence and conduction bands of the host. As a result of the free movement of the holes and electrons to the intermediate electronic states, recombination occurs at this level and causes subsequent changes in light emission properties.[91]

Doping nanoparticles can occur during any of the three different formation stages: (A) before nucleation, (B) during nucleation, or (C) during growth of nanoparticles. Different types of nanoparticles have been previously doped with transition metals such as Cu^{2+} and Mn^{2+}, as well as lanthanides such as Er^{3+}. Semiconductors II-VI quantum dots (QDs) are considered the best example for doping since a decrease in energy band gap occurs upon doping these QDs and eventually reduces the effect of self-quenching.[91] Dye-doped organic nanoparticles were well reported in scientific literature; cyanine-based fluorescent organic nanoparticles (FONs) have been previously doped with an ethidinium dye to cause the emission of white light.[92] Ultimately, pyrazoline-based nanoparticles were doped with a red light-emission material to provide a tunable emission.[93] This tunability in optical properties was also observed in organic binary nanowires composed of a blue emitting material, 1,3,5,triphenyl-2-pyrazoline (TPP) and an orange dye, rubrene. The binary nanostructures exhibited different emission colors (including white light) depending on the doping or molar ratio of TPP/rubrene.[94]

There are several applications associated with doping nanoparticles. For instance, lanthanide-doped nanocrystals with upconversion emission, have been widely used for optical labeling in biological studies.[95] In regard to QDs, doping strategy allows for the use of these nanostructures in sensing applications,[96] bioimaging,[97] and other analytical applications such as mass spectrometry[98] and electrochemistry.[99] However, doping organic nanoparticles promotes mainly the application of these nanostructures in optoelectronic devices.[100]

1.5. NanoGUMBOS: Characterization Tools

1.5.1. Transmission Electron Microscopy

Transmission electron microscopy (TEM) is one of the most common techniques where high-energy electron beams are employed for materials characterization.[101] This technique is based on the detection of signals produced from elastic interactions with matter (Figure 1.12).[102] TEM instrument was invented in 1931 by the German electrical

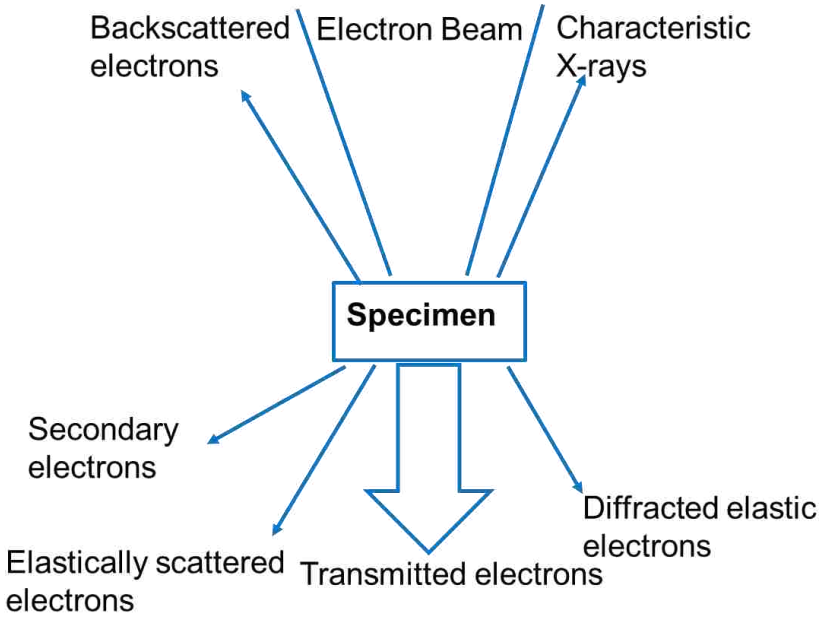

Figure 1.12. Different types of 2° effects (secondary, backscattered, transmitted, characteristic X-ray) occur upon interaction of an electron beam with a specimen. Adapted from Reference 7.

engineer Max Knoll and the German physicist Ernst Ruska.[7] In the operation principle of a TEM instrument, electrons are produced and emitted from a field emission gun (FEG) or a LaB_6 electron emitter. The trajectory of electrons is then deflected by the presence of a magnetic field created by magnetic lenses.[103] The condenser lenses then produce a fine beam of electrons, which interacts with the specimen for imaging purposes. Finally, the objective and projector lenses magnify the image that is analyzed on a CCD camera (Figure 1.13).[104] In a traditional way of generating an image in TEM, a bright-field image is produced by detecting transmitted (non-scattered) electrons.

When imaging the specimen with TEM, the sample thickness needs to be less than

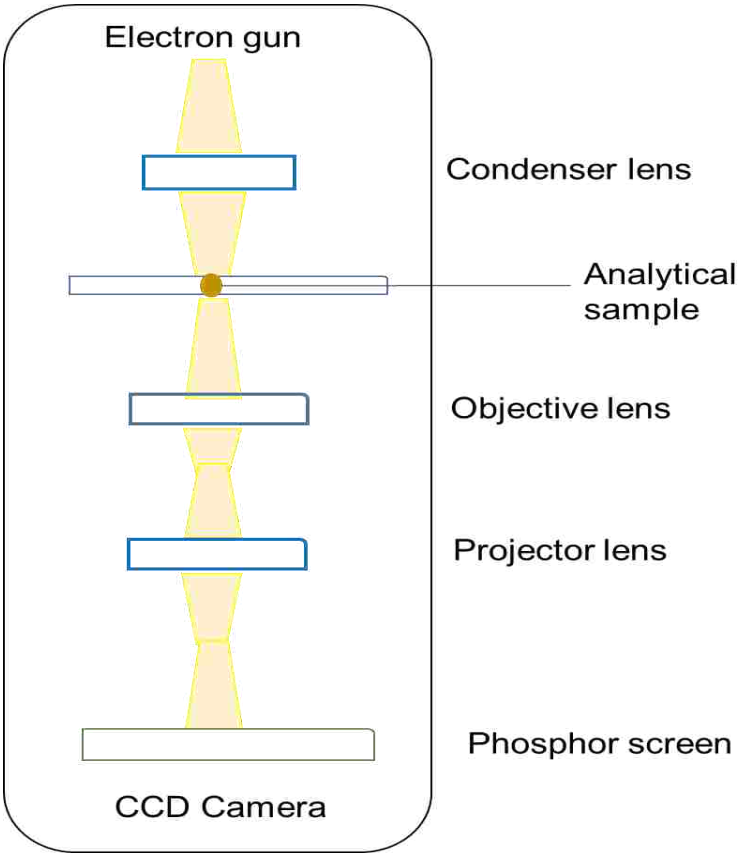

Figure 1.13. A transmission electron microscope enables visualization of nanoparticles. Adapted from Reference 7.

100 nm. Hence, procedures such as grinding and milling are performed for hard inorganic samples. Furthermore, staining biological samples with heavy metals is a common procedure for a better observation of samples with low atomic number. Occasionally, preparation of samples is not required and materials suspended in volatile solvents can be directly spotted on a carbon-coated TEM grid.[7] TEM has two primary drawbacks including the artifacts, which are usually misinterpreted by the operator, and sample damaging caused by electron beam to specimens such as organic materials, minerals, and ceramics.[101]

1.5.2. Dynamic Light Scattering

Dynamic light scattering (DLS) is a common characterization technique which provides information involving the hydrodynamic diameter of particles from the scale of submicron to nanometer.[105] In this technique, a laser irradiating a nanoparticles suspension is elastically scattered by the nanoparticles which are in Brownian motion (Figure 1.14). This motion is caused by the collision of nanoparticles with surrounding

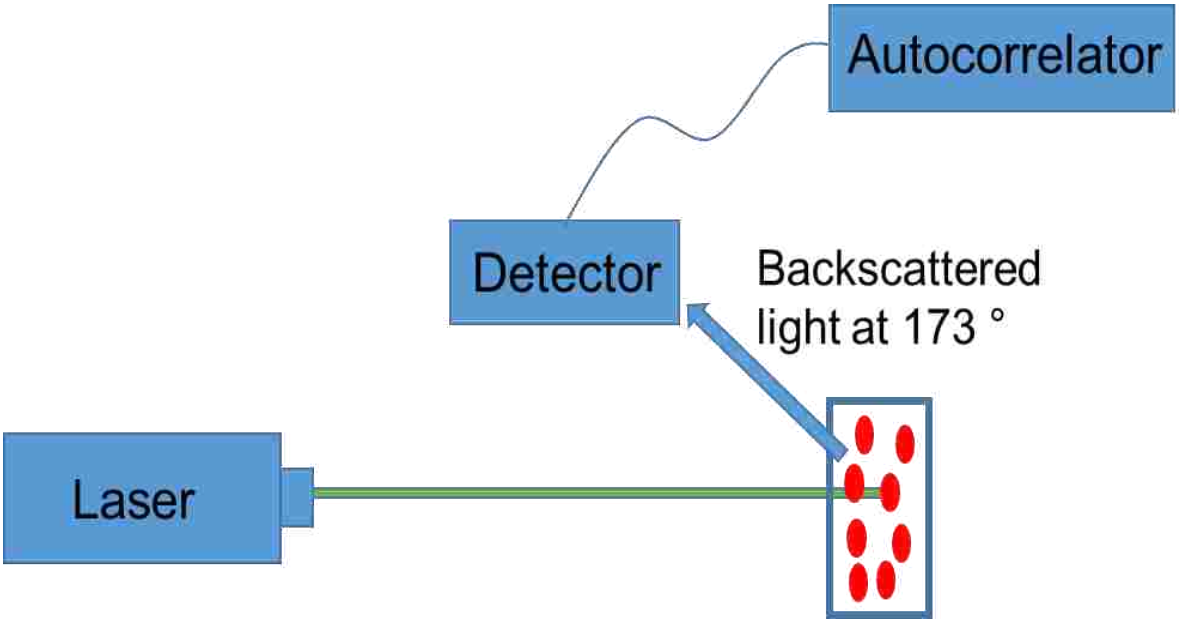

Figure 1.14. A DLS instrument detects the light scattering of nanoparticles suspension.

molecules and contribute to the fluctuations in intensity of scattered light.[106] Small nanoparticles that move quickly in the dispersing medium show a fast decay of scattered light; however, larger nanoparticles with a slower movement have a long decay of fluctuated light. Ultimately, the decay rates are correlated to the size of nanoparticles and a size distribution of the system is obtained as a function of intensity, volume, or number distributions.[107] The particle radius is calculated from the Stokes-Einstein equation (Equation 2), which connects the size to the diffusion coefficient in the medium:

$$r = \frac{k_B T}{6\pi\eta D} \quad (2)$$

Where r is Van der Waals radius of the molecule (m)

K_B is the Boltzmann constant ($1.388X10^{-23}$ $J \cdot K^{-1}$)

T is the absolute temperature (K)

η is the viscosity ($Pa \cdot s^{-1}$)

D is the self-diffusion coefficient ($m^2 \cdot s^{-1}$)

DLS is considered a non-destructive technique where the sample can be completely recovered after measurement. This technique is also rapid and can be performed in any liquid medium, as long as the physical parameters such as viscosity and density are taken into consideration. DLS is suitable and accurate for monodisperse samples; however, in the case of polydisperse samples, the presence of large particles can prevent the signal from the smaller particles to be discerned.[107] In addition, DLS is limited to spherical nanoparticles since the analysis and autocorrelation function are based on the assumption of a spherical shape of particles.[108]

1.5.3. Zeta Potential

Zeta potential (ζ) is the electrostatic surface potential which results from the net charge at the slipping plane, an outer boundary of the electrical double layer surrounding a nanoparticle.[109-110] When a particle moves due to Brownian motion, some ions are strongly attached to the particle and belong to the inner region known as the Stern layer. Beyond this inner boundary, some ions are less attached to the particle and constitute the electrical double layer or the diffuse layer. The boundary to these ions is the slipping plane at which the voltage (zeta potential) is measured (Figure 1.15). Zeta potential can be indirectly determined based on the electrophoretic mobility of the particle or the acoustic and electroacoustic properties.[110]

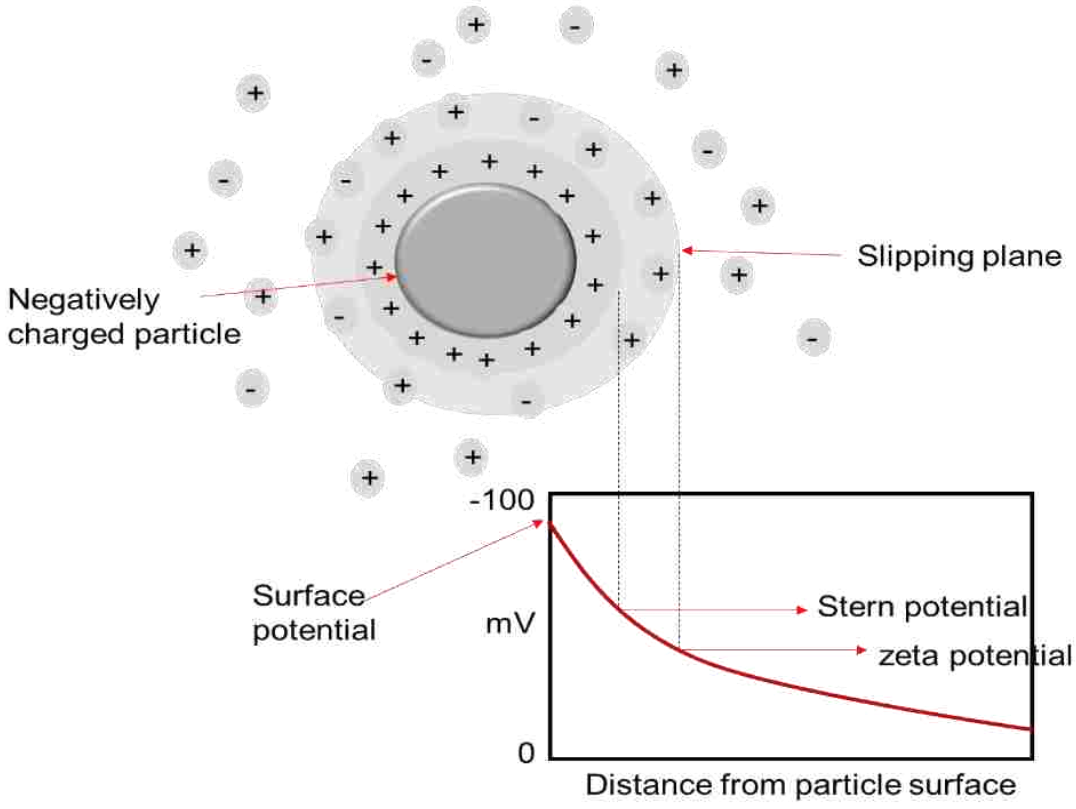

Figure 1.15. Zeta potential measures the charge at the slipping plane of an electrical double layer surrounding a charged nanoparticle.

Laser Doppler electrophoresis (LDE) or laser Doppler velocimetry (LDV) is the process used to measure zeta potential of a particle by tracking its electrophoretic mobility.[111-112] The sample is analyzed in an electrophoresis cell where the charged particles move from one electrode to another upon the application of a voltage. During this phenomenon, a laser is illuminated on the particles in movement, causing a frequency shift in the signal. As the laser wavelength and the scattering angle are known, the electrophoretic mobility can be calculated. The Henry equation relates between the electrophoretic mobility and zeta potential (Equation 3).

$$U_E = \frac{2\varepsilon\zeta f(K_a)}{3\eta} \quad (3)$$

Where U_E is the electrophoretic mobility ($m^2 \cdot V^{-1} \cdot s^{-1}$), ε is the electric permittivity of the medium or dielectric constant ($C^2 \cdot N^{-1} \cdot m^{-2}$), η is the viscosity of the medium, f (ka) is the Henry's function, and ζ is the zeta potential (V).[113] The Henry's function is equal to 1.5 in polar medium (Smoluchowski approximation) and 1.0 in non-polar medium (Hückel approximation). Zeta potential is essential to acquire information about the stability of the colloidal system, aggregation level, reactivity, and toxicology of nanoparticles.[110] Scientists generally consider the systems with zeta potential values between + 30 mV and - 30 mV as unstable systems and the ones with values beyond these limits as stable systems.[114-115]

1.5.4. Spectroscopic Studies

Spectroscopy is the science which deals with the interaction or emission of matter to electromagnetic radiation.[116] Nanomaterials present optical properties that lie between atomic and bulk properties.[7] Organic nanoparticles in particular, can show optical properties different from the relative bulk system. The inter- and intra-molecular

interactions of the aggregates govern the optical properties in these nanoparticles. For example, J- and H- aggregates are the most common type of aggregation encountered mainly in organic dyes-based nanomaterials. The parallel stacking of organic molecules contributes to H-type of aggregates and the head-to-tail stacking to J-type of aggregates.[117] Changes in absorbance and fluorescence spectra of nanomaterials can be related to these types of aggregation, as well as other factors including the size and morphology of nanoparticles.

1.5.4.1. Absorption Spectroscopy

When it interacts with matter, light can be absorbed (entirely or partially) and energy will be transferred to the molecule in form of quanta or photon.[118] The energy of a photon is expressed in Equation 4 as following:

$$E = h \times \nu = \frac{hc}{\lambda} \quad (4)$$

Where E is the energy (J), h is Planck's constant (6.62×10^{-34} J·s), c is the speed of light in a vacuum ($2.997\text{x}10^{8}$ m·s^{-1}), λ is the wavelength (m), and ν is the frequency (s^{-1}). Absorption spectroscopy measures the fraction of light absorbed by an analyte sample.[119] An absorption measurement is able to detect specific functional groups denoted as chromophores. This type of spectroscopy is the most common and useful for quantitative analysis.[120] The amount of light absorbed is related to the concentration via Beer's law (Equation 5), which is applied for diluted solutions (< 0.01 M).

$$A = \log\frac{P_0}{P_t} = \in bC \quad (5)$$

Where A is the absorbance (unitless), P_0 and P_t are the initial and transmitted radiant powers respectively (watts), ∈ is the molar absorptivity (L·moles^{-1}·cm^{-1}), b is the

path length (cm), and C is concentration of the analyte (moles·L^{-1}). There are several parameters that affect absorption measurement such as the nature of the solvent (polarity), pH and temperature of the solution.[121] The basic instrument components in absorbance spectroscopy are presented in Figure 1.16. The spectrophotometer is composed of a light source (*e.g.*, xenon arc), a monochromator, reference and sample cell holders, as well as a detector (*e.g.*, photomultiplier tube).[119]

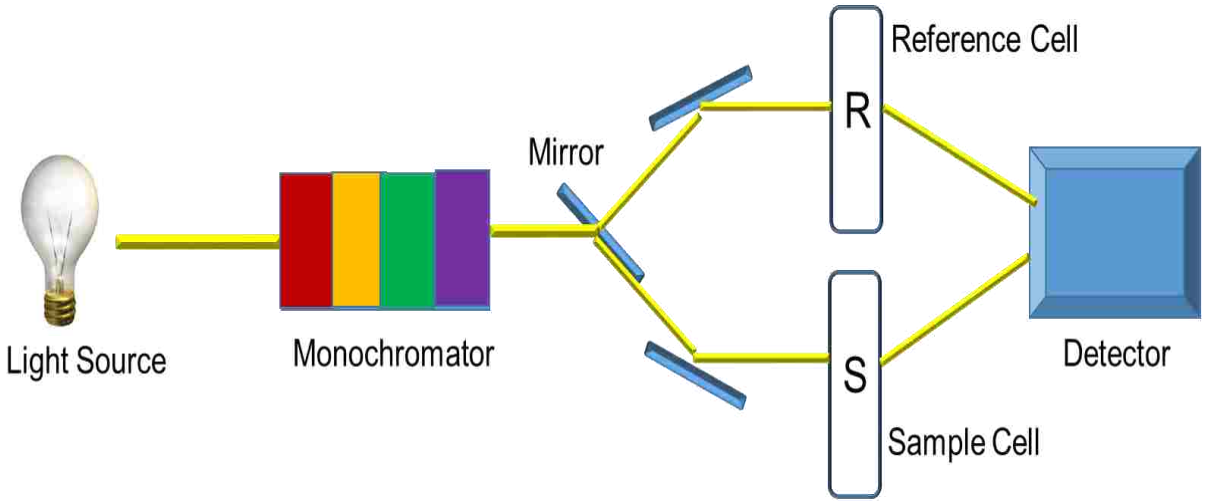

Figure 1.16. A double-beam design is used in absorption spectroscopy.

1.5.4.2. Fluorescence Spectroscopy

An energy-level diagram is used to describe different energy and vibrational levels in a molecule.[118] When light is absorbed (10^{-15} seconds), a molecule can move from a ground energy level to a higher energy level (Figure 1.17). For some molecules, when a higher excited state is attained, subsequent luminescence phenomenon might occur for the molecule to return to the ground state. Fluorescence is observed when the photons are emitted from a singlet excited state. In this case, the emitted light has a lower energy than the light absorbed because the molecule loses some energy through radiationless processes such as vibrational relaxations (10^{-12} seconds); likewise, the solvent

reorientation in the excited state or solvent effect contributes to this loss of energy.[118] A transition from a singlet to a triplet state, a state when an electron shows unpaired spins, occurs via an intersystem crossing. Molecules in a triplet state can return to ground state and emit light by phosphorescence.[118] In fact, phosphorescence decay occurs at a longer lifetime scale (10^{-3} seconds) than the lifetime of fluorescence (10^{-8} seconds).[122]

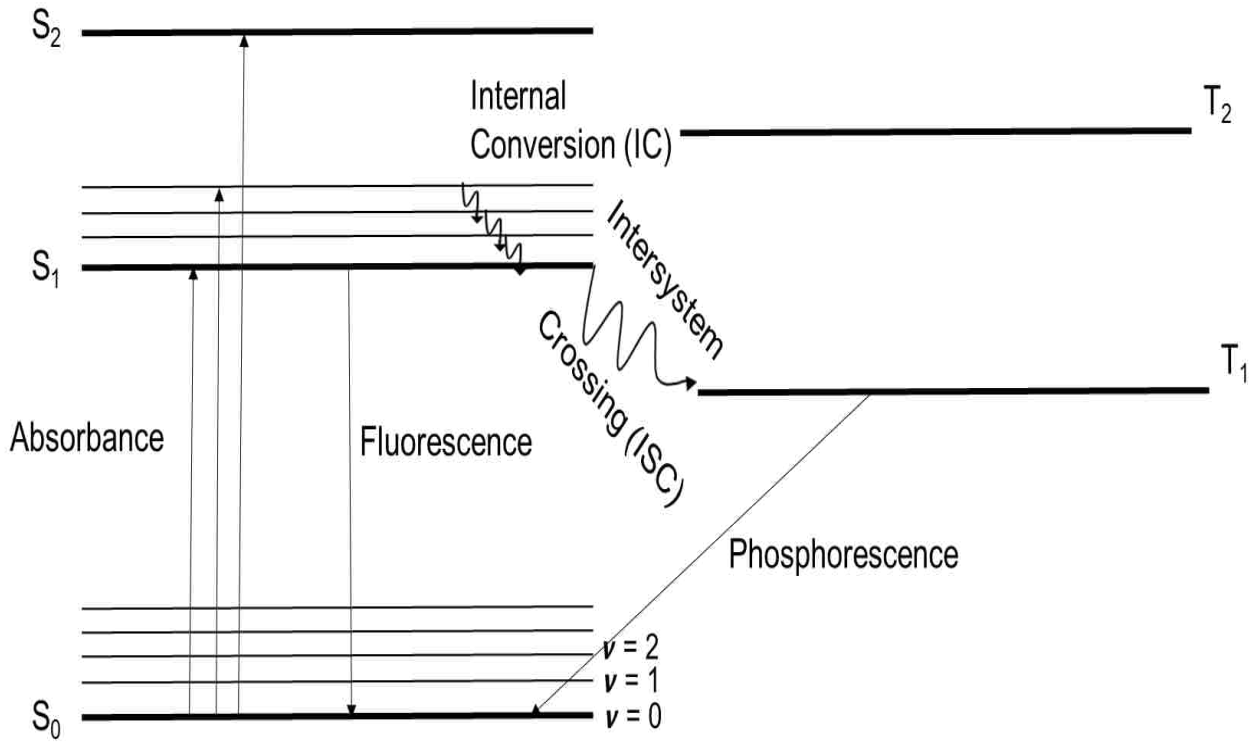

Figure 1.17. Jablonski diagram shows the radiative and non-radiative electron transitions. Adapted from Reference 118.

The instrumental design of a fluorometer has the detector orthogonal relative to the source. This configuration is adopted to decrease the problems caused by scattered light (Figure 1.18). Fluorescence spectroscopy offers more advantages than absorbance spectroscopy when an analyte is strongly fluorescent. This spectroscopy is more sensitive and selective than absorbance, and the output is linear over a broader analyte

concentration range as compared to absorbance. However, sample dilution may be needed prior to fluorescence measurements as a consequence of the self-absorption from a high analyte concentration.[119]

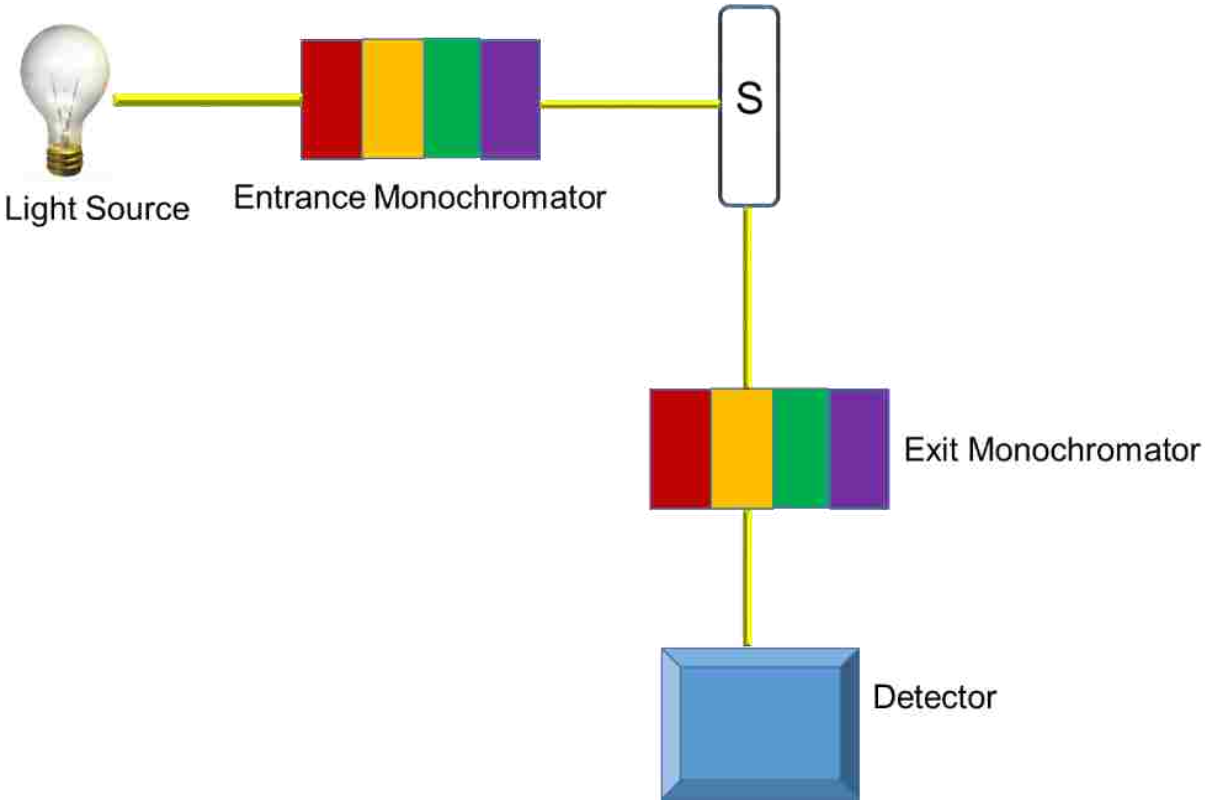

Figure 1.18**.** A fluorometer is designed with right angle detector.

1.6. Applications of NanoGUMBOS

1.6.1. Molecular Imprinting

Molecular imprinting is a technology that allows the creation of specific binding sites to a template within a solid matrix. This technology is usually performed in cross-linked polymers which allow to lock-in the template. An imprinted polymer acquires selective recognition properties for the shape, size, and functionalities of a targeted analyte.[123] This acquisition stems from two basic procedures:

1) the organization of the monomer functional groups around the template to create a monomer-template complex
2) the formation of a selective cavity to the template within the cross-linked polymer.[124]

The interactions between the functional monomers and the print molecule can be formed as a result of non-covalent (*e.g.*, hydrogen bonds, ionic interactions) or covalent interactions depending on the imprinting strategy. Non-covalent imprinting is more common because it doesn't require extensive steps to imprint or remove the template as it is the case for covalent imprinting.[124] Several parameters such as the ratios of template to monomer and cross-linker to monomer, the solvent, as well as the temperature of the medium, control the formation of selective imprinted polymer.[124] Altogether, the success of imprinting is governed by the organization of a pre-polymer complex between the monomer and the template, which follows Le Châtelier's principle (Figure 1.19). Experimental conditions such as the increase in monomer to template ratio or the decrease in temperature may eventually favor the formation of the complex and increase the number of binding sites.

Molecularly imprinted polymers (MIPs) are interesting given the fact that these smart polymers can be used as sorbents for solid phase extraction,[125-126] stationary phases in liquid chromatography,[127] and as replacement for antibodies in binding assays.[128] Particularly, MIP nanoparticles present a higher surface area-to-volume ratio and accessible cavities compared to bulk material, which is highly advantageous in the case of surface imprinting.[129] These nanoparticles have been exploited in several applications such as drug delivery[130] and sensing applications.[131]

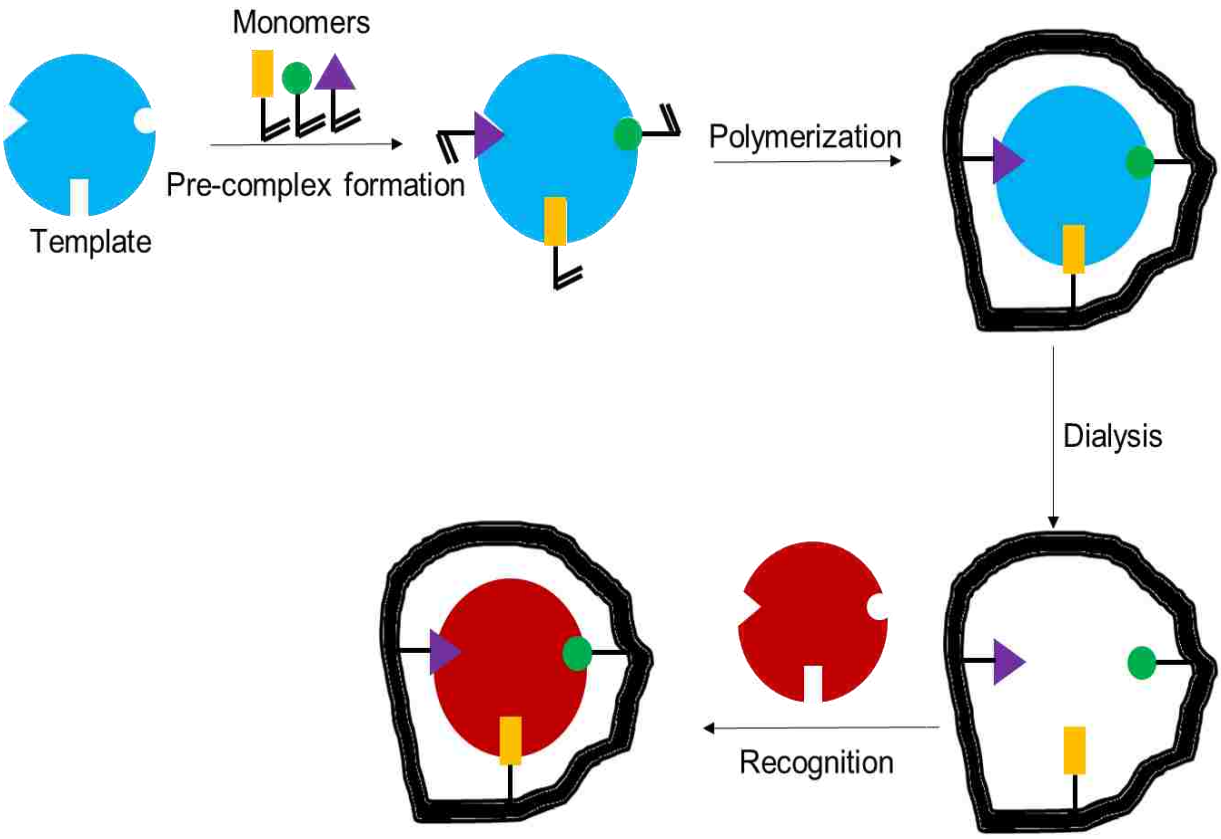

Figure 1.19. Molecular imprinting process forms specific sites in polymers.

1.6.2. Organic Light Emitting Devices

Light emitting diodes (LEDs) are semiconductor devices that achieve solid state lighting, which is more energy efficient than regular lighting.[132] Organic light emitting diodes (OLEDs), in particular, are interesting since these devices are made from non-toxic and less expensive materials in comparison to LEDs. OLEDs are composed of a combination of some or all of the following sandwiched layers: electrodes (anode and cathode), hole injection layer (HIL), hole transport layer (HTL), electron transport layer (ETL), and emissive layer (EML) (Figure 1.20). The recombination between electrons and holes which occurs usually in EML, causes light emission in this device. In some cases, one layer can procure several functions; therefore, different designs of OLEDs can be

fabricated. In a single layer OLED, an organic layer which is placed between two electrodes, functions as electrons and holes transport as well as emissive layer simultaneously.[132] In a double layer geometry, OLED is made of separate electron and hole transporting layers; under these circumstances, light emission occurs at the interface between the two layers. A multi-layer system includes all types of layers which should have specific characteristics such as high luminescence efficiency, good physical and chemical stability, acceptable conductivity, as well as high color rendering index. Among

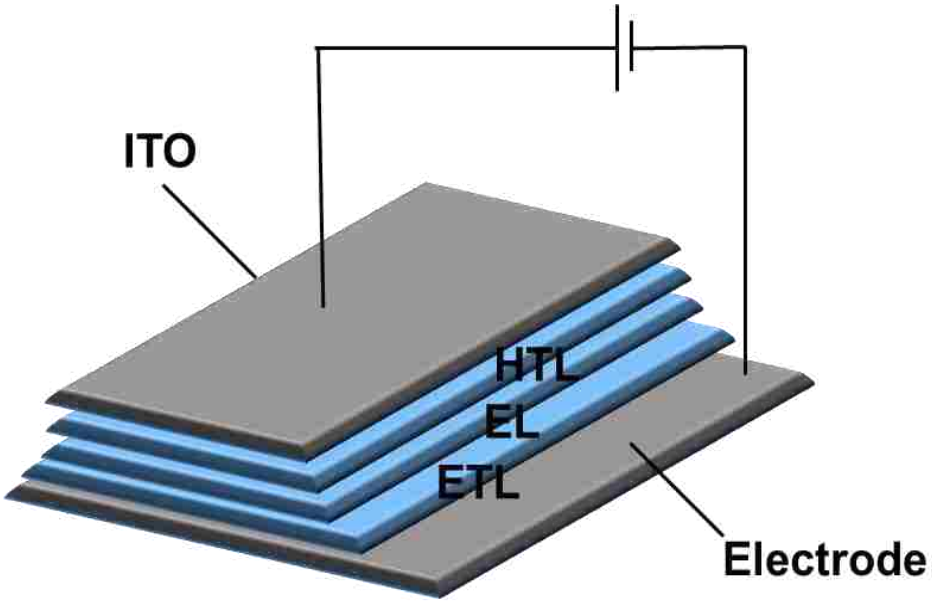

Figure 1.20. A light emitting device can be fabricated from triple layers (HTL, EL, and ETL).

the commercially available OLEDs, green and red OLEDs have been extensively explored; however, blue OLEDs are still considered a challenge due to the short lifetime of these devices.[133] White OLEDs are of a particular interest since these devices offer a full color display. The combination of materials emitting the primary colors (RGB) is one method to produce white light in these devices. Current research focuses on improving the efficiency and lifetime of white OLEDs.[132] In this regard, the tendency to miniaturize

light emitting devices has led to the integration of nanomaterials in these devices.[134] Furthermore, the tunability in optical and physical properties with size and morphology of nanoparticles make these materials highly significant for LEDs.[135]

1.7. Scope of this Dissertation

The primary focus of this dissertation is the syntheses of nanoparticles derived from GUMBOS (*i.e.,* nanoGUMBOS) and the applicability of these nanoparticles as molecularly imprinted polymers for chiral recognition as well as emissive materials in organic light emitting devices. In the second chapter of this dissertation, the fundamentals of nanoGUMBOS synthesis, the procedures that can be used for efficient production of nanoGUMBOS, and the factors that affect the mechanisms of nanoparticles formation are described. The syntheses are developed to have a better control over the engineering of nanoGUMBOS within a specific size and polydispersity. Chapter Three describes our studies on the synthesis of polymeric nanoparticles derived from PILs using UV illumination. Molecular imprinting procedure was used to generate polymeric nanoGUMBOS with chiral recognition properties. Information on the polymerization of GUMBOS at the nanoscale, molecular imprinting, and the recognition of L-tryptophan through fluorescence measurements is discussed in this chapter. Moreover, the synthesis of polymeric nanoGUMBOS using gamma irradiation is investigated in the next chapter. The formation of the nanoparticles and the polymerization mechanism are analyzed; preliminary studies on the potential application of these nanoparticles in drug encapsulation are also presented. Chapter Five highlights the application of semiconductive fluorescent nanoGUMBOS in OLEDs. The knowledge of nanoGUMBOS synthesis was used to control the size and eventually, the optical properties of these

nanoparticles. A doping procedure was also introduced in this chapter as a method to tune the optical properties. Herein, the focus is on the quantum yield of nanoGUMBOS and the factors that influence the light emission from these nanoparticles. The last section of this dissertation highlights the importance of nanoGUMBOS, the significant results from the studies, and the conclusions that can be drawn. Future work covers the possible investigations that can be performed either on polymeric or semiconductor-based nanoGUMBOS. This section includes other projects that involve the synthesis and the surface modification of nanoGUMBOS, in addition to suggested experiments that may improve the usefulness of these organic nanomaterials.

1.8. References

1. Whatmore, R. W. Nanotechnology—What Is It? Should We Be Worried? *Occup. Med.* **2006,** *56* (5), 295-299.

2. Schmid, G.; Decker, M.; Ernst, H.; Fuchs, H.; Grünwald, W.; Grunwald, A.; Hofmann, H.; Mayor, M.; Rathgeber, W.; Simon, U. Small Dimensions and Material Properties. *A Definition of Nanotechnology* **2003,** *11* (03), 13-28.

3. Reichardt, N. C.; Martin-Lomas, M.; Penades, S. Glyconanotechnology. *Chem. Soc. Rev.* **2013,** *42* (10), 4358-4376.

4. Gröning, P. A. Nanotechnology: An Approach to Mimic Natural Architectures and Concepts. *Adv. Eng. Mater*. **2005,** *7* (5), 279-291.

5. Huczko, A. Template-Based Synthesis of Nanomaterials. *Appl. Phys. A* **2000,** *70* (4), 365-376.

6. Faraday, M. The Bakerian Lecture: Experimental Relations of Gold (and Other Metals) to Light. *Philos. Trans. R. Soc. London* **1857,** *147*, 145-181.

7. Hormyak, G. L.; Dotta, J.; Tibbals, H.F.; Rao, A. *Introduction to Nanoscience*; CRC Press: London, 2008.

8. Zsigmondy, R. A. Properties of Colloids, Nobel Lecture in Chemistry, 1926.

9. Gupta, T.; Jayatissa, A. Recent Advances in Nanotechnology: Key Issues & Potential Problem Areas. In *Nanotechnology*, 2003. IEEE-NANO 2003. 2003 Third IEEE Conference on, 2003; pp 469-472.

10. Mamalis, A. G. Recent Advances in Nanotechnology. *J. Mater. Process. Technol.* **2007,** *181* (1–3), 52-58.

11. Klostranec, J. M.; Chan, W. C. W. Quantum Dots in Biological and Biomedical Research: Recent Progress and Present Challenges. *Adv. Mat.* **2006,** *18* (15), 1953-1964.

12. Adams, F. C.; Barbante, C. Nanoscience, Nanotechnology and Spectrometry. *Spectrochim. Acta, Part B* **2013,** *86* (0), 3-13.

13. Saha, K.; Agasti, S. S.; Kim, C.; Li, X.; Rotello, V. M. Gold Nanoparticles in Chemical and Biological Sensing. *Chem. Rev.* **2012,** *112* (5), 2739-2779.

14. Grass, R. N.; Athanassiou, E. K.; Stark, W. J. Covalently Functionalized Cobalt Nanoparticles as a Platform for Magnetic Separations in Organic Synthesis. *Angew. Chem., Int. Ed.* **2007,** *46* (26), 4909-4912.

15. Crooks, R. M.; Zhao, M. Q.; Sun, L.; Chechik, V.; Yeung, L. K. Dendrimer-Encapsulated Metal Nanoparticles: Synthesis, Characterization, and Applications to Catalysis. *Acc. Chem. Res.* **2001,** *34* (3), 181-190.

16. Sun, S. H. Recent Advances in Chemical Synthesis, Self-Assembly, and Applications of Fept Nanoparticles. *Adv. Mat.* **2006,** *18* (4), 393-403.

17. Lu, X. M.; Rycenga, M.; Skrabalak, S. E.; Wiley, B.; Xia, Y. N. Chemical Synthesis of Novel Plasmonic Nanoparticles. In *Annual Review of Physical Chemistry*, 2009; Vol. 60; pp 167-192.

18. Baer, D. R.; Gaspar, D. J.; Nachimuthu, P.; Techane, S. D.; Castner, D. G. Application of Surface Chemical Analysis Tools for Characterization of Nanoparticles. *Anal. Bioanal. Chem.* **2010,** *396* (3), 983-1002.

19. Sang, F. M.; Huang, X. Y.; Ren, J. C. Characterization and Separation of Semiconductor Quantum Dots and Their Conjugates by Capillary Electrophoresis. *Electrophoresis* **2014,** *35* (6), 793-803.

20. Tiwari, J. N.; Tiwari, R. N.; Kim, K. S. Zero-Dimensional, One-Dimensional, Two-Dimensional and Three-Dimensional Nanostructured Materials for Advanced Electrochemical Energy Devices. *Prog. Mater. Sci.* **2012,** *57* (4), 724-803.

21. Murthy, S. K. Nanoparticles in Modern Medicine: State of the Art and Future Challenges. Int. J. Nanomed. **2007,** *2* (2), 129-141.

22. Merkel, T. J.; Herlihy, K. P.; Nunes, J.; Orgel, R. M.; Rolland, J. P.; DeSimone, J. M. Scalable, Shape-Specific, Top-Down Fabrication Methods for the Synthesis of Engineered Colloidal Particles. *Langmuir* **2010,** *26* (16), 13086-13096.

23. Raab, C.; Simkó, M.; Fiedeler, U.; Nentwich, M.; Gazsó, A. Production of Nanoparticles and Nanomaterials, *NanoTrust-Dossiers 06en*, **2011**.

24. Cui, H.; Feng, Y.; Ren, W.; Zeng, T.; Lv, H.; Pan, Y. Strategies of Large Scale Synthesis of Monodisperse Nanoparticles. *Recent Pat. Nanotechnol.* **2009,** *3* (1), 32-41.

25. Mohanraj, V.; Chen, Y. Nanoparticles-a Review. *Trop. J. Pharm. Res.* **2007,** *5* (1), 561-573.

26. Huczko, A. Template-Based Synthesis of Nanomaterials. *Appl. Phys. A: Mater. Sci. Process.* **2000,** *70* (4), 365-376.

27. Fouilloux, S.; Desert, A.; Tache, O.; Spalla, O.; Daillant, J.; Thill, A. SAXS Exploration of the Synthesis of Ultra Monodisperse Silica Nanoparticles and Quantitative Nucleation Growth Modeling. *J. Colloid Interface Sci.* **2010,** *346* (1), 79-86.

28. LaMer, V. K.; Dinegar, R. H. Theory, Production and Mechanism of Formation of Monodispersed Hydrosols. *J. Am. Chem. Soc.* **1950,** *72* (11), 4847-4854.

29. Finney, E. E.; Finke, R. G. Nanocluster Nucleation and Growth Kinetic and Mechanistic Studies: A Review Emphasizing Transition-Metal Nanoclusters. *J. Colloid Interface Sci.* **2008,** *317* (2), 351-374.

30. Sugimoto, T. Underlying Mechanisms in Size Control of Uniform Nanoparticles. *J. Colloid Interface Sci.* **2007,** *309* (1), 106-118.

31. Cao, G. Zero-Dimensional Nanostructures: Nanoparticles. In *Nanostructures and Nanomaterials: Synthesis, Properties and Applications*, Imperial College Press: London, 2004; pp 51-59.

32. Allouche, J. Synthesis of Organic and Bioorganic Nanoparticles: An Overview of the Preparation Methods. In *Nanomaterials: A Danger or a Promise?*; Brayner, R., Ed.; Springer-Verlag: London, 2013.

33. Nakanishi, H.; Oikawa, H. Reprecipitation Method for Organic Nanocrystals. In *Single Organic Nanoparticles*; Masuhara, H.; Nakanishi, H.; Sasaki, K., Eds. Springer: Berlin Heidelberg, 2003; pp 17-31.

34. Asahi, T.; Sugiyama, T.; Masuhara, H. Laser Fabrication and Spectroscopy of Organic Nanoparticles. *Acc. Chem. Res.* **2008,** *41* (12), 1790-1798.

35. Ibanez, A.; Maximov, S.; Guiu, A.; Chaillout, C.; Baldeck, P. L. Controlled Nanocrystallization of Organic Molecules in Sol-Gel Glasses. *Adv. Mat.* **1998,** *10* (18), 1540-1543.

36. Weingaertner, H. Understanding Ionic Liquids at the Molecular Level: Facts, Problems, and Controversies. *Angew. Chem., Int. Ed.* **2008,** *47* (4), 654-670.

37. Huddleston, J. G.; Visser, A. E.; Reichert, W. M.; Willauer, H. D.; Broker, G. A.; Rogers, R. D. Characterization and Comparison of Hydrophilic and Hydrophobic Room Temperature Ionic Liquids Incorporating the Imidazolium Cation. *Green Chem.* **2001,** *3* (4), 156-164.

38. Rogers, R. D.; Seddon, K. R. Ionic Liquids - Solvents of the Future? *Science* **2003,** *302* (5646), 792-793.

39. Welton, T. Room-Temperature Ionic Liquids. Solvents for Synthesis and Catalysis. *Chem. Rev.* **1999,** *99* (8), 2071-2083.

40. Wilkes, J. S. A Short History of Ionic Liquids - from Molten Salts to Neoteric Solvents. *Green Chem.* **2002,** *4* (2), 73-80.

41. Walden, P. Molecular weights and electrical conductivity of several fused salts *Impér. Sci. St. Pétersbourg.* **1914,** *8*, 405-422.

42. Wilkes, J. S.; Zaworotko, M. J. Air and Water Stable 1-Ethyl-3-Methylimidazolium Based Ionic Liquids. *J. Chem. Soc., Chem. Commun.* **1992,** (13), 965-967.

43. Wilkes, J. S.; Levisky, J. A.; Wilson, R. A.; Hussey, C. L. Dialkylimidazolium Chloroaluminate Melts - a New Class of Room-Temperature Ionic Liquids for Electrochemistry, Spectroscopy, and Synthesis. *Inorg. Chem.* **1982,** *21* (3), 1263-1264.

44. Endres, F.; El Abedin, S. Z. Air and Water Stable Ionic Liquids in Physical Chemistry. *Phys. Chem. Chem. Phys.* **2006,** *8* (18), 2101-2116.

45. Ngo, H. L.; LeCompte, K.; Hargens, L.; McEwen, A. B. Thermal Properties of Imidazolium Ionic Liquids. *Thermochim. Acta* **2000,** *357*, 97-102.

46. MacFarlane, D. R.; Seddon, K. R. Ionic Liquids - Progress on the Fundamental Issues. *Aust. J. Chem.* **2007,** *60* (1), 3-5.

47. Joshi, M. D.; Anderson, J. L. Recent Advances of Ionic Liquids in Separation Science and Mass Spectrometry. *RSC Adv.* **2012,** *2* (13), 5470-5484.

48. Ho, T. D.; Canestraro, A. J.; Anderson, J. L. Ionic Liquids in Solid-Phase Microextraction: A Review. *Anal. Chim. Acta* **2011,** *695* (1–2), 18-43.

49. Davis, J. H. Task-Specific Ionic Liquids. *Chem. Lett.* **2004,** *33* (9), 1072-1077.

50. Giernoth, R. Task-Specific Ionic Liquids. *Angew. Chem., Int. Ed.* **2010,** *49* (16), 2834-2839.

51. Visser, A. E.; Swatloski, R. P.; Reichert, W. M.; Mayton, R.; Sheff, S.; Wierzbicki, A.; Davis, J. H.; Rogers, R. D. Task-Specific Ionic Liquids Incorporating Novel Cations for the Coordination and Extraction of Hg^{2+} and Cd^{2+}: Synthesis, Characterization, and Extraction Studies. *Environ. Sci. Technol.* **2002,** *36* (11), 2523-2529.

52. Plechkova, N. V.; Seddon, K. R. Applications of Ionic Liquids in the Chemical Industry. *Chem. Soc. Rev.* **2008,** *37* (1), 123-150.

53. Lu, J.; Yan, F.; Texter, J. Advanced Applications of Ionic Liquids in Polymer Science. *Prog. Polym. Sci.* **2009,** *34* (5), 431-448.

54. Green, O.; Grubjesic, S.; Lee, S.; Firestone, M. A. The Design of Polymeric Ionic Liquids for the Preparation of Functional Materials. *Polym. Rev.* **2009,** *49* (4), 339-360.

55. Yuan, J. Y.; Mecerreyes, D.; Antonietti, M. Poly(Ionic Liquid)s: An Update. *Progress in Polym. Sci* **2013,** *38* (7), 1009-1036.

56. Hsieh, Y.-N.; Ho, W.-Y.; Horng, R.; Huang, P.-C.; Hsu, C.-Y.; Huang, H.-H.; Kuei, C.-H. Study of Anion Effects on Separation Phenomenon for the Vinyloctylimidazolium Based Ionic Liquid Polymer Stationary Phases in GC. *Chromatographia* **2007,** *66* (7-8), 607-611.

57. Sato, T.; Marukane, S.; Narutomi, T.; Akao, T. High Rate Performance of a Lithium Polymer Battery Using a Novel Ionic Liquid Polymer Composite. *J. Power Sources* **2007,** *164* (1), 390-396.

58. Freitas, F. S.; Freitas, J. N. d.; Ito, B. I.; Paoli, M.-A. D.; Nogueira, A. F. Electrochemical and Structural Characterization of Polymer Gel Electrolytes Based on a PEO Copolymer and an Imidazolium-Based Ionic Liquid for Dye-Sensitized Solar Cells. *ACS Appl. Mater. Interfaces* **2009,** *1* (12), 2870-2877.

59. Guo, L.; Deng, Q.; Fang, G.; Gao, W.; Wang, S. Preparation and Evaluation of Molecularly Imprinted Ionic Liquids Polymer as Sorbent for on-Line Solid-Phase Extraction of Chlorsulfuron in Environmental Water Samples. *J. Chromatogr. A* **2011,** *1218* (37), 6271-6277.

60. Bi, W. T.; Tian, M. L.; Row, K. H. Evaluation of Molecularly Imprinted Anion-Functionalized Poly(Ionic Liquid)s by Multi-Phase Dispersive Extraction of Flavonoids from Plant. *J. Chromatogr. B: Anal. Technol. Biomed. Life Sci.* **2013,** *913*, 61-68.

61. Batra, D.; Hay; Firestone, M. A. Formation of a Biomimetic, Liquid-Crystalline Hydrogel by Self-Assembly and Polymerization of an Ionic Liquid. *Chem. Mat.* **2007,** *19* (18), 4423-4431.

62. Yoshio, M.; Kagata, T.; Hoshino, K.; Mukai, T.; Ohno, H.; Kato, T. One-Dimensional Ion-Conductive Polymer Films: Alignment and Fixation of Ionic Channels Formed by Self-Organization of Polymerizable Columnar Liquid Crystals. *J. Am. Chem. Soc.* **2006,** *128* (16), 5570-5577.

63. Batra, D.; Seifert, S.; Varela, L. M.; Liu, A. C. Y.; Firestone, M. A. Solvent-Mediated Plasmon Tuning in a Gold-Nanoparticle–Poly(Ionic Liquid) Composite. *Adv. Funct. Mat.* **2007,** *17* (8), 1279-1287.

64. Warner, I. M.; El-Zahab, B.; Siraj, N. Perspectives on Moving Ionic Liquid Chemistry into the Solid Phase. *Anal. Chem.* **2014,** *86* (15), 7184-7191.

65. Magut, P. K. S.; Das, S.; Fernand, V. E.; Losso, J.; McDonough, K.; Naylor, B. M.; Aggarwal, S.; Warner, I. M. Tunable Cytotoxicity of Rhodamine 6G Via Anion Variations. *J. Am. Chem. Soc.* **2013,** *135* (42), 15873-15879.

66. Cole, M. R.; Li, M.; Jadeja, R.; El-Zahab, B.; Hayes, D.; Hobden, J. A.; Janes, M. E.; Warner, I. M. Minimizing Human Infection from Escherichia Coli O157:H7 Using GUMBOS. *J. Antimicrob. Chemother.* **2013,** *68* (6), 1312-1318.

67. Regmi, B. P.; Monk, J.; El-Zahab, B.; Das, S.; Hung, F. R.; Hayes, D. J.; Warner, I. M. A Novel Composite Film for Detection and Molecular Weight Determination of Organic Vapors. *J. Mater. Chem.* **2012,** *22* (27), 13732-13741.

68. Jordan, A. N.; Das, S.; Siraj, N.; de Rooy, S. L.; Li, M.; El-Zahab, B.; Chandler, L.; Baker, G. A.; Warner, I. M. Anion-Controlled Morphologies and Spectral Features of Cyanine-Based NanoGUMBOS - an Improved Photosensitizer. *Nanoscale* **2012,** *4* (16), 5031-5038.

69. Dumke, J. C.; El-Zahab, B.; Challa, S.; Das, S.; Chandler, L.; Tolocka, M.; Hayes, D. J.; Warner, I. M. Lanthanide-Based Luminescent NanoGUMBOS. *Langmuir* **2010,** *26* (19), 15599-15603.

70. Bwambok, D. K.; El-Zahab, B.; Challa, S. K.; Li, M.; Chandler, L.; Baker, G. A.; Warner, I. M. Near-Infrared Fluorescent NanoGUMBOS for Biomedical Imaging. *ACS Nano* **2009,** *3* (12), 3854-3860.

71. Das, S.; Bwambok, D.; El-Zahab, B.; Monk, J.; de Rooy, S. L.; Challa, S.; Li, M.; Hung, F. R.; Baker, G. A.; Warner, I. M. Nontemplated Approach to Tuning the Spectral Properties of Cyanine-Based Fluorescent NanoGUMBOS. *Langmuir* **2010,** *26* (15), 12867-12876.

72. Tesfai, A.; El-Zahab, B.; Kelley, A. T.; Li, M.; Garno, J. C.; Baker, G. A.; Warner, I. M. Magnetic and Nonmagnetic Nanoparticles from a Group of Uniform Materials Based on Organic Salts. *ACS Nano* **2009,** *3* (10), 3244-3250.

73. Tesfai, A.; El-Zahab, B.; Bwambok, D. K.; Baker, G. A.; Fakayode, S. O.; Lowry, M.; Warner, I. M. Controllable Formation of Ionic Liquid Micro- and Nanoparticles Via a Melt-Emulsion-Quench Approach. *Nano Lett.* **2008,** *8* (3), 897-901.

74. Bang, J. H.; Suslick, K. S. Applications of Ultrasound to the Synthesis of Nanostructured Materials. *Adv. Mat.* **2010,** *22* (10), 1039-1059.

75. Grzelczak, M.; Vermant, J.; Furst, E. M.; Liz-Marzán, L. M. Directed Self-Assembly of Nanoparticles. *ACS Nano* **2010,** *4* (7), 3591-3605.

76. Chuong, T. V.; Dung, L. Q. T.; Luan, N. D. T.; Huy, T. T. Application of Ultrasound for Nanomaterials Synthesis. *Int. J. Nanotechnol.* **2011,** *8* (3-5), 291-299.

77. Caneba, G.; Dutta, C.; Agrawal, V.; Rao, M. Novel Ultrasonic Dispersion of Carbon Nanotubes. *J. Miner. Mater. Charact. Eng.* **2010,** *9* (03), 165.

78. Capelo-Martínez, J. L. *Ultrasound in Chemistry: Analytical Applications*; Wiley: 2008.

79. Lidström, P.; Tierney, J.; Wathey, B.; Westman, J. Microwave Assisted Organic Synthesis—a Review. *Tetrahedron* **2001,** *57* (45), 9225-9283.

80. Zhang, X.; Liu, Z. Recent Advances in Microwave Initiated Synthesis of Nanocarbon Materials. *Nanoscale* **2012,** *4* (3), 707-714.

81. Baba, K.; Kasai, H.; Okada, S.; Oikawa, H.; Nakanishi, H. Fabrication of Organic Nanocrystals Using Microwave Irradiation and Their Optical Properties. *Opt. Mater.* **2003,** *21* (1), 591-594.

82. Kappe, C. O.; Dallinger, D. The Impact of Microwave Synthesis on Drug Discovery. *Nat. Rev. Drug Discovery* **2006,** *5* (1), 51-63.

83. Li, S.; Purdy, W. C. Cyclodextrins and Their Applications in Analytical Chemistry. *Chem. Rev.* **1992,** *92* (6), 1457-1470.

84. Yong, C.; Washington, C.; Smith, W. Structural Behaviour of 2-Hydroxypropyl-β-Cyclodextrin in Water: Molecular Dynamics Simulation Studies. *Pharmaceutical Research* **2008,** *25* (5), 1092-1099.

85. Iohara, D.; Hirayama, F.; Higashi, K.; Yamamoto, K.; Uekama, K. Formation of Stable Hydrophilic C60 Nanoparticles by 2-Hydroxypropyl-Beta-Cyclodextrin. *Mol. Pharm.* **2011,** *8* (4), 1276-1284.

86. Devi, L. B.; Mandal, A. B. Self-Assembly of Ag Nanoparticles Using Hydroxypropyl Cyclodextrin: Synthesis, Characterisation and Application for the Catalytic Reduction of P-Nitrophenol. *RSC Adv.* **2013,** *3* (15), 5238-5253.

87. Xu, J.-Z.; Xu, S.; Geng, J.; Li, G.-X.; Zhu, J.-J. The Fabrication of Hollow Spherical Copper Sulfide Nanoparticle Assemblies with 2-Hydroxypropyl-β-Cyclodextrin as a Template Under Sonication. *Ultrason. Sonochem.* **2006,** *13* (5), 451-454.

88. Liveri, V. T. *Reversed Micelles as Nanometer-Size Solvent Media*; Marcel Dekker: New York: 2002.

89. Trivedi, R.; Kompella, U. B. Nanomicellar Formulations for Sustained Drug Delivery: Strategies and Underlying Principles. *Nanomedicine* **2010,** *5* (3), 485-505.

90. Pileni, M.-P. The Role of Soft Colloidal Templates in Controlling the Size and Shape of Inorganic Nanocrystals. *Nat. Mater.* **2003,** *2* (3), 145-150.

91. Wu, P.; Yan, X.-P. Doped Quantum Dots for Chemo/Biosensing and Bioimaging. *Chem. Soc. Rev.* **2013,** *42* (12), 5489-5521.

92. Yao, H.; Ashiba, K. Efficient Excitation-Energy Transfer in Ion-Based Organic Nanoparticles with Versatile Tunability of the Fluorescence Colours. *Chem. Phys. Chem.* **2012,** *13* (11), 2703-2710.

93. Peng, A. D.; Xiao, D. B.; Ma, Y.; Yang, W. S.; Yao, J. N. Tunable Emission from Doped 1,3,5-Triphenyl-2-Pyrazoline Organic Nanoparticles. *Adv. Mat.* **2005,** *17* (17), 2070-2073.

94. Zhao, Y. S.; Fu, H. B.; Hu, F. Q.; Peng, A. D.; Yang, W. S.; Yao, J. N. Tunable Emission from Binary Organic One-Dimensional Nanomaterials: An Alternative Approach to White-Light Emission. *Adv. Mat.* **2008,** *20* (1), 79-83.

95. Wang, F.; Liu, X. G. Recent Advances in the Chemistry of Lanthanide-Doped Upconversion Nanocrystals. *Chem. Soc. Rev.* **2009,** *38* (4), 976-989.

96. He, Y.; Wang, H.-F.; Yan, X.-P. Exploring Mn-Doped ZnS Quantum Dots for the Room-Temperature Phosphorescence Detection of Enoxacin in Biological Fluids. *Anal. Chem.* **2008,** *80* (10), 3832-3837.

97. Santra, S.; Yang, H.; Holloway, P. H.; Stanley, J. T.; Mericle, R. A. Synthesis of Water-Dispersible Fluorescent, Radio-Opaque, and Paramagnetic CdS:Mn/ZnS Quantum Dots: A Multifunctional Probe for Bioimaging. *J. Am. Chem. Soc.* **2005,** *127* (6), 1656-1657.

98. Kailasa, S. K.; Wu, H.-F. Interference Free Detection for Small Molecules: Probing the Mn^{2+}-Doped Effect and Cysteine Capped Effect on the ZnS Nanoparticles for Coccidiostats and Peptide Analysis in SALDI-TOF MS. *Analyst* **2010,** *135* (5), 1115-1123.

99. Pan, Z. Q.; Fan, H.; Shi, C. G.; Bao, N.; Yu, C. M.; Gu, H. Y. Direct Electrochemistry of Hemoglobin Immobilized on CdS:Mn Nanoparticles. *Microchim. Acta* **2011,** *173* (3-4), 277-283.

100. Jang, J.; Oh, J. H. Facile Fabrication of Photochromic Dye-Conducting Polymer Core-Shell Nanomaterials and Their Photoluminescence. *Adv. Mat.* **2003,** *15* (12), 977-980.

101. Williams, D.; Carter, C. B. The Transmission Electron Microscope. In *Transmission Electron Microscopy*; Springer US: 2009; pp 3-22.

102. Alloyeau, D.; Mottet, C.; Ricolleau, C. *Nanoalloys: Synthesis, Structure and Properties*; Springer: 2012.

103. Sigle, W., Analytical Transmission Electron Microscopy. In *Annual Review of Materials Research*; 2005; Vol. 35, pp 239-314.

104. Wang, Z. L. Transmission Electron Microscopy of Shape-Controlled Nanocrystals and Their Assemblies. *J. Phys. Chem. B* **2000,** *104* (6), 1153-1175.

105. Sapsford, K. E.; Tyner, K. M.; Dair, B. J.; Deschamps, J. R.; Medintz, I. L. Analyzing Nanomaterial Bioconjugates: A Review of Current and Emerging Purification and Characterization Techniques. *Anal. Chem.* **2011,** *83* (12), 4453-4488.

106. Chu, B. Dynamic Light Scattering. In *Soft Matter Characterization;* Borsali, R.; Pecora, R., Eds.; Springer: **2008**, pp 335-372.

107. Lin, P. C.; Lin, S.; Wang, P. C.; Sridhar, R. Techniques for Physicochemical Characterization of Nanomaterials. *Biotechnol. Adv.* **2014,** *32* (4), 711-726.

108. Brar, S. K.; Verma, M. Measurement of Nanoparticles by Light-Scattering Techniques. *TrAC, Trends Anal. Chem.* **2011,** *30* (1), 4-17.

109. Doane, T. L.; Chuang, C. H.; Hill, R. J.; Burda, C. Nanoparticle Zeta-Potentials. *Acc. Chem. Res.* **2012,** *45* (3), 317-326.

110. Wang, N.; Hsu, C.; Zhu, L.; Tseng, S.; Hsu, J.-P. Influence of Metal Oxide Nanoparticles Concentration on Their Zeta Potential. *J. Colloid Interface Sci.* **2013,** *407* (0), 22-28.

111. Jiang, J. K.; Oberdorster, G.; Biswas, P. Characterization of Size, Surface Charge, and Agglomeration State of Nanoparticle Dispersions for Toxicological Studies. *J. Nanopart. Res.* **2009,** *11* (1), 77-89.

112. Morrison, I. D.; Ross, S. *Colloidal Dispersions: Suspensions, Emulsions, and Foams*. Wiley: 2002.

113. Hunter, R. J. Chapter 3 - the Calculation of Zeta Potential. In *Zeta Potential in Colloid Science*; Hunter, R. J., Ed. Academic Press: 1981; pp 59-124.

114. Li, D.; Muller, M. B.; Gilje, S.; Kaner, R. B.; Wallace, G. G, Processable Aqueous Dispersions of Graphene Nanosheets. *Nat. Nanotechnol.* **2008,** *3* (2), 101-105.

115. Everett, D. H.; Everett, D. Basic Principles of Colloid Science. Royal Society of Chemistry London: 1988; Vol. 144.

116. Ingle, J. D.; Crouch, S. R. Spectrochemical Analysis. *Englewood Cliffs, NJ* **1988**, pp 106.

117. Gao, Y. N.; Zhang, X. M.; Ma, C. Q.; Li, X. Y.; Jiang, J. Z. Morphology-Controlled Self-Assembled Nanostructures of 5,15-Di 4-(5-Acetylsulfanylpentyloxy)Phenyl Porphyrin Derivatives. Effect of Metal-Ligand Coordination Bonding on Tuning the Intermolecular Interaction. *J. Am. Chem. Soc.* **2008,** *130* (50), 17044-17052.

118. Guilbault, G. G., *Practical Fluorescence: Theory,Methods and Techniques, by George G. Guilbault, with Contributions from R. F. Chen;* Marcel Dekker: 1973.

119. Rubinson, K. A.; Rubinson, J. F. *Contemporary Instrumental Analysis*. Prentice Hall: 2000.

120. Burgess, C.; Knowles, A.; Group, U. S. *Standards in Absorption Spectrometry*. Chapman and Hall: 1981.

121. Skoog, D. A.; Holler, F. J.; Crouch, S. R. *Principles of Instrumental Analysis*. Thomson Brooks/Cole: 2007.

122. Lakowicz, J. R. *Principles of Fluorescence Spectroscopy*. Springer: 2007.

123. Yan, M. *Molecularly Imprinted Materials: Science and Technology*. CRC press: 2004.

124. Spivak, D. A. Optimization, Evaluation, and Characterization of Molecularly Imprinted Polymers. *Adv. Drug Delivery Rev.* **2005,** *57* (12), 1779-1794.

125. Theodoridis, G.; Manesiotis, P., Selective Solid-Phase Extraction Sorbent for Caffeine Made by Molecular Imprinting. *J. Chromatogr. A* **2002,** *948* (1-2), 163-169.

126. Masque, N.; Marce, R. M.; Borrull, F. Molecularly Imprinted Polymers: New Tailor-Made Materials for Selective Solid-Phase Extraction. *TrAC, Trends Anal. Chem.* **2001,** *20* (9), 477-486.

127. Sellergren, B. Imprinted Chiral Stationary Phases in High-Performance Liquid Chromatography. *J. Chromatogr. A* **2001,** *906* (1-2), 227-252.

128. Subrahmanyam, S.; Piletsky, S. A.; Piletska, E. V.; Chen, B. N.; Karim, K.; Turner, A. P. F. 'Bite-and-Switch' Approach Using Computationally Designed Molecularly Imprinted Polymers for Sensing of Creatinine. *Biosens. Bioelectron.* **2001,** *16* (9-12), 631-637.

129. Poma, A.; Turner, A. P. F.; Piletsky, S. A. Advances in the Manufacture of MIP Nanoparticles. *Trends Biotechnol.* **2010,** *28* (12), 629-637.

130. Ciardelli, G.; Cioni, B.; Cristallini, C.; Barbani, N.; Silvestri, D.; Giusti, P. Acrylic Polymeric Nanospheres for the Release and Recognition of Molecules of Clinical Interest. *Biosens. Bioelectron.* **2004,** *20* (6), 1083-1090.

131. Reimhult, K.; Yoshimatsu, K.; Risveden, K.; Chen, S.; Ye, L.; Krozer, A. Characterization of Qcm Sensor Surfaces Coated with Molecularly Imprinted Nanoparticles. *Biosens. Bioelectron.* **2008,** *23* (12), 1908-1914.

132. Thejokalyani, N.; Dhoble, S. J. Novel Approaches for Energy Efficient Solid State Lighting by RGB Organic Light Emitting Diodes - a Review. *Renewable Sustainable Energy Rev.* **2014,** *32*, 448-467.

133. Zhang, Y. F.; Lee, J.; Forrest, S. R. Tenfold Increase in the Lifetime of Blue Phosphorescent Organic Light-Emitting Diodes. *Nat. Commun*. **2014,** *5:5008,*1-7.

134. Salah, N.; Habib, S. S.; Khan, Z. H.; Alharbi, N. D. Synthesis and Characterization of Pure and Tb/Cu Doped Alq(3) Nanostructures. *J. Lumin.* **2013,** *143*, 640-644.

135. Zhang, Q.; Wang, C. F.; Ling, L. T.; Chen, S. Fluorescent Nanomaterial-Derived White Light-Emitting Diodes: What's Going On. *J. Mater. Chem. C* **2014,** *2* (22), 4358-4373.

CHAPTER TWO
STRATEGIES FOR CONTROLLED SYNTHESIS OF NANOPARTICLES DERIVED FROM A GROUP OF UNIFORM MATERIALS BASED ON ORGANIC SALTS

2.1. Introduction

Materials at the nanoscale level frequently manifest new and interesting functionalities not shown in the corresponding bulk state. The dimensions and uniformity of such particles are often important to tailoring these functionalities, and in turn, allow expansion of the possible scope of applications. Thus, much of the current interest in nanoparticles stems from interest in the improved physical, chemical, and electronic properties of these colloidal systems.[1-2] In this regard, non-conventional superconductive and magnetic properties that are not present in the corresponding bulk state in combination with quantum size effects have garnered considerable attention.[2,3] Such properties are highly dependent on the dimensions and stacking arrangements (*e.g.*, assemblies of molecular aggregates) of these materials, which result in variable electronic states confined within the nanoparticles.[2, 4] The significance of this size and stacking dependence is embedded in the ability to improve physical properties such as the strength and rigidity of solids and to control the electrical/optical properties of nanoparticles.[2, 4] In particular, synthesis of nanoparticles with a desired size, narrow size distribution, and minimal aggregation is necessary for reliable performance in many applications.[5,6*]

---

[*] This chapter previously appeared as Suzana Hamdan, Jonathan C. Dumke, Bilal El-Zahab, Susmita Das, Dorin Boldor, Gary A. Baker, and Isiah M. Warner. Strategies for controlled synthesis of nanoparticles derived from a group of uniform materials based on organic salts, *Journal of Colloid and Interface Science*, **2015**, *446*, 163-169. It is reproduced by permission of Elsevier (Appendix F).

Over the past several years, organic-based nanoparticles have been the subject of much research as a result of the inherent physiological compatibility of these nanomaterials. In addition, the poor water solubility of these compounds favors the conversion of bulk into nanoscale materials within aqueous media.[3, 7] Many organic nanoparticles have also been shown to display size-dependent changes in electronic transitions that are often attributed to the appearance of inter- and intra-molecular overlapping structures at the nanoscale level.[8] Changes in spectroscopic properties resulting from size dependence of organic nanoparticles have been described as "structural confinement" effects.[8] Therefore, tuning the size of organic nanoparticles is of great interest to researchers because size-control of such materials can widen potential applications for photonic crystals and various light-emitting materials.[8,9]

In the recent realm of organic-based nanomaterials, nanoGUMBOS which are derived from a group of uniform materials based on organic salts (GUMBOS), emerge as solid-phase materials that possess many of the ionic liquids properties. By definition, GUMBOS are organic salts with a defined melting point range of 25-250 °C and, as is true for ionic liquids, have a broad tunability via manipulation of the cation or anion.[10-11] NanoGUMBOS thus combine the versatility of GUMBOS with the enhanced properties often obtained at the nanoscale, offering the flexible design of organic nanomaterials. Within the last few years, nanoGUMBOS which possess fluorescent,[12-14] magnetic,[15] luminescent,[16] pH-sensitive,[17] optoelectronic,[18] and anticancer[19] properties have been described. Previous studies from our laboratory have demonstrated the wide tunability in their spectral and physical properties, as well as the morphologies of nanoGUMBOS through variation in the associated counter ion.[14, 18, 20] Therefore, nanoGUMBOS have

found application in various fields including analytical chemistry, biomedicine, and electronics. So far, little work has been done to formulate reliable approaches for generation of nanoGUMBOS of controlled size, uniformity, and sphericity. However, improved synthetic control of nanoGUMBOS is essential for tailoring these materials for target applications. In 2008, the Warner research group published the first report on the synthesis of ionic liquid-derived nanoparticles using a melt-emulsion-quench method.[21] Nevertheless, the size-control of melt-emulsion-quench-derived nanoparticles was still considered a major challenge. In some of our more recent studies, a reprecipitation approach commonly employed in the synthesis of organic nanoparticles[22-23] was extended to the preparation of nanoGUMBOS in an aqueous medium.[12, 14, 18-19] Although this method can be used to produce nanoparticles with average sizes in the nanometer regime, it is difficult to deliver nanoparticles smaller than 20 nm without using additives such as surfactants or polymers.[24] Furthermore, there are often limitations associated with the selection of poor and good solvents suitable for organic compounds used for reprecipitation.[25] Historically, nanoGUMBOS synthesis with size uniformity of 10% standard deviation alongside size-control is not easily accomplished. Templated approaches, such as reverse microemulsion[15] and hydrogel-assisted synthesis,[13] have been successfully applied for the synthesis of nanoGUMBOS; however, both techniques present some limitations. Reverse microemulsions are suitable to achieve smaller nanoGUMBOS sizes, but frequently introduce unwanted agglomeration. In contrast, hydrogel-assisted synthesis routes can achieve low dispersity, yet cannot easily produce reduced-size nanoGUMBOS.

Here, we present our studies aimed at developing strategies for producing nanoGUMBOS with controlled sizes and narrow size distributions. The GUMBOS used in this study are derived from imidazolium ionic liquids, which have been widely used as task-specific ionic liquids (TSILs) for metal extractions,[26] for producing antimicrobial activity,[27] and as electrolytes for electrochemistry, gas separations, and lignocellulose processing.[28] This study focuses on efforts to produce refined nanoGUMBOS using i) sonochemical, ii) microwave-assisted, iii) cyclodextrin-assisted, and iv) surfactant-assisted procedures. Sonochemical synthesis in this study employs a non-templating approach in the presence of ultrasonication acoustic waves (20 and 55 kHz), as well as a templating approach which involves use of a soft template (*i.e.,* 2-hydroxypropyl-β-cyclodextrin (2HP-β-CD)). A microwave approach was employed with bath sonication in the absence of a template. In addition, we consider a surfactant-assisted approach that includes the use of Triton X-100 (TX-100) to form a normal micellar template. Overall, this study contrasts non-templated and templated techniques for the formation of uniform particles derived from GUMBOS, at the nanoscale level. Our goal of producing nanoGUMBOS with relatively low polydispersity was primarily achieved through the use of soft templating methods which yielded spherical and quasi-spherical nanoGUMBOS between 12 and 99 nm in mean size with relatively low polydispersity of 2-13 nm.

2.2. Experimental Section

2.2.1. Materials

1-Hexyl-3-methylimidazolium chloride [Hmim][Cl] (97%), 2-hydroxypropyl-β-cyclodextrin (MS = 0.6 and 0.8), 2-hydroxypropyl-α-cyclodextrin, TX-100 were purchased from Sigma Aldrich (St. Louis, MO) and used as received. Sodium tetraphenylborate [Na][TPB] (99.5%) was purchased from TCI America (Portland, OR) and used as

received. Ultrapure water (18.2 MΩ cm) was obtained from an Elga model PURELAB ultra water filtration system.

2.2.2. Melting Point and Thermogravimetric Measurements

Melting point and thermogravimetric measurements were both performed on bulk [Hmim][TPB]. For acquisition of melting point data, a DigiMelt MPA 160 from SRS (Sunnyvale, CA) was used and a Hi Res Modulated TGA 2950 thermogravimetric analyzer from TA instruments (New Castle, DE) was employed for measurement of thermal decomposition temperatures. In our experimental procedure, equal volumes of equimolar aqueous solutions of [Hmim][Cl] and [Na][TPB] reactants were mixed. This mixture was magnetically stirred for a few hours and then centrifuged at a speed of 3800 rpm (3180 rcf) for 30 minutes. The white precipitate [Hmim][TPB] was washed twice with water to remove the sodium chloride by-product and then lyophilized to eliminate water.

2.2.3. Transmission Electron Microscopy

Transmission electron microscopy (TEM) micrographs were obtained using a JEOL JEM-1011 TEM (München, Germany). A volume of 4 to 8 µL nanoGUMBOS sample was drop-casted onto ultrathin carbon-coated 400-mesh Ted Pella, Inc TEM grids (Redding, CA). Grids were washed with water to avoid any unwanted adsorption of by-products resulting from the anion-exchange reaction.

2.2.4. Light Scattering and Zeta Potential Measurements

Dynamic light scattering (DLS) and zeta potential measurements were performed on a Malvern Zetasizer Nano ZS from Malvern Instruments Ltd (Worcestershire, England). DLS samples were prepared in a disposable sizing cuvet while zeta potential

measurements were performed in a disposable capillary cell. The hydrodynamic diameter of nanoGUMBOS obtained from DLS was displayed using intensity values.

2.2.5. Non-Templated Synthesis Methods

2.2.5.1. Synthesis of NanoGUMBOS by Use of an Ultrasonication Method

A procedure reported by Ou *et al.* was adopted for the synthesis of nanoGUMBOS in the absence of a template.[7] This synthetic approach was performed using two different ultrasonication modes to control the homogeneity of the colloidal system: an ultrasonic bath (55 kHz) and a sonicator probe (ultrasonic processor) operated at 20 kHz. An aqueous [Na][TPB] solution was added to an aqueous solution of [Hmim][Cl] at the same concentration while keeping the total volume constant at 10 mL under ultrasonication. Three different concentrations of reactants were separately tested: 0.25, 0.1, and 0.05 mM of [Hmim][Cl] and [Na][TPB]. This experiment was performed using two different volumetric ratios of the cation to anion of 1:1 (*i.e.*, 5 mL of each reactant) and 1:6 (*i.e.,* 1.43 mL of [Hmim][Cl] to 8.57 mL of [Na][TPB]). The ultrasonic processor, Model VC-750 from SONICS (Newton, CT) was set to provide continuous ultrasonication for 10 min at 25% amplitude in a 20 mL borosilicate reaction vial.

2.2.5.2. Microwave-Assisted Synthesis of NanoGUMBOS

In this approach, equal volumes of [Hmim][Cl] and [Na][TPB] (0.05 mM) were first allowed to react for 10 min using the ultrasonication bath. The resultant sample was transferred to a borosilicate glass vial in an Anton Paar Monowave 300 instrument (Graz, Austria) for microwave irradiation heating. Magnetic stirring at 600 rpm was conducted during temperature-controlled microwave heating. The temperature of the reaction mixture was monitored by use of a ruby thermometer for internal temperature

measurement and an IR sensor for external temperature measurement of reaction vials. The mixture was heated using microwave irradiation to a specified temperature (120, 150, 180 or 200°C) followed by cooling down to 30 °C. The total cycle time was fixed at 10-11 min, including heating for 5 min. For a better understanding of the materials produced under microwave reaction conditions, dielectric properties were measured using an open-ended coaxial probe method with a slim-form probe[29] and a properly calibrated vector network analyzer (ENA 5071C, Agilent Tech, Santa Clara, CA).

2.2.6. Templated Synthesis Method

2.2.6.1. Synthesis of NanoGUMBOS using Ultrasonication and 2HP-β-CD

In this templated procedure, modified from Xu *et al*.[30], formation of nanoGUMBOS occurs during ultrasonication in the presence of the template 2HP-β-CD. An aqueous solution of 5 mL [Na][TPB] was mixed with a 5 mL volume of aqueous [Hmim][Cl] containing 0.8 mg of 2HP-β–CD. The ultrasonication probe was operated at 25% amplitude for a period of 10 min. In this approach, two different concentrations of the aqueous solutions of [Hmim][Cl] and [Na][TPB] were tested: 4 and 0.25 mM. Heat generated during sonication was duly dissipated by jacketing the vial with ice-water during the ultrasonication treatment.

2.2.6.2. Synthesis of NanoGUMBOS Using a Normal Micellar Template

The cation and anion precursors (100 µL of 12.5 mM aqueous solutions of [Hmim][Cl] and [Na][TPB]) were added separately to 5 mL aqueous surfactant solutions of 20 mM TX-100. These solutions were magnetically stirred for 30 min in order to allow the micellar system to stabilize. Ultimately, the aqueous surfactant solutions containing the precursors were mixed for 24 h under continuous magnetic stirring (380 rpm). In this

case, the self-assembled surfactant TX-100 phase was used to control the formation of the nanoGUMBOS in the aqueous system through creation of a single phase of normal micelles.

2.3. Results and Discussion

2.3.1. Metathesis Reaction

The GUMBOS studied in this work was composed of 1-hexyl-3-methylimidazolium tetraphenylborate [Hmim][TPB] prepared by metathesis reaction between the initial reactants 1-hexyl-3-methylimidazolium chloride, [Hmim][Cl], and sodium tetraphenylborate, [Na][TPB], in an aqueous medium (refer to Scheme 2.1). [Hmim][Cl], a water-miscible ionic liquid, was chosen in particular because of the length of its alkyl chain which imparts hydrophobicity to the final product. The anion of the room temperature ionic liquid [Hmim][Cl] was exchanged with tetraphenylborate anion (TPB) to form a hydrophobic solid phase compound. In this case, the formation of the nanoparticles occurs simultaneously with the exchange reaction in the medium.

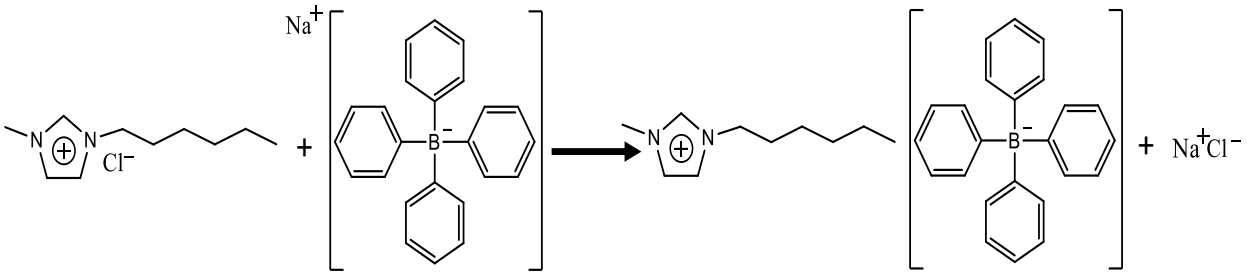

Scheme 2.1. Anion-exchange reaction between [Hmim][Cl] and [Na][TPB].

The product of the reaction is insoluble in water, thus favoring the formation of nanoparticles in aqueous medium under these experimental conditions. The melting point of the product [Hmim][TPB] was determined to be 111.2 ± 0.4 °C (clear point) which classifies this product as a GUMBOS, but not a frozen ionic liquid. The decomposition

temperature of this compound was 308 °C as determined by use of thermogravimetric analysis (TGA) (Figure 2.1).

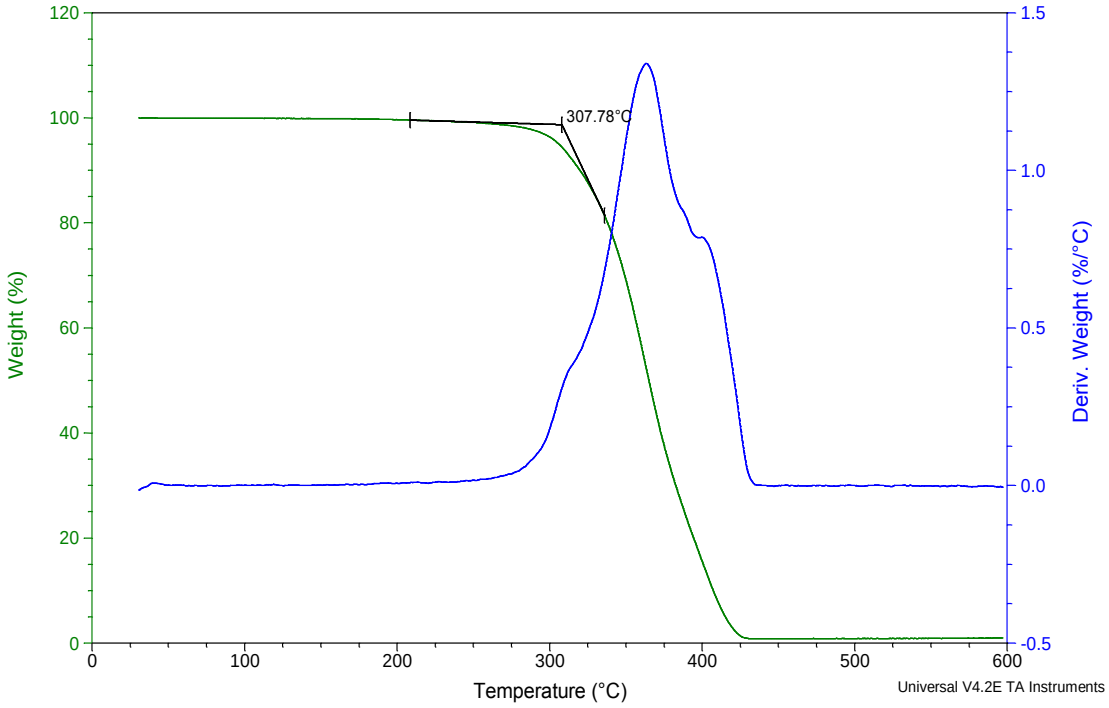

Figure 2.1. Weight percent loss of [Hmim][TPB] in function of temperature and its first derivative variation. The measurements show a thermal decomposition temperature of 307.8 °C.

2.3.2. Size Studies

2.3.2.1. Template-Free Sonochemical Routes: Bath vs. Probe

The use of an ultrasonication bath resulted in the formation of zero-dimensional particles with an average size of 785 ± 199 nm as compared to the use of an ultrasonication probe that delivered a fibrous network of aggregated particles (Figure 2.2b). In the absence of a template, the ultrasonication technique produced mesoparticles (or mesoGUMBOS) with high polydispersity. The particle formation is attributed to the presence of free-energy driven molecular self-assemblies in the medium.[31]

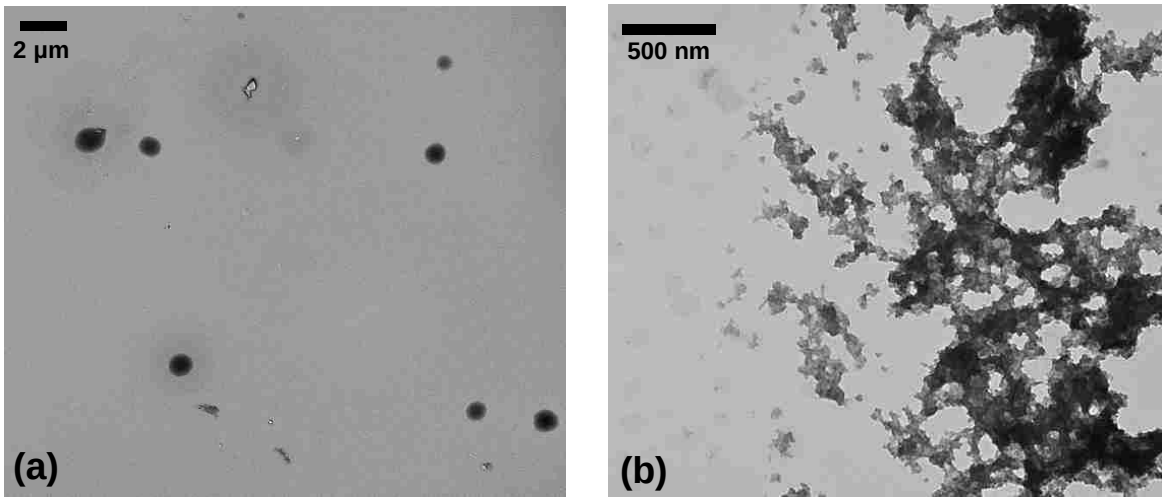

Figure 2.2. Transmission electron micrographs of mesoGUMBOS obtained at 0.25 mM concentration of reactants for 1:1 volume ratio of cation to anion when using (a) a low-power ultrasonication bath (scale bar: 2 µm) and (b) an ultrasonication probe (scale bar: 500 nm).

Self-assemblies are generally based on non-covalent interactions (van der Waals, electrostatic, and hydrophobic forces, π-π interactions, etc.) that spontaneously direct the formation of materials toward formation of spherical aggregates without external intervention; therefore, in this case, the defined structure of these nanoGUMBOS is consistent with formation by a self-assembly mechanism.[31-32] NanoGUMBOS synthesis using an ultrasonication probe was investigated in order to study the variation of particles size with the type and speed of acoustic agitation. The type of stirring employed during nucleation and growth phases has been associated with the level of aggregation in the colloidal system.[33] In terms of synthesizing nanoGUMBOS at high ultrasonication power, the nucleation and growth kinetics of the system changes the interactions between GUMBOS and increases the level of aggregation (Figure 2.1b). Ultrasonication has been widely used for the synthesis of nanoparticles because ultrasonic irradiation creates high temperature and pressure around a collapsing vapor bubble or acoustic cavitation known as a “hot spot” where intermolecular collisions are promoted.[34-37]

Variation in the nanoGUMBOS hydrodynamic diameter was also achieved using non-templating syntheses in the presence of ultrasonication (bath or probe) at different reactant concentrations and volume ratios of cation [$Hmim^+$] and anion [TPB^-] (Table 2.1). Both sonochemical methods using a bath and probe ultrasonicator resulted in a decrease in hydrodynamic diameter with a decrease in reactant concentration for a 1:1 ratio. The

Table 2.1. Effects of reactant concentration and volume ratio on hydrodynamic diameter from ultrasonication bath and probe methods were studied by use of DLS measurements. R symbolizes the ratio of anion to cation.

	Concentration (mM)		
Sonochemical syntheses	**0.25**	**0.1**	**0.05**
Hydrodynamic diameter using sonication bath (nm)	725 ± 40 (R=1) 428 ± 66 (R=6)	622 ± 13 (R=1) 427 ± 27 (R=6)	511 ± 4 (R=1) 240 ± 21 (R=6)
Hydrodynamic diameter using sonication probe (nm)	416 ± 85 (R=1) 429 ± 28 (R=6)	371 ± 68 (R=1) 255 ± 63 (R=6)	269 ± 61 (R=1) 376 ± 58 (R=6)

relationship between concentration and size of particles originates from dependence of the latter on the growth kinetics of the process. The rate of diffusion, k_D, is related to size of zero-dimensional nanoGUMBOS according to equations 1 and 2:

$$r^2 = k_D t + r_0^2 \quad (1)$$

$$k_D = 2D(C - C_s)V_m \quad (2)$$

where r is the radius of the nuclei, C is the bulk concentration, C_s is the concentration on the surface of the solid particles, V_m is the molar volume of the nuclei, and D is the

diffusion coefficient. These equations are used to explain how nanoGUMBOS size increases with the availability of growth species to adsorb onto the surface of the nuclei.[38] Examination of DLS measurements shows that smaller sizes of nanoGUMBOS were obtained for the same concentration of reactants using the ultrasonication probe, as compared to use of an ultrasonication bath. The decrease in size of particles can be attributed to an increase in nucleation rate caused by high intensity ultrasonication probe that creates more cavitation sites in the medium. Higher nucleation rates for a given concentration of solute results in a larger number of smaller nuclei.[38] Furthermore, the change in the cation:anion volume ratio from 1:1 to 1:6 produced an approximately 200 to 100 nm decrease in hydrodynamic diameter using bath ultrasonication. It is apparent that the presence of excess anion leads to electrostatically-stable nanoparticles and thus a decrease in particle size and aggregation level.[7] However, when using the ultrasonication probe, the excess anion had a negligible effect on the size of nanoparticles because of the high level of aggregation.

Another use of ultrasonication was demonstrated for the precipitation of nanoGUMBOS from a poor-good solvents mixture; the detailed procedure is explained in Figure A1, Appendix A.

2.3.2.2. Template-Free Sonication Bath Plus Microwave Assistance

Zero-dimensional nanoGUMBOS with an average diameter of 133 nm (Figure 2.3) were formed using an ultrasonication bath, followed by microwave irradiation to a temperature higher than the melting point (> 111 °C) and lower than the decomposition temperature (308 °C). The sample was subsequently cooled to 30 °C for reformation of nanoGUMBOS. The decrease in size of particles (Figure 2.4), observed after

microwave treatment, is attributed to promotion of collisions between species and new assembly states of molecules.[39-40] Polydispersity of the system is also improved as compared to nanoGUMBOS before microwave irradiation because of the volumetric absorption capacity of the medium when exposed to microwave radiation. Thus, heating is more homogeneous and efficient than via regular conduction and convection heating, subsequently affecting the rate of nanoparticle formation.[41-43]

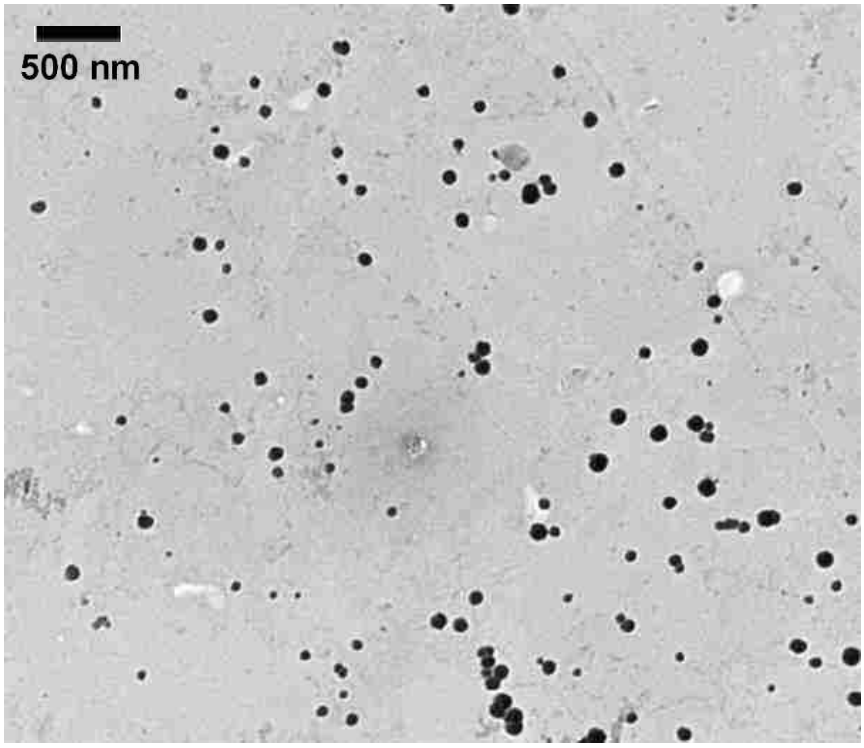

Figure 2.3. Transmission electron micrograph of nanoGUMBOS (133 ± 16 nm) obtained at 0.05 mM concentration of reactants when using the ultrasonication bath followed by microwave heating at 120 °C (scale bar: 500 nm).

Studies of the dielectric properties of water and nanoGUMBOS suspension indicated quite different dissipation paths for microwave energy in the medium at low (30 °C) and high temperatures (95°C). The loss tangent (*tan δ*) which is expressed as the ratio of dielectric loss factor over dielectric constant, reflects the ability of a medium to

convert microwave energy into heat.[44] This value is reported for the water medium and the nanoGUMBOS suspension in water at different temperatures in Figure 2.5. At 30 °C,

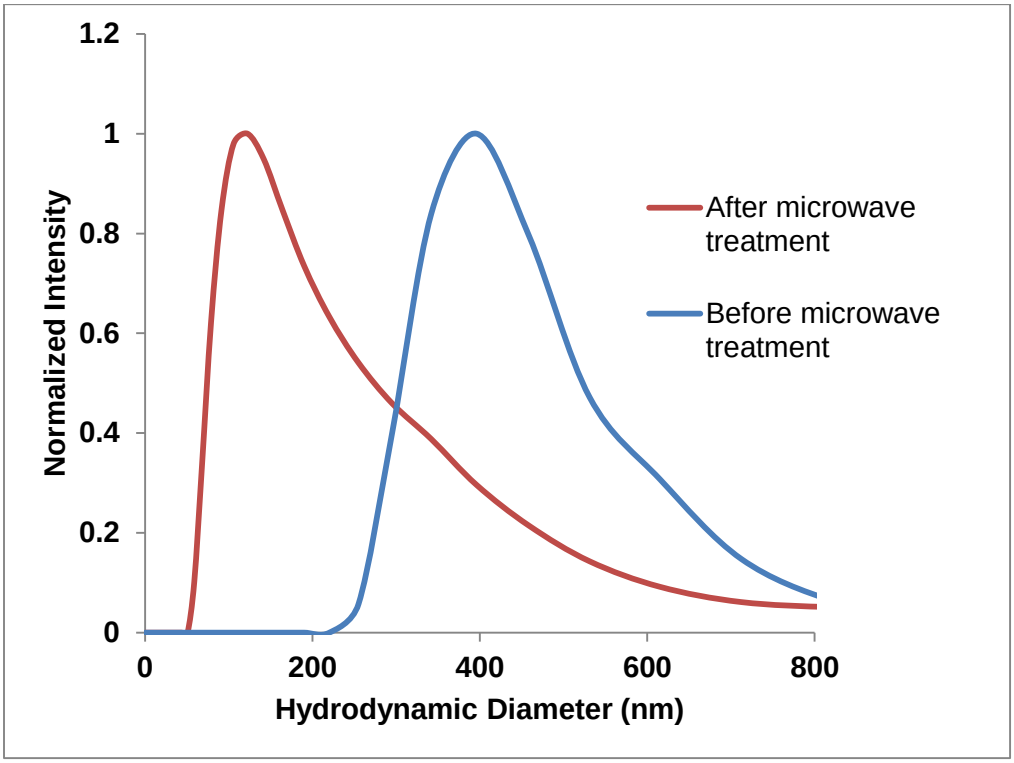

Figure 2.4. Variation of hydrodynamic diameter of nanoGUMBOS synthesized using the ultrasonication bath before (average size: 437 nm) and after microwave treatment (average size: 199 nm)

tan δ of water (0.11 ± 0.011) is much higher than that for the nanoGUMBOS suspension (0.083 ± 0.00019) due to the presence of a solvation shell around the nanoparticles in the latter case. The binding of water molecules to the nanoparticles causes a decrease in the polarizability of water in the medium and a decrease in the mobility of the polar molecules and ionic species. However, the effect of heating due to the absorption of microwave energy by the nanoGUMBOS suspension is enhanced as compared to pure water at high temperature (95 °C). At this temperature, nanoGUMBOS begin to partially melt and

dissociate into free ions that dissipate microwave energy via ionic oscillations. The loss tangent of a nanoGUMBOS suspension in water (0.052 ± 0.0013) is higher than water (0.030 ± 0.0021) in this case. It is expected that similar (or even more divergent) behavior of nanoGUMBOS suspension regarding absorption of microwaves will be observed at temperatures above 95 °C. This phenomenon showcases the efficiency of the process of microwave heating and its effect on the formation of reduced-size nanoGUMBOS. This method is similar in concept to a microwave-assisted reprecipitation method that has been previously introduced by Baba *et al*. for synthesis of organic nanoparticles.[39]

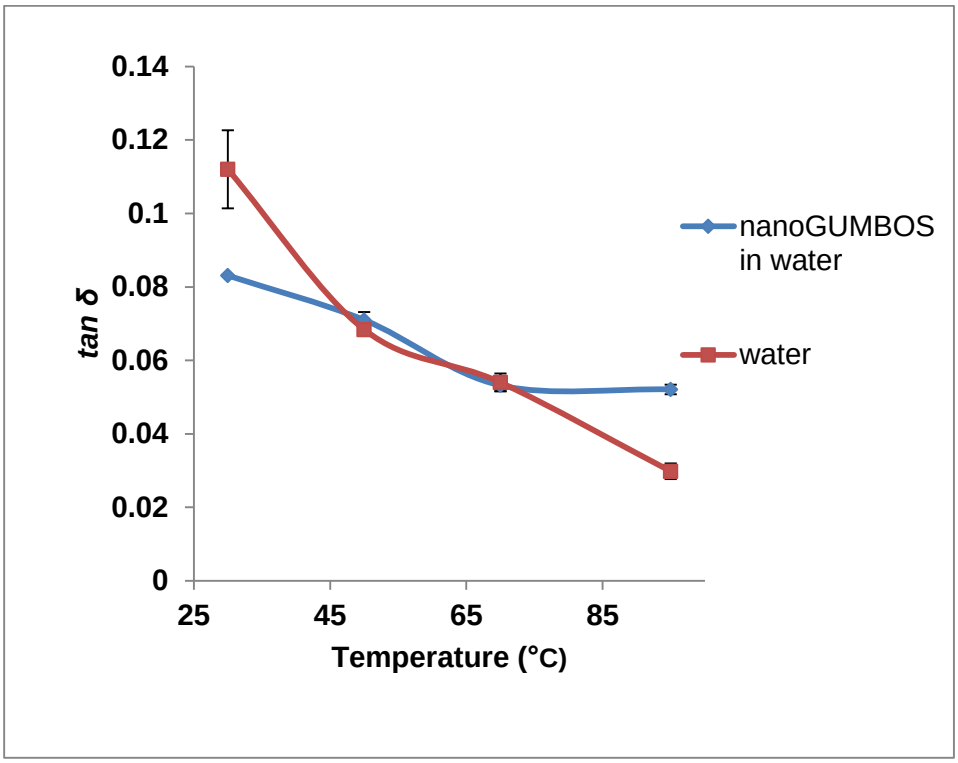

Figure 2.5. Variation of *tan δ* values of water medium and nanoGUMBOS suspended in water at various temperatures (values obtained at 2.45 GHz).

The materials irradiated by use of microwave energy at various temperatures resulted in similar nanoGUMBOS hydrodynamic diameter (Table 2.2). The negligible

effect of the temperature increase on the hydrodynamic diameter is due to all temperatures being above the GUMBOS melting point (111 °C).

Table 2.2. Increase in temperature during the microwave-assisted synthesis results in an overall unchanged hydrodynamic diameter (measured by use of DLS).

Temperature (°C)	**Size (nm)**
120	227 ± 59
150	225 ± 45
180	207 ± 15
200	214 ± 37

2.3.2.3. Ultrasonication Using a Modified Cyclodextrin

Production of NanoGUMBOS was evaluated by employing 2HP-β-CD as a template in concert with probe ultrasonication at two different reactant concentrations (Figure 2.6). TEM micrographs revealed that these nanoGUMBOS were primarily spherical in shape. The average diameter of these nanoGUMBOS was 19 ± 2 nm and 12 ± 2 nm using 4 mM as well as 0.25 mM of reactant concentration, respectively. Thus, 2HP-β-CD template aided in control of the formation of nanoGUMBOS by significantly decreasing the size and aggregation of the nanoGUMBOS observed for ultrasonication in the absence of a template.

In order to clarify the templating mechanism of 2HP-β-CD and confirm the role of the hydroxyl groups in the procedure for formation of nanoparticles, we used a template with a different molar substitution (MS) of hydroxypropyl groups (*i.e.,* MS = 0.6 and 0.8).

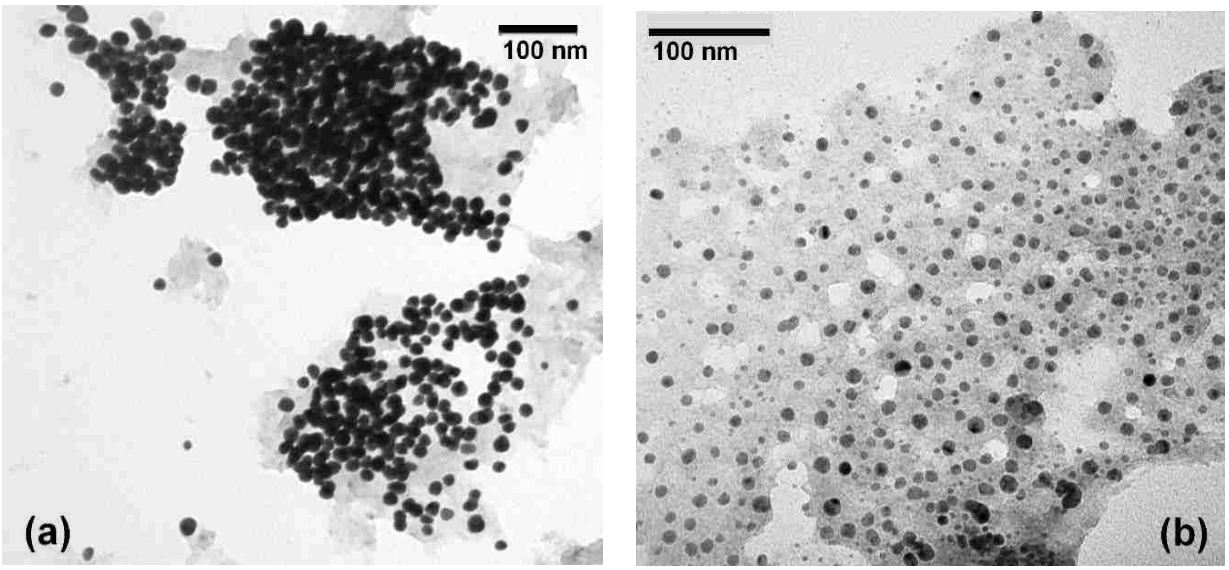

Figure 2.6. Transmission electron micrographs of nanoGUMBOS (scale bars: 100 nm) obtained using 2HP-β-CD (MS = 0.6) as template at (a) 4 mM concentration of reactants and (b) 0.25 mM concentration of reactants.

The results were an increase in the size of nanoparticles from 19 ± 2 nm to an average of 73 ± 9 nm when the molar substitution of hydroxypropyl groups on 2HP-β-CD was increased (Figure 2.7). It is hypothesized that the 2HP-β-CD template molecularly cross-links in the presence of ultrasonication via hydrogen bonding between hydroxyl groups.[30] This molecular cross-linking produces spherical assemblies forming complexes with [$Hmim^+$]. The [TPB^-] anion then ionically binds with [$Hmim^+$] to form the [Hmim][TPB] compound. In the present study, it is also observed that hydroxyl groups of the template 2HP-β-CD, with the aid of probe ultrasonicator, lead to rapid nucleation of nanoGUMBOS and subsequent formation of relatively uniform nanoGUMBOS. A similar observation has been validated by Li *et al*. wherein the formation of beta-cyclodextrin (β-CD)

self-assemblies in water has been explained and the application of β-CD as a template for TiO_2 nanoparticles has been demonstrated.[45]

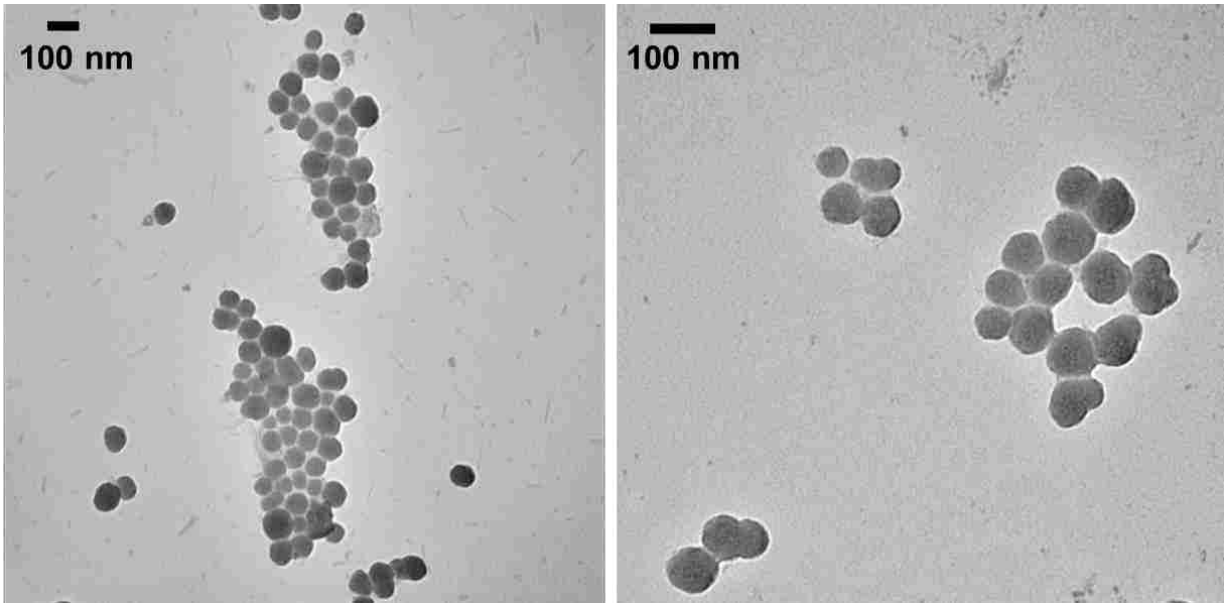

Figure 2.7. Transmission electron micrographs of nanoGUMBOS obtained using 2HP-β-CD (MS = 0.8) as a template at 4 mM concentration of reactants (scale bar: 100 nm).

A similar experiment regarding the templated synthesis of nanoGUMBOS was conducted with 2HP-α-CD; the TEM micrographs of these nanoGUMBOS are reported in Figure A2, Appendix A.

2.3.2.4. TX-100 Micellar Template

The neutral surfactant TX-100 was chosen for studying the effect of another soft template on the size of the nanoGUMBOS and avoidance of ionic interferences with [Hmim][TPB]. The use of a TX-100 micellar template resulted in zero-dimensional nanoGUMBOS with an average diameter of 87 ± 13 nm (Figure 2.8a). In this synthesis, organized microemulsion systems formed by TX-100 normal micelles can be used as reaction media for formation of nanoparticles where the surfactant functions as a capping

agent to control the size and dispersity of nanoparticles at the nanoscale level.[46-47] One advantage of using microemulsion synthesis is the possibility of tailoring nanoparticle size by making simple changes in the synthetic conditions.[47] However, decreasing reactant concentration from 12.5 to 5 mM yielded very similar nanoGUMBOS sizes (Figure 2.8b). This observation suggests a templating effect of the TX-100, which allows formation of nanoGUMBOS within the hydrophobic pockets of the normal micelles.

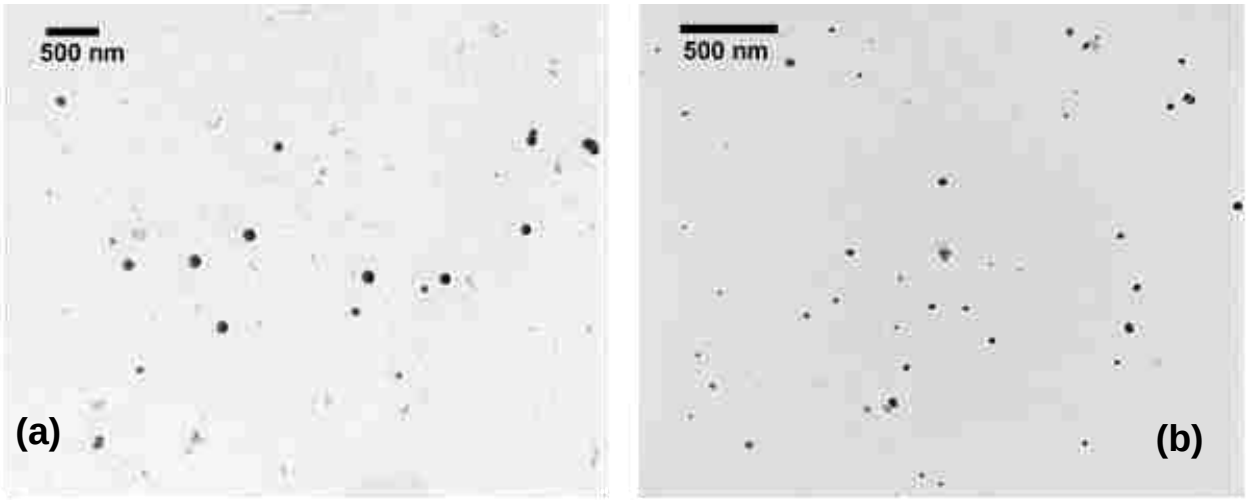

Figure 2.8. Transmission electron micrographs of monodisperse nanoGUMBOS obtained using a TX-100 micellar template method at a concentration of (a) 12.5 mM reactants (87 ± 13 nm) and (b) 5 mM reactants (99 ± 10 nm) (scale bar: 500 nm).

2.3.3. Stability Studies

To further investigate the relationship between size and surface charge of our nanoparticles, the zeta potential was measured at different concentrations for the template-free sonochemical route (Table 2.3). In this study, the net surface charge of the nanoGUMBOS interfacial double layer and, subsequently, the stability of the colloidal systems was determined. For a 1:1 cation:anion ratio, our nanoGUMBOS were negatively charged, implying that the [TPB] anions preferably adsorb onto the particle surface. A high negative zeta potential indicates a negligible tendency to electrostatically

agglomerate at the concentrations studied. Previous studies have suggested that excess anion increases the magnitude of the negative zeta potential of the particles, resulting in increased electrostatic repulsion and thereby suppression of nanoparticle growth.[7] However, in this study, the zeta potential values differ slightly between cation:anion molar ratios of 1:1 and 1:6. Nevertheless, excess anion did correlate with a decreased nanoGUMBOS size for ultrasonication bath synthesis, indicating that excess anions might

Table 2.3. The decrease in concentration of reactants and cation:anion molar ratio resulted in lower zeta potential values (pH between 7.5 and 8.7).

NanoGUMBOS syntheses	0.25 mM	0.1 mM	0.05 mM
Ultrasonication Bath	–70.4 ± 1.1 mV (R=1) –64.3 ± 1.4 mV (R=6)	–66.4 ± 0.7 mV (R=1) –66.1 ± 3.6 mV (R=6)	–66.2 ± 1.4 mV (R=1) –53.1 ± 5.8 mV (R=6)
Ultrasonication Probe	–77.7 ± 2.9 mV (R=1) –75.8 ± 1.7 mV (R=6)	–72.6 ± 2.1 mV (R=1) –71.9 ± 4.3 mV (R=6)	–54.6 ± 1.7 mV (R=1) –58.8 ± 1.2 mV (R=6)
Ultrasonication Probe with 2HP-β-CD (MS=0.6)	–84.1 ± 3.5 mV (R=1)	–67.3 ± 3.7 mV (R=1)	–62.8 ± 1.5 mV (R=1)

indeed be responsible for suppressing the growth of nanoGUMBOS. This observation infers that an intentional excess of anions may increase the surface charge density, resulting in formation of smaller nanoGUMBOS.[7] The 2HP-β-CD template method resulted in similar zeta potential values as compared to template-free ultrasonication methods. Zeta potential values were more negative (especially at high concentration)

than values obtained from the assembled 2HP-β-CD alone (–57.3 ± 2 mV; pH=8.4) suggesting that the position of the nuclei is more likely on the surface of the template rather than inside the cyclodextrin cavity. However, the surfactant-assisted synthesis method resulted in a lower magnitude zeta potential of –19.3 ± 1.7 mV (pH between 5.9 and 7.7) than other nanoGUMBOS syntheses. This lower negative zeta potential likely stems from the surface of nanoGUMBOS being partially covered by uncharged micelles (possibly, hemi-micelles) of TX-100, shielding electrostatic interactions.

2.4. Conclusions

This study demonstrates strategies for the size, uniformity, and sphericity-control of nanoGUMBOS, which have been deemed to be a new class of nanomaterials highly beneficial for analytical, biological, and technological applications. Herein, facile and reliable solution-based procedures were explored to achieve size tunability of nanoGUMBOS. Throughout this investigation, different sizes and dispersities of the meso/nanoGUMBOS were produced through variations in experimental factors such as concentration of reactants, presence of template, and modes of formation. Large-size and polydisperse mesoGUMBOS were obtained using a non-templated ultrasonication method at high concentration of reactants. In that study, the size was controlled by changing the concentration of reactants, the intensity of ultrasonication, as well as the volume ratio of cation to anion. When using the ultrasonication bath, presence of excess anion caused a decrease in the average particles size. The presence of hgh intensity ultrasonication resulted in a similar effect on average size, however, in this case, the nanomaterials presented a high level of aggregation. Microwave-assisted ultrasonication synthesis produced size-reduced nanoGUMBOS to an average diameter of 133 nm, as

compared to mesoGUMBOS synthesized by a single step ultrasonication. Moreover, the size of these nanoGUMBOS approached a value lower than 100 nm and uniformity was improved, when using the templates 2HP-β-CD and TX-100. As previously noted, this study introduces facile and efficient strategies for synthesis and size-tuning of nanoGUMBOS. This is an important task that allows control of the properties of these systems and expands the applications of these versatile organic nanomaterials.

2.5. References

1. Auffan, M.; Rose, J.; Bottero, J.; Lowry, G. V.; Jolivet, J.; Wiesner, M. R. Towards a Definition of Inorganic Nanoparticles from an Environmental, Health and Safety Perspective. *Nat. Nano* **2009,** *4* (10), 634-641.

2. Huczko, A. Template-Based Synthesis of Nanomaterials. *Appl. Phys. A: Mater.* **2000,** *70* (4), 365-376.

3. Horn, D.; Rieger, J. Organic Nanoparticles in the Aqueous Phase - Theory, Experiment, and Use. *Angew. Chem. Int. Ed.* **2001,** *40* (23), 4331-4361.

4. Ray, P. C. Size and Shape Dependent Second Order Nonlinear Optical Properties of Nanomaterials and Their Application in Biological and Chemical Sensing. *Chem. Rev.* **2010,** *110* (9), 5332-5365.

5. Zhang, Q.; Xie, J.; Yang, J.; Lee, J. Y. Monodisperse Icosahedral Ag, Au, and Pd Nanoparticles: Size Control Strategy and Superlattice Formation. *ACS Nano* **2009,** *3* (1), 139-148.

6. Pang, X.; Zhao, L.; Han, W.; Xin, X.; Lin, Z. A General and Robust Strategy for the Synthesis of Nearly Monodisperse Colloidal Nanocrystals. *Nat. Nano* **2013,** *8* (6), 426-431.

7. Ou, Z.-m.; Yao, H.; Kimura, K. Organic Nanoparticles of Cyanine Dye in Aqueous Solution. *Bull. Chem. Soc. Jpn.* **2007,** *80* (2), 295-302.

8. Asahi, T.; Sugiyama, T.; Masuhara, H. Laser Fabrication and Spectroscopy of Organic Nanoparticles. *Acc. Chem. Res.* **2008,** *41* (12), 1790-1798.

9. Xiao, D.; Xi, L.; Yang, W.; Fu, H.; Shuai, Z.; Fang, Y.; Yao, J. Size-Tunable Emission from 1,3-Diphenyl-5-(2-Anthryl)-2-Pyrazoline Nanoparticles. *J. Am. Chem. Soc.* **2003,** *125* (22), 6740-6745.

10. Davis, J. H. Task-Specific Ionic Liquids. *Chem. Lett.* **2004,** *33* (9), 1072-1077.

11. Plechkova, N. V.; Seddon, K. R. Applications of Ionic Liquids in the Chemical Industry. *Chem. Soc. Rev.* **2008,** *37* (1), 123-150.

12. Bwambok, D. K.; El-Zahab, B.; Challa, S. K.; Li, M.; Chandler, L.; Baker, G. A.; Warner, I. M. Near-Infrared Fluorescent Nanogumbos for Biomedical Imaging. *ACS Nano* **2009,** *3* (12), 3854-3860.

13. Das, S.; de Rooy, S. L.; Jordan, A. N.; Chandler, L.; Negulescu, I. I.; El-Zahab, B.; Warner, I. M. Tunable Size and Spectral Properties of Fluorescent NanoGUMBOS in Modified Sodium Deoxycholate Hydrogels. *Langmuir* **2011,** *28* (1), 757-765.

14. Das, S.; Bwambok, D.; El-Zahab, B.; Monk, J.; de Rooy, S. L.; Challa, S.; Li, M.; Hung, F. R.; Baker, G. A.; Warner, I. M. Nontemplated Approach to Tuning the Spectral Properties of Cyanine-Based Fluorescent NanoGUMBOS. *Langmuir* **2010,** *26* (15), 12867-12876.

15. Tesfai, A.; El-Zahab, B.; Kelley, A. T.; Li, M.; Garno, J. C.; Baker, G. A.; Warner, I. M. Magnetic and Nonmagnetic Nanoparticles from a Group of Uniform Materials Based on Organic Salts. *ACS Nano* **2009,** *3* (10), 3244-3250.

16. Dumke, J. C.; El-Zahab, B.; Challa, S.; Das, S.; Chandler, L.; Tolocka, M.; Hayes, D. J.; Warner, I. M. Lanthanide-Based Luminescent NanoGUMBOS. *Langmuir* **2010,** *26* (19), 15599-15603.

17. Das, S.; Paul, K.; de Rooy, S. L.; Hasan, F.; Warner, I. M. Ionic Liquid-Based Fluorescein Colorimetric pH Nanosensors. *RSC Adv.* **2013,** *3* (43), 21054-21061.

18. Jordan, A. N.; Das, S.; Siraj, N.; de Rooy, S. L.; Li, M.; El-Zahab, B.; Chandler, L.; Baker, G. A.; Warner, I. M. Anion-Controlled Morphologies and Spectral Features of Cyanine-Based Nanogumbos - an Improved Photosensitizer. *Nanoscale* **2012,** *4* (16), 5031-5038.

19. Magut, P. K.; Das, S.; Fernand, V. E.; Losso, J.; McDonough, K.; Naylor, B. M.; Aggarwal, S.; Warner, I. M. Tunable Cytotoxicity of Rhodamine 6G Via Anion Variations. *J. Am. Chem. Soc.* **2013,** *135* (42), 15873-15879.

20. de Rooy, S. L.; Das, S.; Li, M.; El-Zahab, B.; Jordan, A.; Lodes, R.; Weber, A.; Chandler, L.; Baker, G. A.; Warner, I. M. Ionically Self-Assembled, Multi-Luminophore One-Dimensional Micro-and Nanoscale Aggregates of Thiacarbocyanine GUMBOS. *J. Phys. Chem. C* **2012,** *116* (14), 8251-8260.

21. Tesfai, A.; El-Zahab, B.; Bwambok, D. K.; Baker, G. A.; Fakayode, S. O.; Lowry, M.; Warner, I. M. Controllable Formation of Ionic Liquid Micro-and Nanoparticles Via a Melt–Emulsion–Quench Approach. *Nano lett.* **2008,** *8* (3), 897-901.

22. Van Keuren, E.; Nishida, M. Synthesis of Nanocomposite Materials Using the Reprecipitation Method. *CMC - Comp. Mater. Cont.* **2009,** *14* (1), 61-77.

23. Kasai, H.; Nalwa, H. S.; Oikawa, H.; Okada, S.; Matsuda, H.; Minami, N.; Kakuta, A.; Ono, K.; Mukoh, A.; Nakanishi, H. A Novel Preparation Method of Organic Microcrystals. *JJAP Part 2-Letters* **1992,** *31* (8A), L1132-L1134.

24. Suk, J.; Bard, A. J. Electrochemistry and Electrogenerated Chemiluminescence of Organic Nanoparticles. *J. Solid State Electr.* **2011,** *15* (11-12), 2279-2291.

25. Kwon, E.; Oikawa, H.; Kasai, H.; Nakanishi, H. A Fabrication Method of Organic Nanocrystals Using Stabilizer-Free Emulsion. *Cryst. Growth Des.* **2007,** *7* (4), 600-602.

26. Wasserscheid, P.; Welton, T. *Ionic Liquids in Synthesis*; Wiley Online Library, 2008; Vol. 7.

27. Rogalsky, S.; Fatyeyeva, K.; Lyoshina, L.; Tarasyuk, O.; Bulko, O.; Lobok, S. Antimicrobial Properties and Thermal Stability of Polycarbonate Modified with 1-Alkyl-3-Methylimidazolium Tetrafluoroborate Ionic Liquids. *J. App. Polym. Sci.* **2014,** *131* (7), 40050-40057.

28. Tang, S.; Baker, G. A.; Zhao, H. Ether- and Alcohol-Functionalized Task-Specific Ionic Liquids: Attractive Properties and Applications. *Chem. Soc. Rev.* **2012,** *41* (10), 4030-4066.

29. Muley, P. D.; Boldor, D. Investigation of Microwave Dielectric Properties of Biodiesel Components. *Biores. Tech.* **2013,** *127* (0), 165-174.

30. Xu, J. Z.; Xu, S.; Geng, J.; Li, G. X.; Zhu, J. J. The Fabrication of Hollow Spherical Copper Sulfide Nanoparticle Assemblies with 2-Hydroxypropyl-Beta-Cyclodextrin as a Template under Sonication. *Ultrason. Sonochem.* **2006,** *13* (5), 451-454.

31. Jin, J.; Iyoda, T.; Cao, C.; Song, Y.; Jiang, L.; Li, T. J.; Zhu, D. B. Self-Assembly of Uniform Spherical Aggregates of Magnetic Nanoparticles through Π–Π Interactions. *Angew. Chem. Int. Ed.* **2001,** *113* (11), 2193-2196.

32. Grzelczak, M.; Vermant, J.; Furst, E. M.; Liz-Marzán, L. M. Directed Self-Assembly of Nanoparticles. *ACS Nano* **2010,** *4* (7), 3591-3605.

33. Li, D.; Kaner, R. B. Shape and Aggregation Control of Nanoparticles: Not Shaken, Not Stirred. *J. Am. Chem. Soc.* **2006,** *128* (3), 968-975.

34. Bang, J. H.; Suslick, K. S. Applications of Ultrasound to the Synthesis of Nanostructured Materials. *Adv. Mater.* **2010,** *22* (10), 1039-1059.

35. Esmaeih-Zare, M.; Salavati-Niasari, M.; Sobhani, A. Simple Sonochemical Synthesis and Characterization of Hgse Nanoparticles. *Ultrason. Sonochem.* **2012,** *19* (5), 1079-1086.

36. Suslick, K. S.; Price, G. J. Applications of Ultrasound to Materials Chemistry. *Ann. Rev. Mater. Sci.* **1999,** *29*, 295-326.

37. Kiel, S.; Grinberg, O.; Perkas, N.; Charmet, J.; Kepner, H.; Gedanken, A. Forming Nanoparticles of Water-Soluble Ionic Molecules and Embedding Them into Polymer and Glass Substrates. *Beilstein J. Nanotechnol.* **2012,** *3* (1), 267-276.

38. Cao, G. Zero-Dimensional Nanostructures: Nanoparticles. In *Nanostructures and Nanomaterials: Synthesis, Properties and Applications*, Imperial College Press: London, 2004; pp 51-59.

39. Baba, K.; Kasai, H.; Okada, S.; Oikawa, H.; Nakanishi, H. Fabrication of Organic Nanocrystals Using Microwave Irradiation and Their Optical Properties. *Opt. Mater.* **2003,** *21* (1–3), 591-594.

40. Gerbec, J. A.; Magana, D.; Washington, A.; Strouse, G. F. Microwave-Enhanced Reaction Rates for Nanoparticle Synthesis. *J. Am. Chem. Soc.* **2005,** *127* (45), 15791-15800.

41. Zhang, X.; Liu, Z. Recent Advances in Microwave Initiated Synthesis of Nanocarbon Materials. *Nanoscale* **2012,** *4* (3), 707-714.

42. Baba, K.; Kasai, H.; Nishida, K.; Nakanishi, H. Functional Organic Nanocrystals. In *Nanocrystal*, InTech: 2011; pp 397-414.

43. Kappe, C. O.; Dallinger, D. The Impact of Microwave Synthesis on Drug Discovery. *Nat. Rev. Drug Discov.* **2006,** *5* (1), 51-63.

44. Baghbanzadeh, M.; Carbone, L.; Cozzoli, P. D.; Kappe, C. O. Microwave-Assisted Synthesis of Colloidal Inorganic Nanocrystals. *Angew. Chem. Int. Ed.* **2011,** *50* (48), 11312-11359.

45. Li, L.; Sun, X.; Yang, Y.; Guan, N.; Zhang, F. Synthesis of Anatase TiO_2 Nanoparticles with B-Cyclodextrin as a Supramolecular Shell. *Chem. Asian J.* **2006,** *1* (5), 664-668.

46. Eastoe, J.; Warne, B. Nanoparticle and Polymer Synthesis in Microemulsions. *Curr. Opin. Colloid Interface Sci.* **1996,** *1* (6), 800-805.

47. Vestal, C. R.; Zhang, Z. J. Normal Micelle Synthesis and Characterization of $MgAl_2O_4$ Spinel Nanoparticles. *J. Solid State Chem.* **2003,** *175* (1), 59-62.

CHAPTER THREE
POLYMERIC IMPRINTED NANOGUMBOS FOR CHIRAL RECOGNITION

3.1. Introduction

Ionic liquids (ILs) are molten salts which possess a range of relatively low melting points due to inefficient packing of bulky cations and small anions (or vice versa).[1-2] ILs show interesting physical and chemical properties such as low volatility, chemical stability, and high conductivity;[1, 3] and can be tailored by molecular design of either the anionic or cationic component for task-specific functions.[4-5] An emerging class of solid phase materials based on tunable ionic liquids collectively referred to as GUMBOS (group of uniform materials based on organic salts) has been demonstrated as capable of forming nanoparticles (nanoGUMBOS) with magnetic, fluorescent, pH sensitive, and anticancer properties.[6-14] To combine one or more of these properties into nanoparticle based theranostic agents, incorporation of a molecular recognition element using the method of molecular imprinting was investigated for formation of nanoGUMBOS molecularly imprinted polymers (referred to as NGMIPs).[15-16]

Scheme 3.1 outlines the methodology envisioned for molecular imprinting of nanoGUMBOS which begins with formation of a pre-polymer complex of interactive monomers with the target molecular compound. The complex is subsequently polymerized to immobilize the positions of the interactive monomers within the surrounding polymer matrix. Removal of the template leaves a shape selective binding cavity lined with interactive functional groups in a complementary array within the cavity.[17] An advantage of using polymerizable ionic liquids is the ability to carry out the molecular

imprinting process in aqueous media, which has only shown a few successes to date[18] and even fewer examples of chiral recognition[19-25] (the most challenging test of molecular recognition).

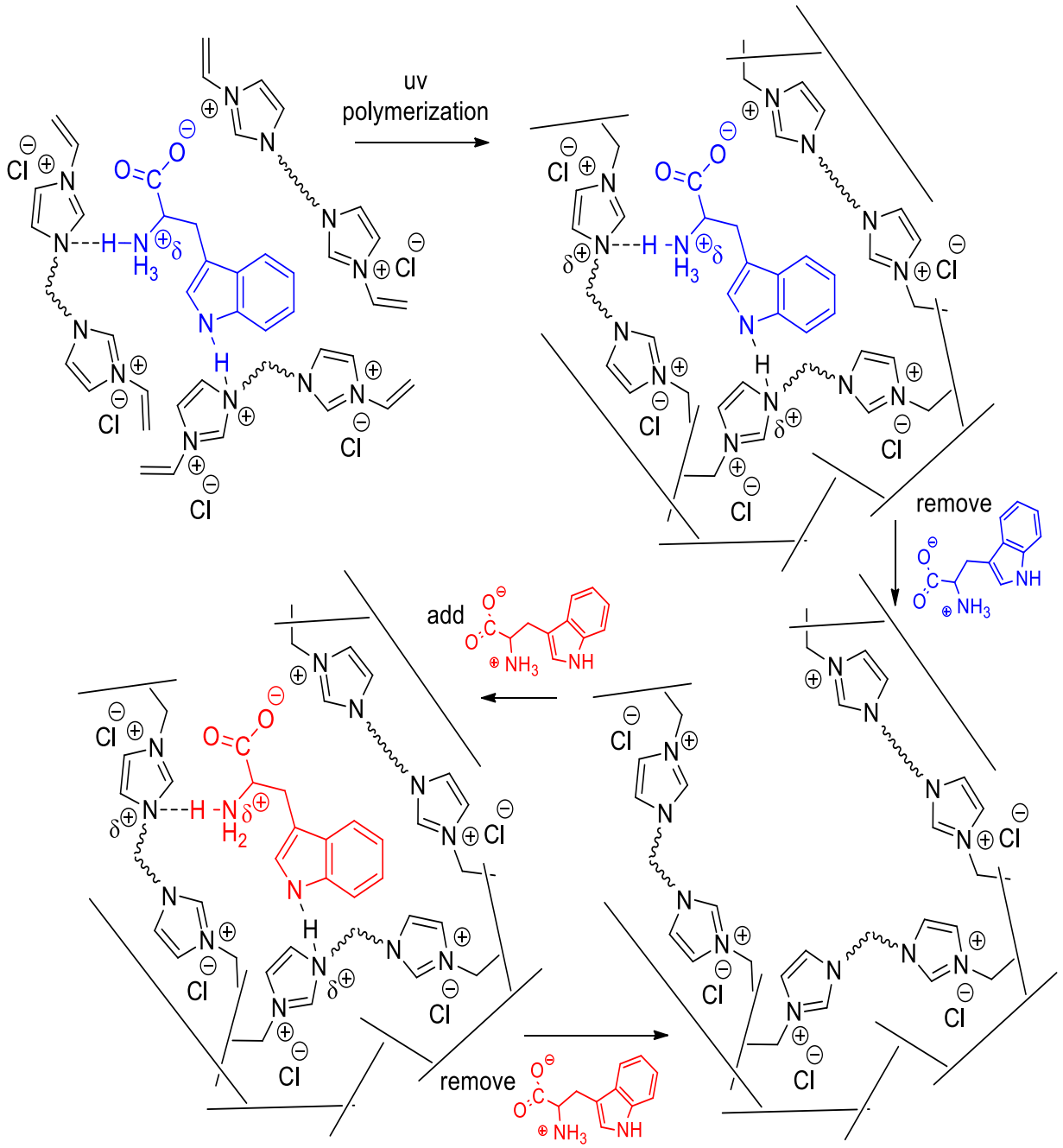

Scheme 3.1. Outline of the molecular imprinting method using crosslinking ionic liquids.

This study reports on the development of molecularly imprinted polymeric nanoGUMBOS directed toward molecular recognition of chiral amino acids using ionic liquid crosslinking monomers. A series of crosslinking ionic liquid monomers with different molecular spacers was synthesized and molecularly imprinted with L-tryptophan (L-Trp) as the target compound.[26-30] To date, the utility of crosslinking ionic liquids for molecular imprinting has not been reported; however, imprinting with only a single crosslinking monomer has been shown to improve molecularly imprinted polymer (MIP) performance in other systems.[31-33] The enantiomer discrimination of chiral imprinted nanoGUMBOS synthesized with the different crosslinkers was compared and correlated with the molecular structure of the crosslinkers.

3.2. Experimental Section

3.2.1. Materials

Ionic liquids and GUMBOS used in this study were received from the laboratories of Dr. Doug Gin and Dr. Richard D. Noble at the University of Colorado, Boulder.[26-30] Triton X-100 (TX-100), sodium bis(2-ethylhexyl) sulfosuccinate (AOT), L-tryptophan (L-Trp), D-tryptophan (D-Trp), as well as the initiator 2,2′-Azobis(2-methylpropionamidine) dihydrochloride (AAPH) were purchased from Sigma Aldrich (St. Louis, MO) and used as received. Ultrapure water (18.2 MΩ cm) was obtained from an Elga model PURELAB ultra water filtration system and an ARIES High Purity Water System.

3.2.2. Characterization Techniques

3.2.2.1. Nuclear Magnetic Resonance (NMR) Spectroscopy

^{1}H-NMR experiments were performed by dissolving the polymerizable monomers in deuterated dimethylsulfoxide DMSO. The spectra were obtained using a Bruker AV-400 liquid instrument (Billerica, MA) that operates at 400 MHZ (Figure B1 in Appendix B).

For ^{19}F-NMR, the studies on the monomers were performed on Bruker AVIII-400-Nanobay (AVB 400) instrument (Billerica, MA).

3.2.2.2. Fourier Transform Infrared (FTIR) Spectroscopy

The polymerized NGMIPs in aqueous suspensions were lyophilized and the formed pellet made of nanoparticles and surfactant was deposited on an ATR cell in a Bruker Tensor 27 instrument (Billerica, MA). The background signal of the surfactant was subtracted from the sample spectrum.

3.2.2.3. Transmission Electron Microscopy (TEM)

TEM micrographs were obtained using a JEOL JEM-1011 TEM (München, Germany). An 8 µL volume of sample was spotted onto ultrathin carbon coated 400-mesh Ted Pella, Inc TEM grids (Redding, CA). The grids were mainly washed with water to avoid any unwanted adsorption of unpolymerized monomers and surfactant.

3.2.2.4. Fluorescence Spectroscopy

Fluorescence measurements were performed using a Fluorolog-3 fluorometer (HORIBA Scientific, Edison, NJ) at a right angle detection. The quartz sample cuvette was purchased from Starna Cells (Atascadero, CA) and had a 0.4 cm path length.

3.2.3. Synthesis Procedures

3.2.3.1. Anion Exchange

The [NTf_2] anion of polymerizable monomers was exchanged with chloride [Cl] anion using an ion exchange resin. In a separation column, Dowex 1x8 chloride form (purchased from Sigma Aldrich) was packed and rinsed with 0.1 M aqueous solution of sodium chloride. After flushing the column with distilled water, monomeric aqueous solutions were loaded on the column and eluted with deionized water. The eluted samples

were spotted on a thin layer chromatography plate. Presence of the product was detected by appearance of a dark spot upon illumination with ultraviolet light. Water was removed by lyophilizing the samples. ^{19}F-NMR of the final product showed the disappearance of fluorine peak, which confirmed that ion exchange took place.

3.2.3.2. Synthesis of Polymeric NanoGUMBOS Using UV-Initiated Polymerization

For UV-initiated polymerization, 0.1 mL of monomeric aqueous solution (0.1 M) and 5 mL of Triton X-100 (TX-100) aqueous surfactant solution (0.02 M) were mixed under magnetic stirring. Ultimately, 0.2 mL of 0.005 M aqueous AAPH solution was added to the mixture. After 30 minutes of magnetic stirring, the sample was purged with nitrogen and then exposed to UV light for 8 hours.

3.2.3.3. Imprinting Procedure: Synthesis of the NGMIPs

To imprint the nanoGUMBOS with the chiral amino acid L-tryptophan, 0.26 mg of L-tryptophan was added to the surfactant solution (described earlier) prior to UV- initiated polymerization. After polymerization, 1 mL of the polymerized sample was centrifuged for 30 minutes at 14000 rpm speed (procedure performed in triplicate). To determine the theoretical number of binding sites created in the NGMIPs, samples were obtained from the supernatant and subsequent fluorescence measurement of supernatant gave the amount of free L-tryptophan that was not encapsulated into the polymeric matrices. The difference between the original tryptophan concentration and that found in the supernatant is recorded as the amount of tryptophan bound to the NGMIP sample, and represents the number of theoretical sites (maximum uptake) created inside the polymeric matrix. To remove L-tryptophan from the cavities of synthesized nanoparticles, the NGMIPs were suspended in 1 mL of fresh water and dialyzed against deionized water

using a Float-A-Lyzer obtained from spectrum laboratories (Irving, TX). The release of L-Trp was monitored by measuring the fluorescence of the retentate over time. The dialysis medium was changed initially each 4 hours and then each day for a period of two weeks.

3.2.3.4. Recognition Studies

After template removal, quantitative evaluation of tryptophan rebinding to the NGMIPs was carried out by adding a solution of L- or D-tryptophan to the nanoGUMOS particles resuspended in water. An amount of tryptophan equal to the maximum uptake capacity was added to each aliquot of nanoGUMBOS suspensions (500 µL each). After vortexing followed by incubation for 20 hr on a shaker platform, the particles were removed by centrifugation and the supernatant analyzed by fluorescence to determine the amount of L-tryptophan and D-tryptophan unbound. The measurements were compared to controls of L- and D-tryptophan representing the initial amount added to the nanoparticles. The amount of L-or D-tryptophan recognized is calculated by using the difference between the integrated surface areas of fluorescence spectra.

3.3. Results and Discussion

Four different crosslinking ionic liquids distinguished by unique functional group spacers between the vinylimidazolium groups were investigated (Figure 3.1).[26-30] The different crosslinkers are referred to by the chemical structures as follow: benzene-based monomer (1), (PEG)-based monomer (2), alkane-based monomer (3), and alkyne-based monomer (4). The [NTf_2] counterions of the synthesized crosslinkers were exchanged with Cl^- using an anion exchange column to render the compounds

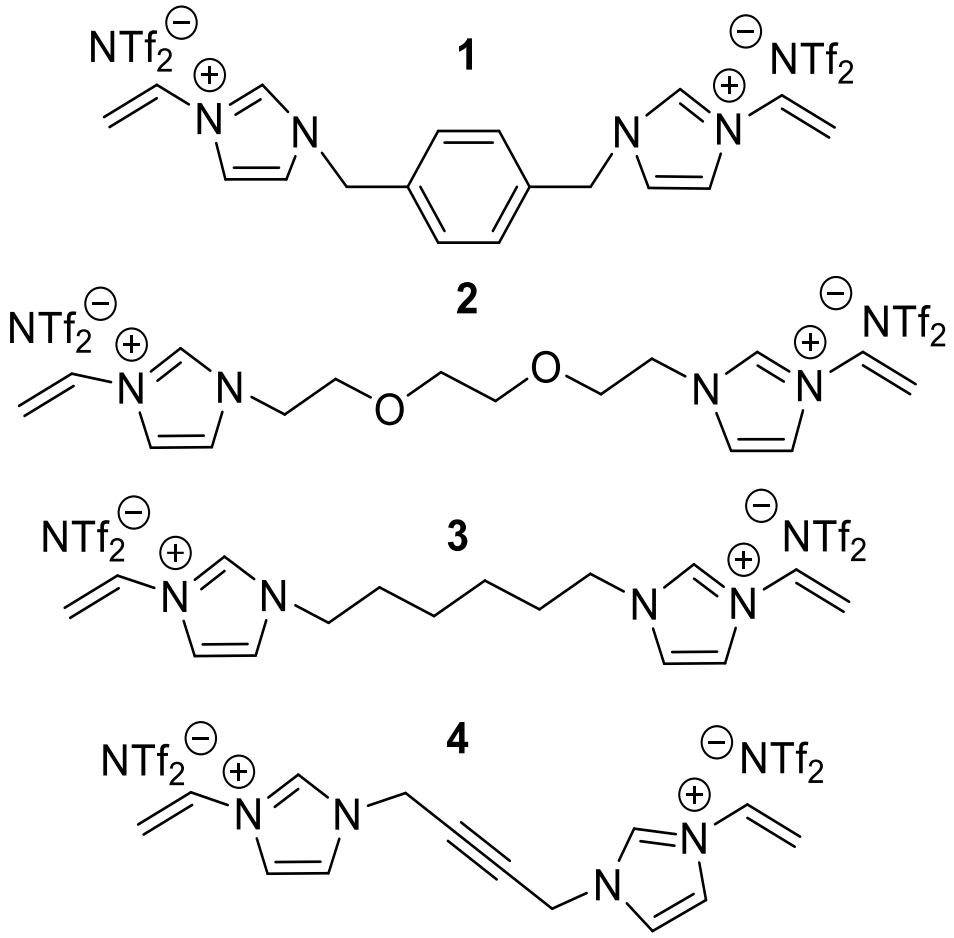

Figure 3.1. Structures of polymerizable crosslinkers: (1) benzene-based monomer, (2) (PEG)-based monomer, (3) alkane-based monomer, and (4) alkyne-based monomer.

hydrophilic for aqueous imprinting.[34] Prior anion exchange, all the monomers coupled with NTf_2 counteranion presented a peak at -78.7 ppm in ^{19}F-NMR spectra, the absence of this peak confirmed that NTf_2 anions were fully exchanged with Cl^- (Figure 3.2). ^{19}F-NMR spectra of benzene, alkane, and alkyne monomers are available in Figure B2, Appendix B. Before advancing to molecular imprinting, the synthesis of blank nanoGUMBOS (nanoGUMBOS non-imprinted polymers with the acronym NGNIP) in the absence of template was carried out using the four different crosslinkers. The NGNIPs were synthesized by dispersion polymerization of an aqueous solution using each of the

four crosslinkers in the presence of Triton-X100 surfactant and 2,2′-Azobis(2-methylpropionamidine) dihydrochloride (AAPH) initiator under UV photoinitiation. TEM micrographs obtained after polymerization confirm the formation of

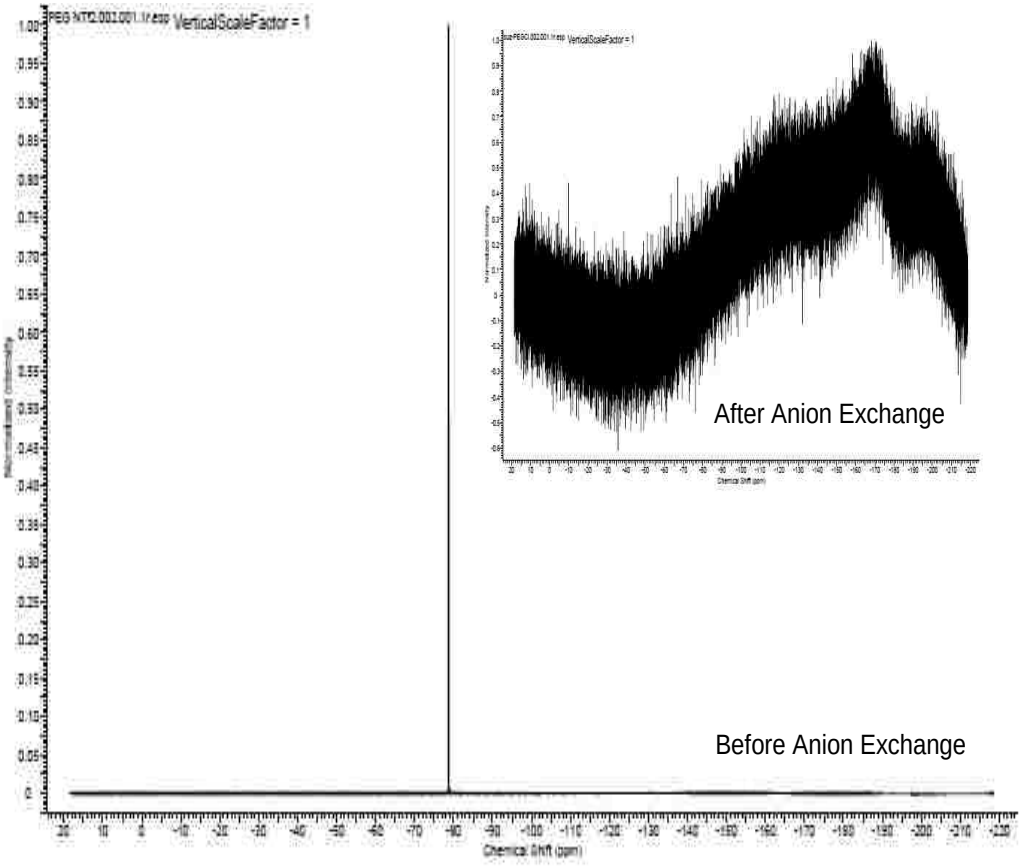

Figure 3.2. ^{19}F-NMR for (PEG)-based monomer before and after anion exchange.

nanoGUMBOS particles for each of the different crosslinkers (Figure 3.3). As shown in TEM micrographs, the (PEG)- and alkyne-based polymerized NGNIPs had smaller average sizes of 87 ± 10 nm and 44 ± 5 nm, respectively (Figures 3.3A and 3.3C). The two other polymerized NGNIPs had average sizes of 109 ±16 nm for the alkane-based NGNIP and 118 nm ± 23 nm for the benzene-based NGNIP. FTIR spectra were obtained before and after UV exposure of the monomer solutions. The surfactant peak was subtracted from the NGNIP spectra after the polymerization (Figure 3.4). The decrease

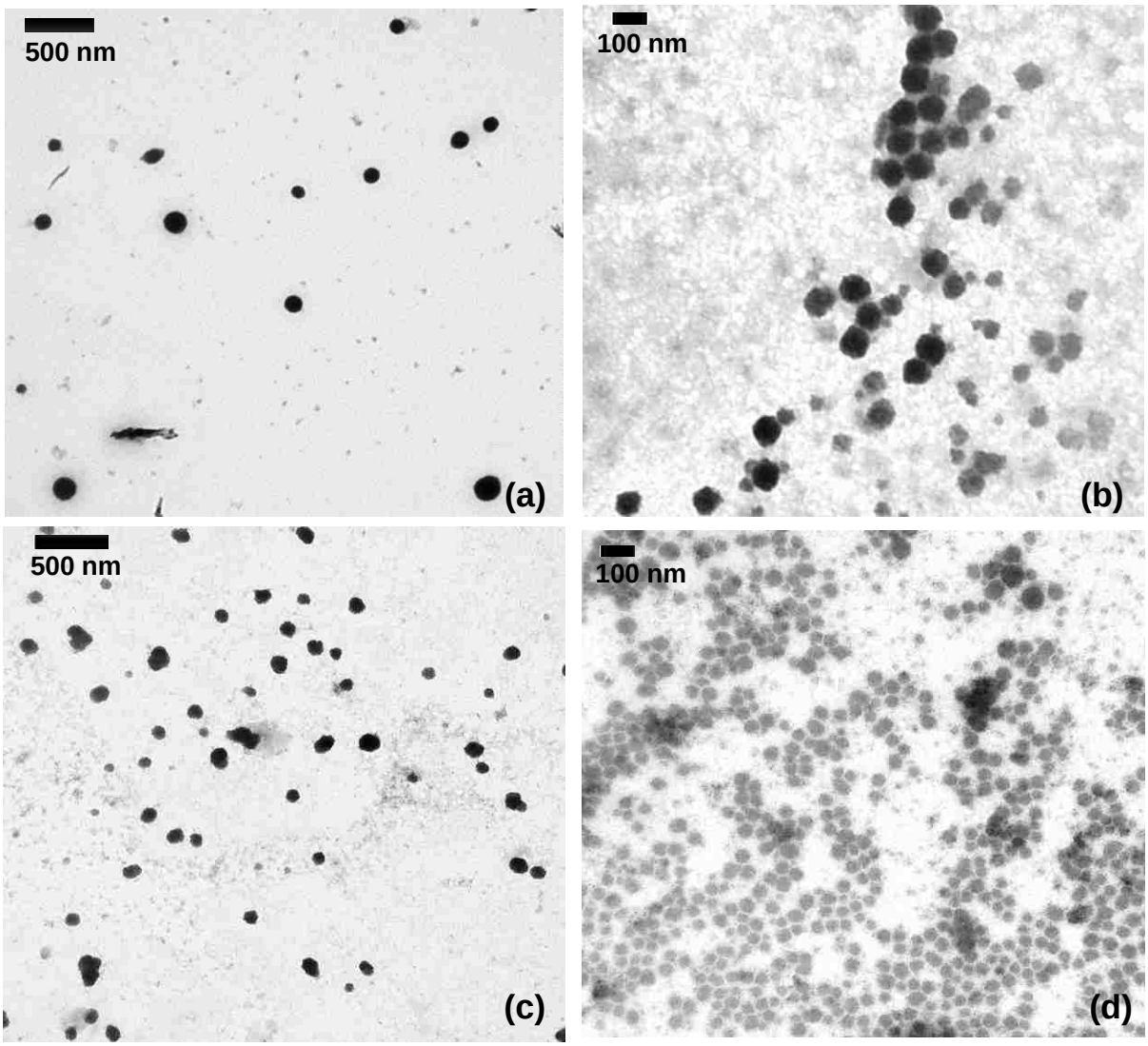

Figure 3.3. Transmission electron micrographs of non-imprinted nanoGUMBOS (NGNIPs) polymerized with the with the following crosslinker types (a) benzene, (b) (PEG), (c) alkane, and (d) alkyne.

or disappearance of the vibration peak at 3080 cm^{-1} (=CH_2 stretch vibration) compared to the standard peak at 1559 cm^{-1} confirms polymerization of the monomers.[35] Centrifugation of the polymerized samples gave a solid pellet as shown in Figure 3.5, also confirming polymerization had taken place.

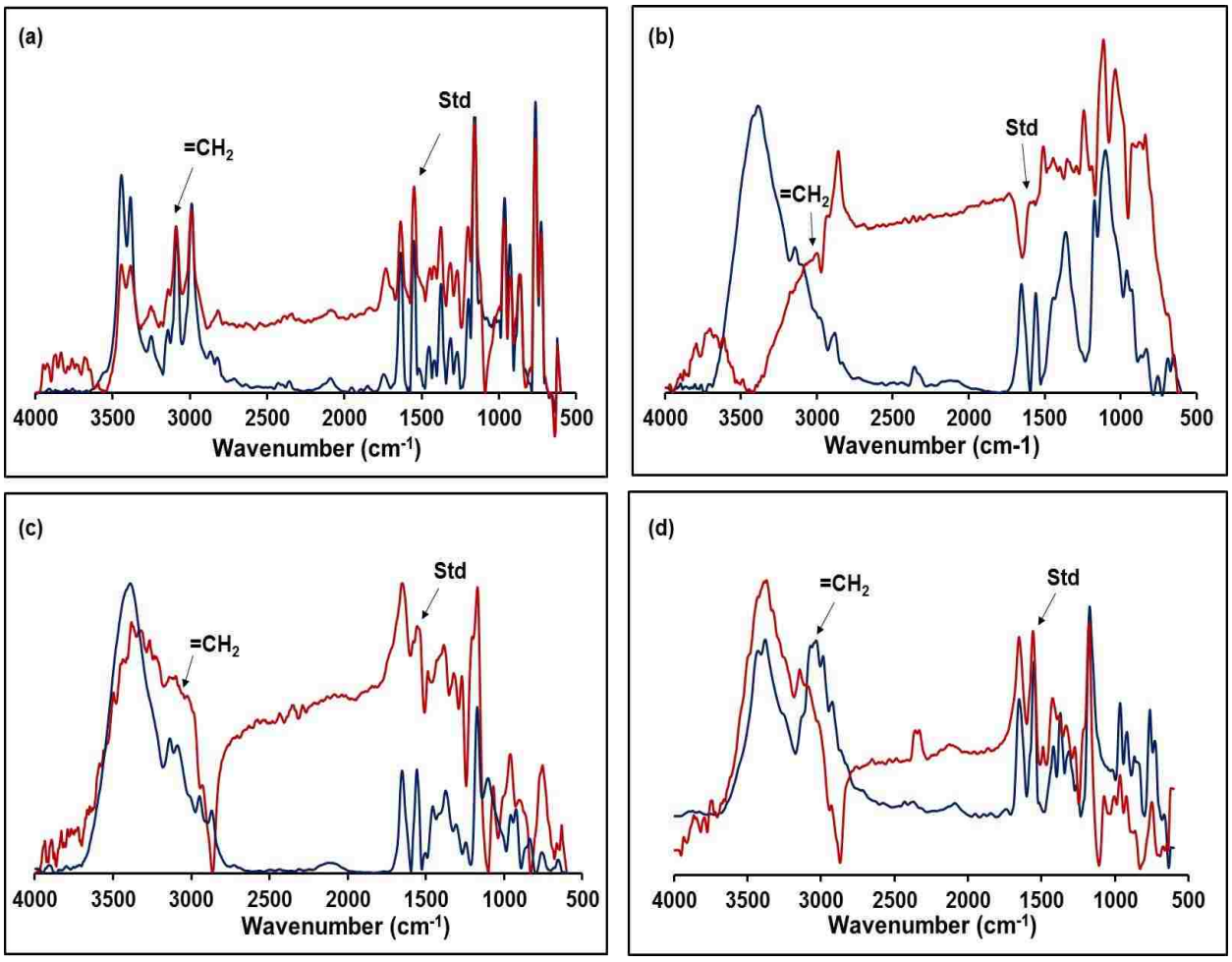

Figure 3.4. FTIR spectra of (a) benzene-, (b) (PEG)-, (c) alkane-, and (d) alkyne-based monomers and polymers (before and after irradiation respectively). The blue line represents the signal of monomers and the red line represents the signal of polymeric nanoparticles. The peak at 1559 cm^{-1} is the standard peak to which the intensity of vibration peak at 3080 cm^{-1} is compared.

Having established good protocols for the polymerization of NGNIPs, the ability to imprint in these materials with L-tryptophan was explored. It is known from the literature that the mole ratio of template to monomer is critical for eliciting the imprinting effect.[36] This is a result of balancing the number of binding sites arising from non-covalent pre-polymer complexes that increase with increased template concentration (*via* Le Châtelier's principle), versus the quality of binding sites that improves from a

Figure 3.5. Photographs showing formation of a pellet made of alkane polymerized nanoGUMBOS.

decrease of the template to monomer ratio. Preliminary studies on the NGMIPs using the (PEG)-based monomer were performed using the same formulation as the NGNIPs to compare template:monomer ratios of 1:6 and 1:8 (Figure 3.6). After polymerization and centrifugation, analysis by fluorescence of the supernatant indicated that 29% of the L-Trp remained in the NGMIP with the template:monomer ratio 1:8, while 24% of the L-Trp remained in the particles formulated with a ratio 1:6. Thus, NGMIPs were synthesized using the 1:8 template:monomer ratio for all further studies. The amount of initiator and the time of photoinitiation were also optimized, arriving at a final procedure using 10 mol % initiator and an 8 hour period of UV illumination with a Hanovia medium pressure mercury arc lamp.

The optimized formulation and procedure were subsequently used to synthesize NGMIPs using each of the four different crosslinking ionic liquids. TEM micrographs of the NGMIPs provided in Figure 3.7 show that average sizes of imprinted particles

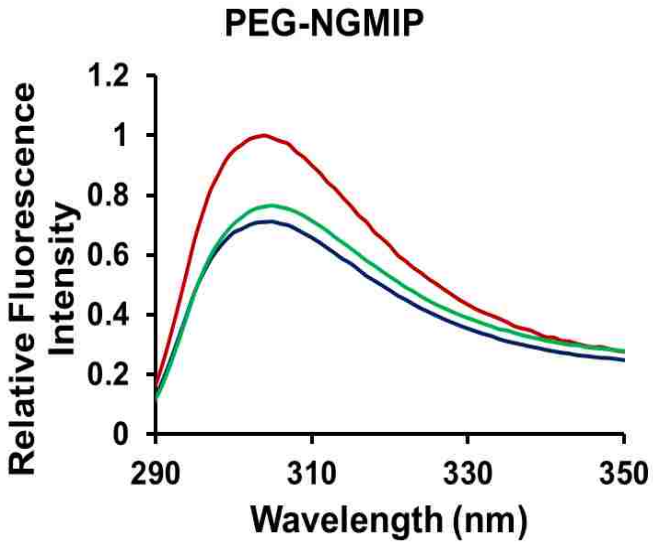

Figure 3.6. Fluorescence measurements on (PEG)-NGMIPs formulated with 1:6 and 1:8 template to monomer ratios. The blue and green lines express the amount of free L-Trp in the (PEG)-NGMIPs formulated using a template to monomer 1:8 and 1:6 mol ratios, respectively. The difference between the amount of L-Trp added (red line) and amount of L-Trp in supernatants (green and blue lines) designates the theoretical sites created in the polymeric matrix.

increased significantly versus the non-imprinted particles (Figure 3.3) for the benzene-based NGMIPs (294 nm ± 46 nm), (PEG)-based NGMIPs (289 ± 117 nm), alkane-based NGMIPs (196 ± 37 nm), and alkyne-based NGMIPs (205 ± 71 nm) in Figures 3.7a-d respectively. The increased sizes for the NGMIPs must be due to inclusion of the tryptophan template, which may be a result of changes in the surface tension characteristics from the equivalent polymers shown in Figure 3.3. After polymerization and centrifugation, the supernatants of each of the NGMIPs were quantified by fluorescence spectroscopy to determine the amount of L-Trp remained in each of the particles, and estimate the maximum uptake capacity of the respective NGMIPs (Figure 3.8).

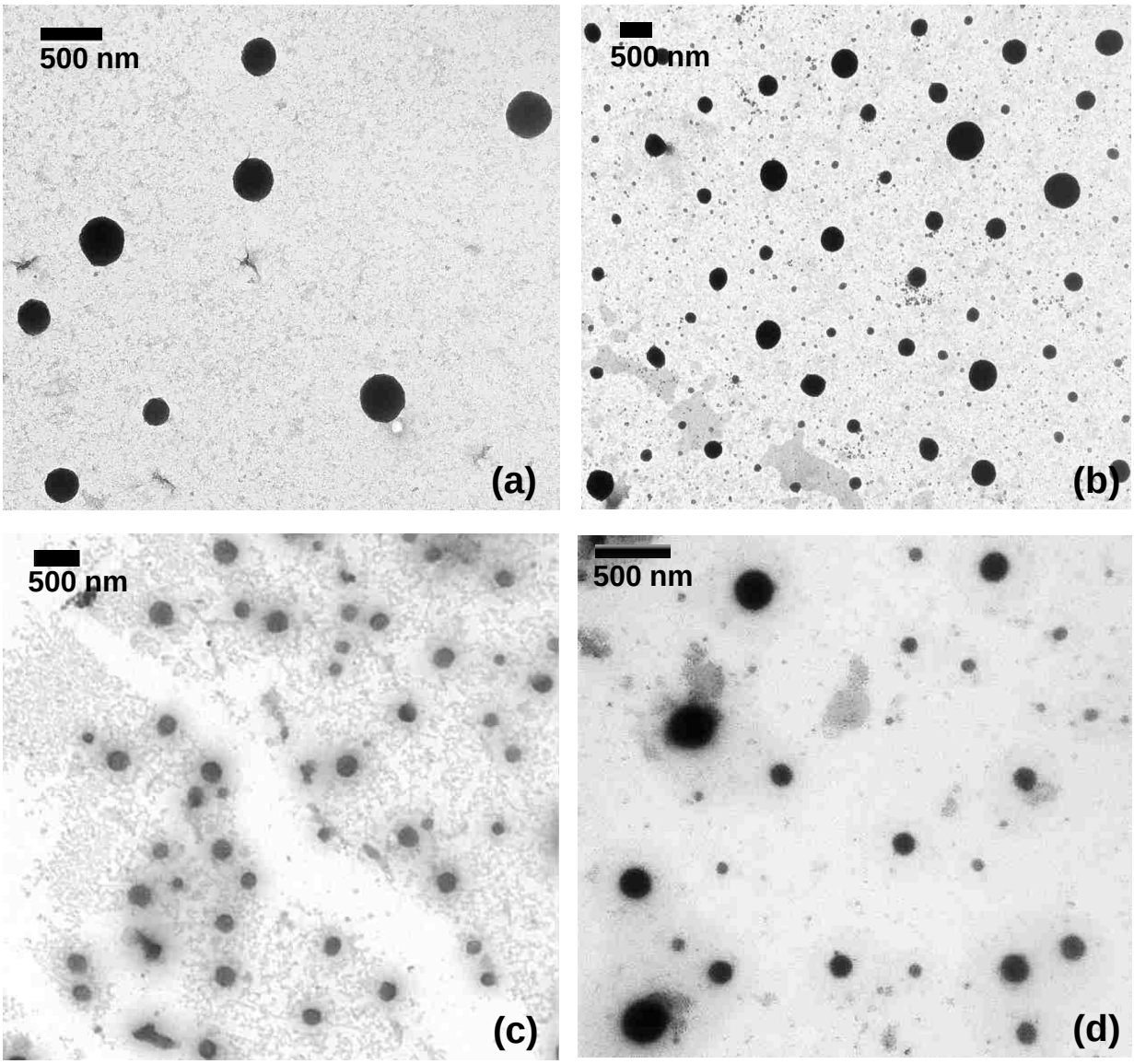

Figure 3.7. Transmission electron micrographs of imprinted nanoGUMBOS (NGMIPs) polymerized with the with the following crosslinker types (a) benzene, (b) (PEG), (c) alkane, and (d) alkyne.

Removal of the remaining L-Trp was carried out by dialysis over a two week period, until the dialysate showed no change in fluorescence (Figure 3.9). TEM micrograph of the (PEG)-based NGMIPs after dialysis displays a grainy structure that could result from tryptophan removal (Figure 3.10). The greater aggregation of the dialyzed NGMIPs

versus the non-dialyzed NGMIPs (Figure 3.4) is due to the removal of surfactant used in the initial imprinting of the particles.

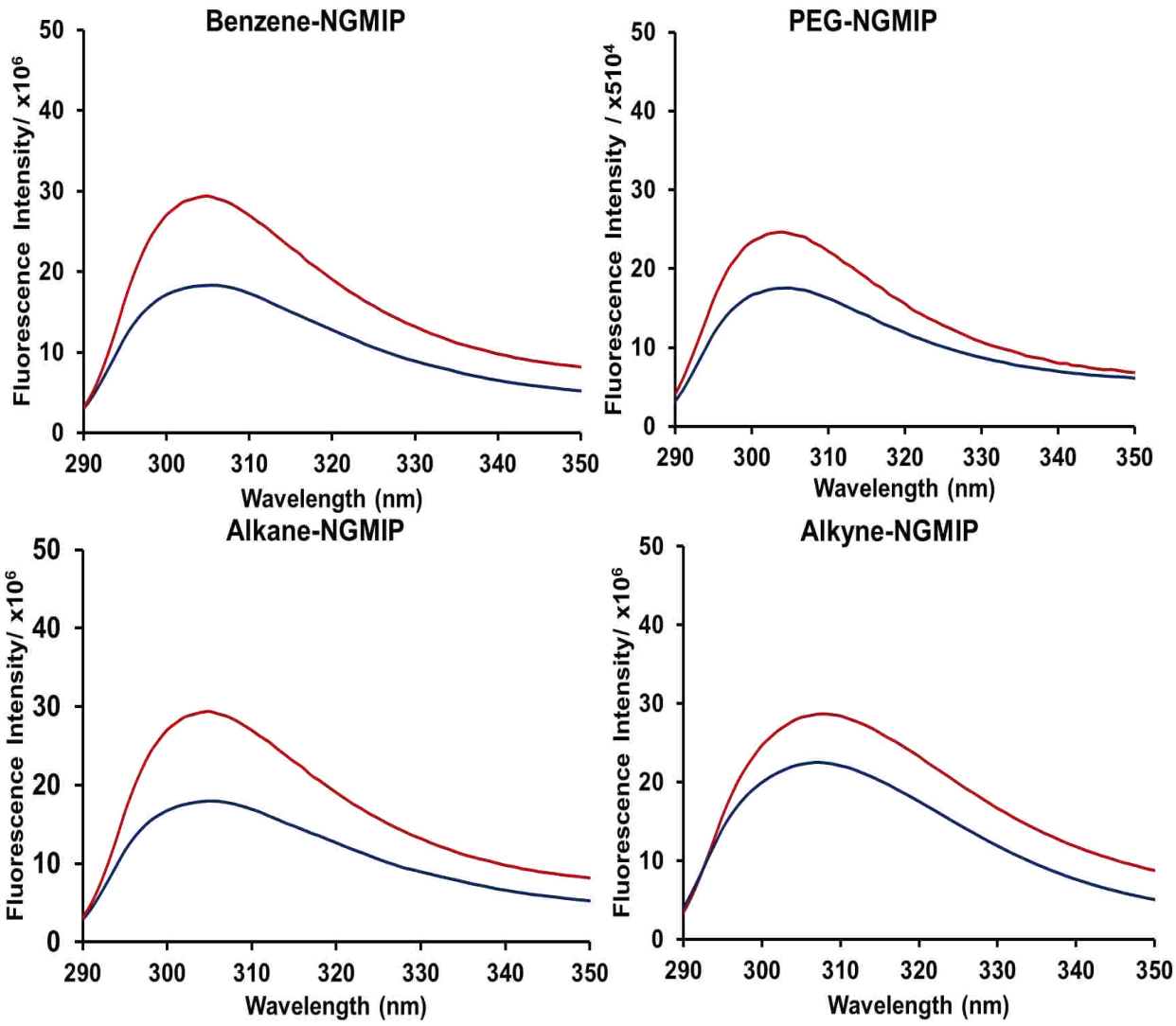

Figure 3.8. Fluorescence spectra showing the theoretical sites of the NGMIPs. All NGMIPs in this case were formulated with 1:8 template to monomer mol ratio. The difference between the amount of L-Trp added (red line) and amount of L-Trp in supernatant (blue line) represents the theoretical sites created in the polymeric matrices. The maximum percent uptakes (theoretical sites) were 38% for benzene-NGMIP, 29% for (PEG)-NGMIP, 39% for alkane-NGMIP, and 21% for alkyne-NGMIP.

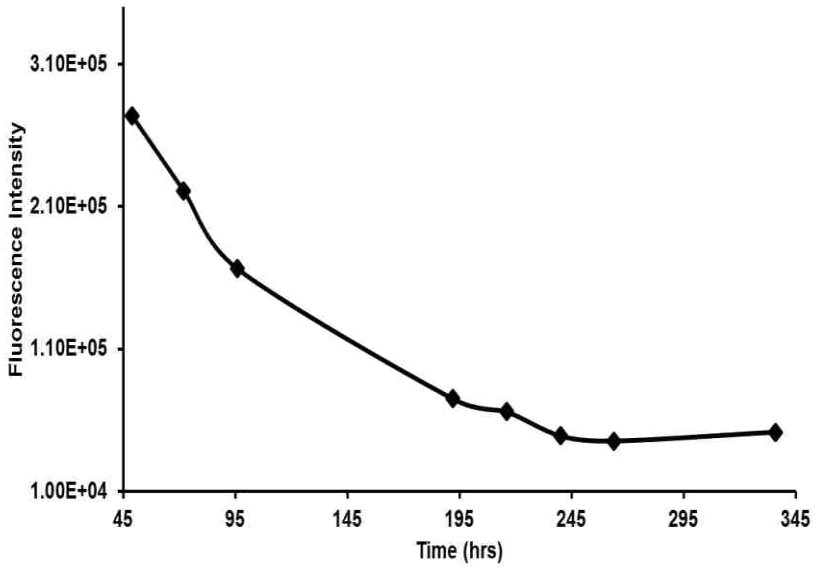

Figure 3.9. Dialysis profile of L-Trp released from benzene-NGMIP. Fluorescence measurements were taken from the retentate to track the decrease in the signal upon diffusion of L-Trp to the release medium (water).

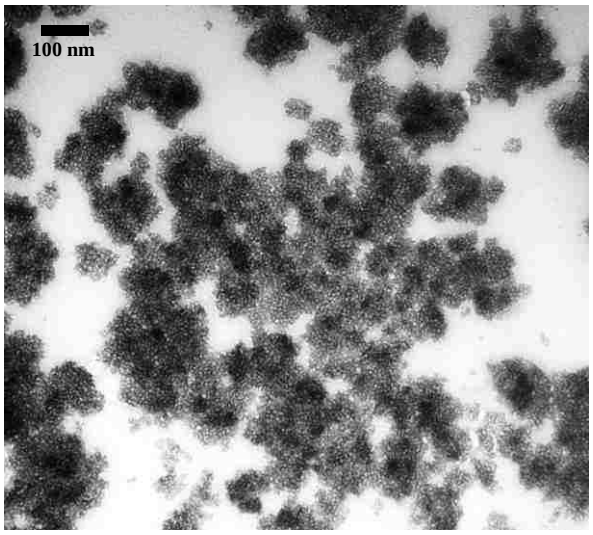

Figure 3.10. TEM of the NGMIP particles shown in Figure 3.7a after dialysis in deionized water for 2 weeks.

Rebinding of both enantiomers of tryptophan was analyzed in batch rebinding mode by adding to NGMIP particles, a solution of tryptophan with the concentration

matching the maximum capacity determined for each type of NGMIP (Figure 3.8). After incubation with L- or D-Trp, the particles were removed by centrifugation and the amount of tryptophan remaining in the supernatant was measured by fluorescence (Figure 3.11). The difference between the original solution concentration and the amount remaining in the supernatant gives the amount of tryptophan bound to the polymer, which is reported in Table 3.1 as the amount of tryptophan bound per gram of each NGMIP. The binding capacities of the NGMIPs were found to be in the range of 13 μmoles/g – 87 μmoles/g, which is approximately ten-fold higher in magnitude versus traditionally formed MIPs.[36-37] Two factors that may be responsible for the high capacity of these materials is the strong binding of the cationic imidazolium group to the tryptophan molecule, and the large number of these interactions possible because two equivalents of imidazolium groups are incorporated for each monomer. The higher uptake value of the benzene-based nanomaterial (benzene-NGMIP) compared to the other nanomaterials may be due to the pi-stacking and/or induced dipole interactions with the aromatic L-Trp that increases the affinity to these materials. This may also be true to some degree for the alkyne-NGMIP; however, the sizeable uptake by the alkyne-NGMIP is overshadowed by its poor selectivity (vide infra). The uptake by the alkane-NGMIP is a little lower due to the lack of pi-stacking interactions; and considerably lower for the (PEG)-NGMIP. The (PEG)-NGMIP is unique in this group of materials in the fact that it has glycol units that are hydrated by several water molecules per unit, which may disrupt some of the polar interactions between tryptophan and the binding site functionality in the (PEG)-NGMIP.

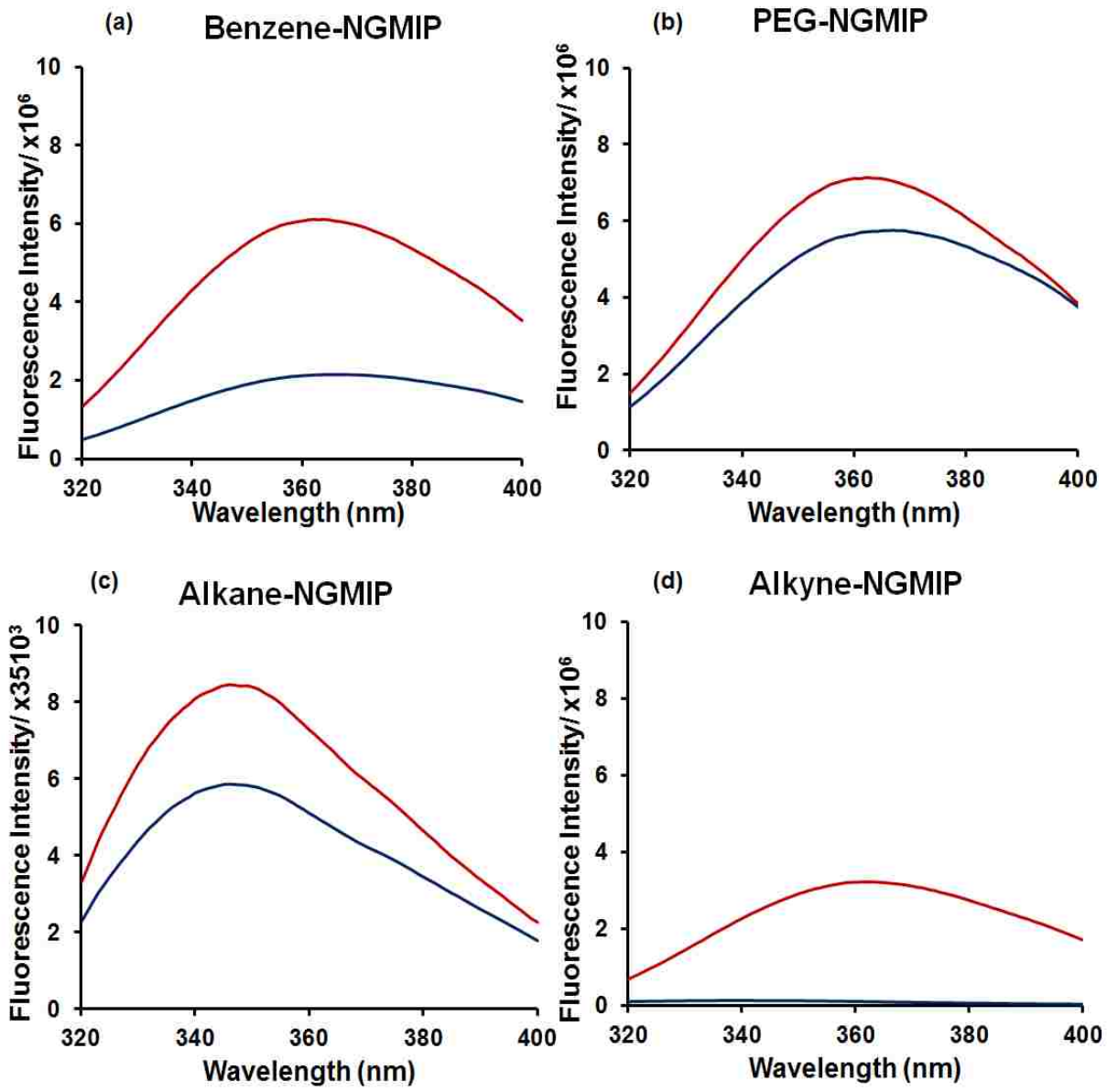

Figure 3.11. Fluorescence spectra showing the relative amount of L-Trp (a-d) or D-Trp (e-h) rebound to the polymeric matrices. The red lines represent the amount of Trp in the incubation solution, and the blue line represents the amount of Trp left in the supernatant after the polymer with adsorbed Trp was removed. The difference between both spectra represents the amount of L-Trp rebound to the polymeric matrices, and the data reported in Table 3.1 as an average over three trials.

(Figure continued)

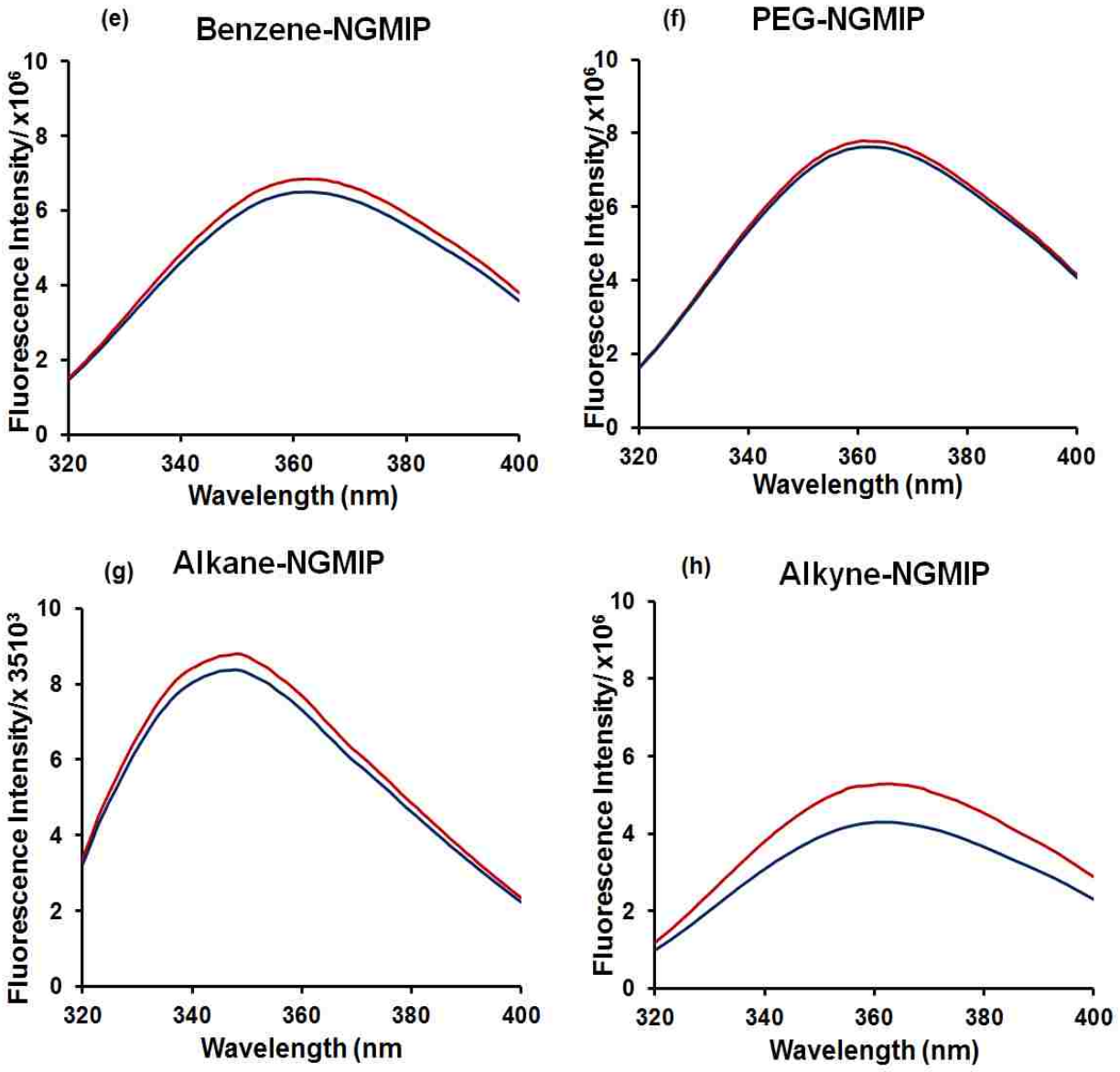

While binding affinity measured via the uptake by the NGMIPs is important, the greatest advantage of the NGMIPs, and all molecularly imprinted polymers as adsorbents or sensor materials, is the high level of molecular recognition possible for rebinding the template. Furthermore, the most challenging test of molecular recognition by any material is differential binding of enantiomers which differ only in their three dimensional

configuration. In fact, enantiorecognition has long been known as the best indicator for testing the imprinting effect, because the specific binding in MIPs arises from complementary three-dimensional binding interactions. Therefore, enantiorecognition was evaluated for each of the NGMIPs by comparing the binding uptake of both L- and D-Trp on the L-Trp imprinted particles (Table 3.1).

Table 3.1. Comparison of the uptake and enantiomer binding ratio of each NGMIP.*

OMNiMIP Crosslinker	Benzene-NGMIP	(PEG)-NGMIP	Alkane-NGMIP	Alkyne-NGMIP
L-Trp Rebinding Uptake (mmol/gram)	0.087 ± 0.029	0.013 ± 0.0038	0.042 ± 0.027	0.081 ± 0.0010
D-Trp Rebinding Uptake (mmol/gram)	0.0068 ± 0.0054	0.0019 ± 0.0011	0.0069 ± 0.0007	0.016 ± 0.0055
Enantiomer Binding Ratio	13:1	7:1	6:1	5:1

*Error is reported as the standard deviation of the mean

As shown in Table 3.1, all of the different NGMIP materials showed good enantiomer differentiation, with the benzene-NGMIP exhibiting the highest enantiorecognition seen by the ratio of 13:1 for binding L-Trp preferred over D-Trp. While the primary interactions of the crosslinkers with template are inferred to occur with imidazolium moiety, secondary interactions are postulated to exist between the aromatic spacer and the L-Trp template. The increased affinity and/or number of template-

crosslinker contacts would provide more complementary interactions that are specific to the L-Trp template than the D enantiomer. This would account for the high chiral discrimination found for the benzene-NGMIP where secondary interactions arise from pi-stacking of the benzene spacer with the aromatic region of the L-Trp template. Enantiorecognition values are virtually the same for the other three NGMIPs, indicating that none of these spacer groups contribute significant interactions with the template (L-Trp) beyond the imidazolium-template contacts.

3.4. Conclusions

Four crosslinking ionic liquids were employed in the synthesis of novel nanomaterials that were successfully imprinted with the chiral template L-Trp under aqueous conditions. The fact that imprinting was carried out in water is significant because in spite of many reports of rebinding analyses by MIPs in aqueous solutions, most of these examples do not perform the actual molecular imprinting process under aqueous conditions, but rather in organic solvents. The reason for this is that the non-covalent molecular imprinting technique relies on formation of pre-polymer complexes based on hydrogen-bonding and weak-to-moderate ionic interactions which are severely disrupted in the presence of water.[18, 39-42] However, many desirable templates, especially those of biological origin, are only soluble in aqueous matrices and cannot be adapted to organic soluble MIP methods. Thus, polymerizable ionic liquids are an important class of monomers for imprinting these water-soluble targets. A few examples of molecularly imprinted polymers using non-crosslinking IL monomers have been published;[43-48] however there have not been any reports of chiral recognition by imprinted ionic liquids. Thus, a chiral template was imprinted for this purpose using crosslinking ILs developed

by the groups of Gin and Noble that uniquely provide the necessary components to form nanoGUMBOS and simultaneously provide the crosslinking required for the molecular imprinting process. Four different crosslinking ionic liquids were available with different functional groups as spacers between the vinylimidazolium groups, and the corresponding NGMIPs from each of these was compared. All four NG-MIPs provided the first examples of enantiorecognition by molecularly imprinted polymeric ILs, indicating that multi-functional nanoGUMBOS with specific molecular recognition can be effectively synthesized for theranostic applications toward a spectrum of aqueous-based templates.

3.5. References

1. Plechkova, N. V.; Seddon, K. R. Applications of Ionic Liquids in the Chemical Industry. *Chem. Soc. Rev.* **2008,** *37* (1), 123-150.

2. Del Popolo, M. G.; Voth, G. A. On the Structure and Dynamics of Ionic Liquids. *J. Phys. Chem. B* **2004,** *108* (5), 1744-1752.

3. Welton, T. Room-Temperature Ionic Liquids. Solvents for Synthesis and Catalysis. *Chemi. Rev.* **1999,** *99* (8), 2071-2083.

4. Davis, J. H. Task-Specific Ionic Liquids. *Chem. Lett.* **2004,** *33* (9), 1072-1077.

5. Lee, S. G. Functionalized Imidazolium Salts for Task-Specific Ionic Liquids and Their Applications. *Chem. Commun.* **2006,** (10), 1049-1063.

6. Bwambok, D. K.; El-Zahab, B.; Challa, S. K.; Li, M.; Chandler, L.; Baker, G. A.; Warner, I. M. Near-Infrared Fluorescent Nanogumbos for Biomedical Imaging. *ACS Nano* **2009,** *3* (12), 3854-3860.

7. Tesfai, A.; El-Zahab, B.; Kelley, A. T.; Li, M.; Garno, J. C.; Baker, G. A.; Warner, I. M. Magnetic and Nonmagnetic Nanoparticles from a Group of Uniform Materials Based on Organic Salts. *ACS Nano* **2009,** *3* (10), 3244-3250.

8. Das, S.; Bwambok, D.; El-Zahab, B.; Monk, J.; de Rooy, S. L.; Challa, S.; Li, M.; Hung, F. R.; Baker, G. A.; Warner, I. M. Nontemplated Approach to Tuning the Spectral Properties of Cyanine-Based Fluorescent NanoGUMBOS. *Langmuir* **2010,** *26* (15), 12867-12876.

9. Das, S.; de Rooy, S. L.; Jordan, A. N.; Chandler, L.; Negulescu, I. I.; El-Zahab, B.; Warner, I. M. Tunable Size and Spectral Properties of Fluorescent NanoGUMBOS in Modified Sodium Deoxycholate Hydrogels. *Langmuir* **2012,** *28* (1), 757-765.

10. Dumke, J. C.; El-Zahab, B.; Challa, S.; Das, S.; Chandler, L.; Tolocka, M.; Hayes, D. J.; Warner, I. M. Lanthanide-Based Luminescent NanoGUMBOS. *Langmuir* **2010,** *26* (19), 15599-15603.

11. Dumke, J. C.; Oureshi, A.; Hamdan, S.; El-Zahab, B.; Das, S.; Hayes, D. J.; Boldor, D.; Rupnik, K.; Warner, I. M. Photothermal Response of Near-Infrared-Absorbing NanoGUMBOS. *App. Spectrosc.* **2014,** *68* (3), 340-352.

12. Jordan, A. N.; Das, S.; Siraj, N.; de Rooy, S. L.; Li, M.; El-Zahab, B.; Chandler, L.; Baker, G. A.; Warner, I. M. Anion-Controlled Morphologies and Spectral Features of Cyanine-Based NanoGUMBOS - an Improved Photosensitizer. *Nanoscale* **2012,** *4* (16), 5031-5038.

13. Das, S.; Magut, P. K. S.; de Rooy, S. L.; Hasan, F.; Warner, I. M. Ionic Liquid-Based Fluorescein Colorimetric pH Nanosensors. *RSC Adv.* **2013,** *3* (43), 21054-21061.

14. Magut, P. K. S.; Das, S.; Fernand, V. E.; Losso, J.; McDonough, K.; Naylor, B. M.; Aggarwal, S.; Warner, I. M. Tunable Cytotoxicity of Rhodamine 6G Via Anion Variations. *J. Am. Chem. Soc.* **2013,** *135* (42), 15873-15879.

15. Alexander, C.; Andersson, H. S.; Andersson, L. I.; Ansell, R. J.; Kirsch, N.; Nicholls, I. A.; O'Mahony, J.; Whitcombe, M. J. Molecular Imprinting Science and Technology: A Survey of the Literature for the Years up to and Including 2003. *J. Mol. Recognit.* **2006,** *19* (2), 106-180.

16. Chen, L.; Xu, S.; Li, J. Recent Advances in Molecular Imprinting Technology: Current Status, Challenges and Highlighted Applications. *Chem. Soc. Rev.* **2011,** *40* (5), 2922-2942.

17. Wulff, G. Molecular Imprinting in Cross-Linked Materials with the Aid of Molecular Templates— a Way Towards Artificial Antibodies. *Angew. Chem., Int. Ed. Eng.* **1995,** *34* (17), 1812-1832.

18. Zhang, H. Water-Compatible Molecularly Imprinted Polymers: Promising Synthetic Substitutes for Biological Receptors. *Polymer* **2014,** *55*, 699-714.

19. Ramstrom, O.; Ye, L.; Gustavsson, P. E. Chiral Recognition by Molecularly Imprinted Polymers in Aqueous Media. *Chromatographia* **1998,** *48* (3-4), 197-202.

20. Jiang, Z.; Yu, Y.; Wu, H. Preparation of Cs/Gptms Hybrid Molecularly Imprinted Membrane for Efficient Chiral Resolution of Phenylalanine Isomers. *J. Membr. Sci.* **2006,** *280* (1-2), 876-882.

21. Zhang, Y.; Pan, Z.; Yuan, Y.; Sun, Z.; Ma, J.; Huang, G.; Xing, F.; Gao, J. Molecularly Imprinted Photonic Crystals for the Direct Label-Free Distinguishing of L-Proline and D-Proline. *Phys. Chem. Chem. Phys.* **2013,** *15* (40), 17250-17256.

22. Monier, M.; El-Mekabaty, A. Preparation of Molecularly Imprinted Resin Based on Chitosan for Chiral Recognition of S-Mandelic Acid. *Int. J. Biol. Macromol.* **2013,** *55*, 207-213.

23. Prasad, B. B.; Srivastava, A.; Pandey, I.; Tiwari, M. P. Electrochemically Grown Imprinted Polybenzidine Nanofilm on Multiwalled Carbon Nanotubes Anchored Pencil Graphite Fibers for Enantioselective Micro-Solid Phase Extraction Coupled with Ultratrace Sensing of D- and L-Methionine. *J. Chromatogr. B: Anal. Technol. Biomed. Life Sci.* **2013,** *912*, 65-74.

24. Prasad, B. B.; Pandey, I.; Srivastava, A.; Kumar, D.; Tiwari, M. P. Multiwalled Carbon Nanotubes-Based Pencil Graphite Electrode Modified with an Electrosynthesized Molecularly Imprinted Nanofilm for Electrochemical Sensing of Methionine Enantiomers. *Sens. Act. B-Chem.* **2013,** *176*, 863-874.

25. Yue, C-Y.; Ding, G-S.; Liu, F-J.; Tang, A-N. Water-compatible surface molecularly imprinted silica nanoparticles as pseudostationary phase in electrokinetic chromatography for the enantioseparation of tryptophan. *J. Chrom. A* **2013**, 1311, 176-182.

26. Carlisle, T. K. Design, Synthesis, and Evaluation of New Ionic Liquid-Based Solvents, Polymers, and Composites for Enhanced Membranebased Carbon Dioxide/Light Gas Separations. Ph.D. Dissertation, University of Colorado, Boulder, CO, 2011.

27. Bara, J. E. New Ionic Liquids and Ionic Liquid-Based Polymers and Liquid Crystals for Gas Separations. Ph.D. Dissertation, University of Colorado, Boulder, CO, 2007.

28. Carlisle, T. K.; Nicodemus, G. D.; Gin, D. L.; Noble, R. D. Co2/Light Gas Separation Performance of Cross-Linked Poly(Vinylimidazolium) Gel Membranes as a Function of Ionic Liquid Loading and Cross-Linker Content. *J. Membr. Sci.* **2012,** *397-398*, 24-37.

29. Robertson, L. A.; Schenkel, M. R.; Wiesenauer, B. R.; Gin, D. L. Alkyl-Bis(Imidazolium) Salts: A New Amphiphile Platform That Forms Thermotropic and Non-Aqueous Lyotropic Bicontinuous Cubic Phases. *Chem. Commun.* **2013,** *49*, 9407-9409.

30. Carlisle, T. K.; McDanel, W. M.; Cowan, M. G.; Noble, R. D.; Gin, D. L. Vinyl-Functionalized Poly(Imidazolium)S: A Curable Polymer Platform for Cross-Linked Ionic Liquid Gel Synthesis. *Chem. Mater.* **2014,** *26*, 1294-1296.

31. Sibrian-Vazquez, M.; Spivak, D. A. Enhanced Enantioselectivity of Molecularly Imprinted Polymers Formulated with Novel Cross-Linking Monomers. *Macromolecules* **2003,** *36* (14), 5105-5113.

32. Sibrian-Vazquez, M.; Spivak, D. A. Improving the Strategy and Performance of Molecularly Imprinted Polymers Using Cross-Linking Functional Monomers. *J. Org. Chem.* **2003,** *68* (25), 9604-9611.

33. LeJeune, J.; Spivak, D. A. Chiral Effects of Alkyl-Substituted Derivatives of N,O-Bismethacryloyl Ethanolamine on the Performance of One Monomer Molecularly Imprinted Polymers (OMNiMIPs). *Anal. Bioanal. Chem.* **2007,** *389* (2), 433-440.

34. Marcilla, R.; Blazquez, J. A.; Rodriguez, J.; Pomposo, J. A.; Mecerreyes, D. Tuning the Solubility of Polymerized Ionic Liquids by Simple Anion-Exchange Reactions. *J. Polym. Sci. A Polym. Chem.* **2004,** *42* (1), 208-212.

35. Svatos, A.; Attygalle, A. B. Characterization of Vinyl-Substituted, Carbon-Carbon Double Bonds by GC/FT-IR Analysis. *Anal. Chem.***1997,** *69* (10), 1827-1836.

36. Spivak, D. A. Optimization, Evaluation, and Characterization of Molecularly Imprinted Polymers. *Adv. Drug Del. Rev.* **2005,** *57* (12), 1779-1794.

37. Kotrotsiou, O.; Chaitidou, S.; Kiparissides, C. Boc-L-Tryptophan Imprinted Polymeric Microparticles for Bioanalytical Applications. *Mat. Sci. Eng. C* **2009,** *29* (7), 2141-2146.

38. Chaitidou, S.; Kotrotsiou, O.; Kotti, K.; Kammona, O.; Bukhari, M.; Kiparissides, C. Precipitation Polymerization for the Synthesis of Nanostructured Particles. *Mat. Sci. Eng. B* **2008,** *152* (1–3), 55-59.

39. Janiak, D. S.; Kofinas, P. Molecular Imprinting of Peptides and Proteins in Aqueous Media. *Anal. Bioanal. Chem.* **2007,** *389*, 399-404.

40. Kubo, T.; Hosoya, K.; Otsuka, K. Molecularly Imprinted Adsorbents for Selective Separation and/or Concentration of Environmental Pollutants. *Anal. Sci.* **2014,** *30*, 97-104.

41. Murray, A.; Ormeci, B. Application of Molecularly Imprinted and Non-Imprinted Polymers for Removal of Emerging Contaminants in Water and Wastewater Treatment: A Review. *Environ. Sci. Pollut. Res.* **2012,** *19*, 3820-3830.

42. Pichon, V.; Chapuis-Hugon, F. Role of Molecularly Imprinted Polymers for Selective Determination of Environmental Pollutants-a Review. *Anal. Chim. Acta* **2008,** *622*, 48-61.

43. Qian, L.; Hu, X.; Guan, P.; Gao, B.; Li, J.; Wang, C.; Tang, Y. Preparation of Bovine Serum Albumin Imprinting Sensitive Hydrogels Using Ionic Liquid as Co-Monomer and Stabilizer. *Talanta* **2014,** *121*, 56-64.

44. Luo, X.; Dong, R.; Luo, S.; Zhan, Y.; Tu, X.; Yang, L. Preparation of Water-Compatible Molecularly Imprinted Polymers for Caffeine with a Novel Ionic Liquid as a Functional Monomer. *J. Appl. Polym. Sci.* **2013,** *127* (4), 2884-2890.

45. Fan, J.-P.; Tian, Z.-Y.; Tong, S.; Zhang, X.-H.; Xie, Y.-L.; Xu, R.; Qin, Y.; Li, L.; Zhu, J.-H.; Ouyang, X.-K. A Novel Molecularly Imprinted Polymer of the Specific Ionic Liquid Monomer for Selective Separation of Synephrine from Methanol-Water Media. *Food Chem.* **2013,** *141* (4), 3578-3585.

46. Guo, L.; Deng, Q.; Fang, G.; Gao, W.; Shuo, W. Preparation and Evaluation of Molecularly Imprinted Ionic Liquids Polymer as Sorbent for on-Line Solid-Phase Extraction of Chlorsulfuron in Environmental Water Samples. *J. Chromatogr. A* **2011,** *1218* (37), 6271-6277.

47. Bi, W.; Tian, M.; Row, K. H. Separation of Phenolic Acids from Natural Plant Extracts Using Molecularly Imprinted Anion-Exchange Polymer Confined Ionic Liquids. *J. Chromatogr. A* **2012,** *1232*, 37-42.

48. Luo, X.; Zhan, Y.; Tu, X.; Huang, Y.; Luo, S.; Yan, L. Novel Molecularly Imprinted Polymer Using 1-(Alpha-Methyl Acrylate)-3-Methylimidazolium Bromide as Functional Monomer for Simultaneous Extraction and Determination of Water-Soluble Acid Dyes in Wastewater and Soft Drink by Solid Phase Extraction and High Performance Liquid Chromatography. *J. Chromatogr. A* **2011,** *1218* (8), 1115-1121.

CHAPTER FOUR
SYNTHESIS OF POLYMERIC NANOGUMBOS VIA GAMMA RAYS INDUCED POLYMERIZATION

4.1. Introduction

Ionic liquids (ILs), defined as organic salts with melting points at or below 100 °C, exhibit interesting physical and chemical properties such as low volatility, high thermal stability, high ionic conductivity, and the ability to dissolve compounds with assorted polarities.[1-3] ILs are dubbed “designer” solvents as a result of the finely tuned organization, which garner these materials.[7, 3] In this regard, polymeric ionic liquids (PILs) emerge as an example of task-specific ionic liquids, which encompass the properties of ILs as well as the mechanical stability, improved durability, dimensional control, and processability of polymers.[4-5] PILs are ionic liquids with the monomer anion or cation as the recurring entity; these materials are usually formed by polymerization of either the alkene (*i.e.*, vinyl) or the acrylate functional group linked to imidazolium or ammonium structure in the IL monomer.[11] Recently, the potential applications of PILs as polymer electrolytes,[6] CO_2 sorbents,[7-8] and dispersing agents,[9] have garnered attention toward preparing these polymers at the meso/nanoscale level.[10-11]

The group of uniform materials based on organic salts (GUMBOS) has been introduced into scientific literature as an ensemble of organic salts which exhibit the properties of ILs but show higher melting points ranging from 25 °C to 250 °C.[12] The flexible design of a GUMBOS promotes the production of polymeric nanoparticles (*i.e.,* polymeric nanoGUMBOS) for task-specific applications, depending on the choice of cation and anion structures. Hence, polymeric nanoGUMBOS offer a potential use in drug

cargo and delivery[13] or as a binder in Li-ion battery electrodes,[14] in view of the dimensionality and physical stability of these materials.

Gamma irradiation has been widely used as a tool for polymers photo-crosslinking.[15-17] Inter- and intra-crosslinking were observed in polymers produced by this method.[18] Gamma irradiation is more advantageous than other irradiation techniques in terms of the deep penetrability, the temperature independence, and the needless presence of an initiator in the system.[18] Thus, this approach has been implemented for the preparation of micro/nanogels,[19-21] nanolatices,[18] and nanocomposites.[22-24]

To the best of our knowledge, synthesis of polymeric nanoGUMBOS using gamma irradiation has not been previously explored. In this study, four imidazolium-based ionic liquids, were polymerized at the nanoscale level by means of the gamma-ray radiation. The formed polymeric nanoparticles were then loaded with the fluorescein sodium salt to study the potential of these materials as drug carriers. Transmission electron microscopy (TEM) and fourier transform infrared (FTIR) spectroscopy were used to characterize the polymeric nanoGUMBOS, while fluorescence microscopy was employed to evaluate the loading capacity of the nanoparticles.

4.2. Experimental Section

4.2.1. Materials

(PEG), alkane, and alkyne ionic liquids coupled with NTf_2 counteranion, were received from Dr. Doug Gin and Dr. Richard D. Noble laboratory at the University of Colorado, Boulder. The anion in these ionic liquids was exchanged with Cl^- using an anion exchange column (detailed information are in Chapter Three). Heptane anhydrous (99%), sodium bis(2-ethylhexyl) sulfosuccinate (NaAOT), as well as 2,2′-Azobis(2-methylpropionitrile) (AIBN) were purchased from Sigma Aldrich (St. Louis, MO) and used

as received. Ultrapure water (18.2 MΩ cm) was obtained from an Elga model PURELAB ultra water filtration system.

4.2.2. Characterization Techniques

4.2.2.1. Melting Point Determination

To acquire the melting point data, a DigiMelt MPA 160 from SRS (Sunnyvale, CA) was used. The clear point was reported as the samples melting point.

4.2.2.2. Fourier Transform Infrared (FTIR)

The organic solvent was first removed from the polymerized nanoGUMBOS suspensions using a rotary evaporator. The formed pellet was then lyophilized and deposited on an ATR cell in a Bruker Tensor 27 instrument (Billerica, MA). The background signal of the surfactant was subtracted from the sample spectrum (signal of polymeric nanoGUMBOS).

4.2.2.3. Transmission Electron Microscopy (TEM)

Transmission electron micrographs were obtained using a JEOL JEM-1011 TEM (München, Germany). An 8 µL volume of sample was spotted onto ultrathin carbon coated 400-mesh Ted Pella, Inc TEM grids (Redding, CA). The grids were washed with water and heptane for nanoparticles synthesized in water-in-oil microemulsion to avoid any unwanted adsorption of unpolymerized monomers and surfactant. However, the grids were only washed with heptane when imaging the monomers.

4.2.3. Synthesis of Polymeric NanoGUMBOS

A monomeric aqueous solution (0.2 M) was dispersed, under magnetic stirring, in a water-in-oil microemulsion in presence of the surfactant NaAOT (100 µL of water per 5 mL of heptane). The solution was then exposed to gamma irradiation, provided by a ^{60}Co

source (Nuclear Science Department, LSU), for 1 to 5 days. The dose rate provided by the gamma source was estimated around 500 cGy/min.

4.2.4. Encapsulation of Fluorescein Sodium Salt

Fluorescein sodium salt (3.5 mg) was dissolved in a 100 µL volume of aqueous monomeric solution (0.2 M). This solution was then added to a 5 mL of heptane; the mixture was magnetically stirred for 30 min and exposed to gamma irradiation for two days. A few drops of the sample were then spotted on a glass slide which was rinsed with deionized water to remove the excess of dye before imaging with a fluorescence microscope (Leica DM RXA2, Germany).

4.3. Results and Discussion

The ILs, which are included in this study, present distinctive spacer groups, incorporated between two vinylimidazoles (Figure 4.1). (PEG) monomer, a room temperature ionic liquid (RTIL), is highly viscous; however, alkane and alkyne monomers are solid salts, *i.e.,* GUMBOS, with melting points of 46 °C and 51 °C respectively.

The dosage of gamma rays used for polymerization was optimized by fixing the exposure time of water-in-oil monomer emulsions to irradiation. To monitor the effect of radiation on the nanoparticles average size, TEM microscopy was employed. An analysis of the system was conducted before and after irradiation to identify the mechanism of polymerization taken place. TEM micrographs show a decrease in average size of the materials when comparing prior to and following the irradiation of monomers (Figure 4.2). After two days of exposure to gamma rays, the average size of the materials was reduced from 682 to 283 nm, 766 to 239 nm, and 2287 to 346 nm for (PEG), alkane, and alkyne

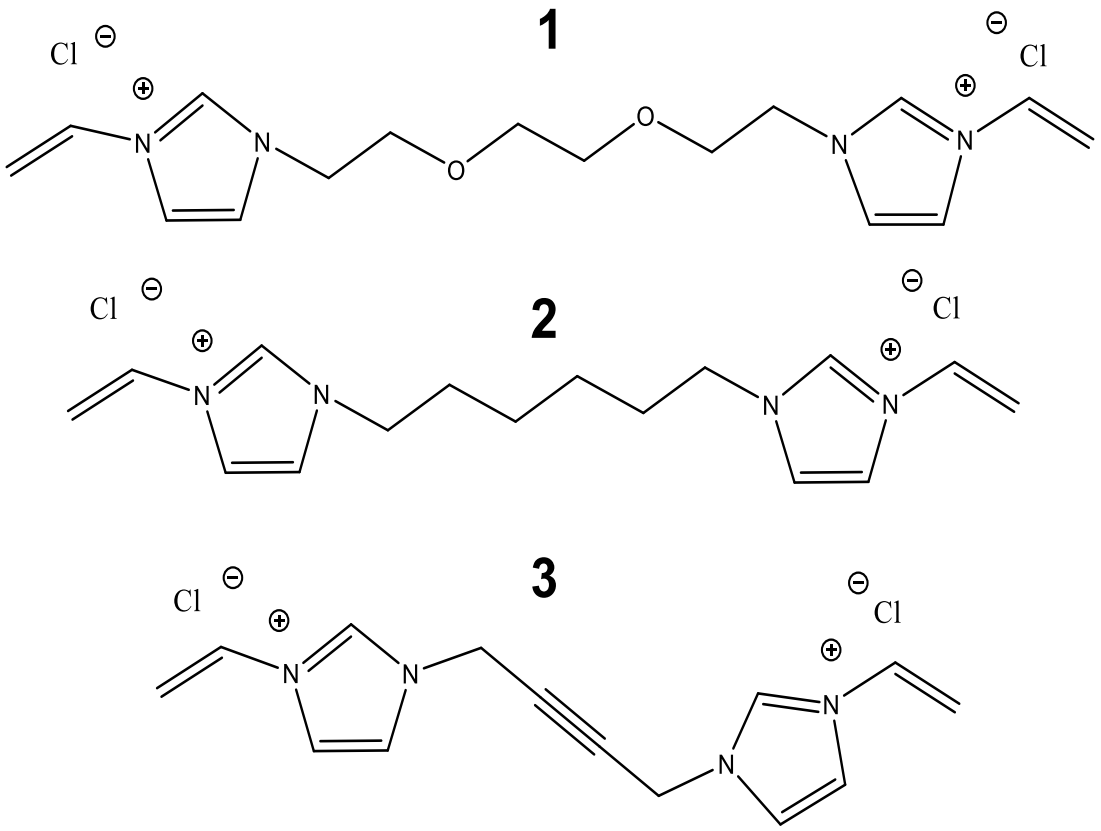

Figure 4.1. Structures of (1) (PEG), (2) alkane, and (3) alkyne ILs monomers.

monomers, respectively. These observations suggest that the nucleation of nanoGUMBOS initiates externally to the monomers droplets and proceeds until the total consumption of monomers.[25] In this scenario, large monomer droplets which are stabilized by the surfactant, and empty surfactant micelles are present in the medium before irradiation. During the emulsion polymerization, the monomer species diffuse to the micelle entity and promote the cross-linking and growth of nanoparticles (Scheme 4.1).[16] The average sizes of the polymeric nanoparticles formed after the first and second day of irradiation, were not significantly different (Table C1 in Appendix C), which implies

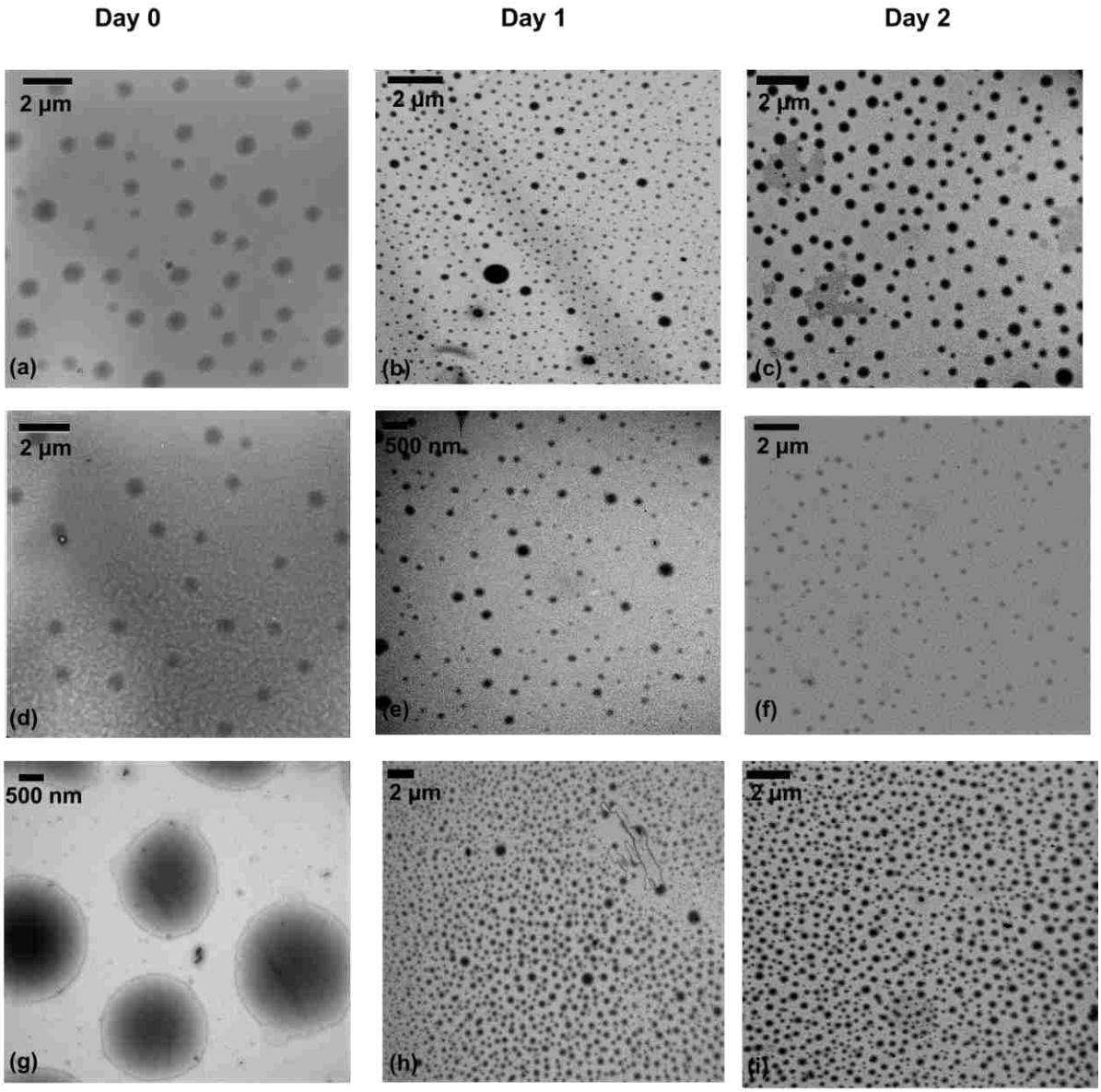

Figure 4.2. TEM micrographs for (a-c) (PEG), (d-f) alkane, and (g-i) alkyne monomers before and after gamma irradiation.

that two days irradiation is totally sufficient for the synthesis of stable nanoparticles. Further studies were also performed after five days irradiation to perceive any change in size or morphology of the synthesized nanoparticles (Figure C1 in Appendix C).

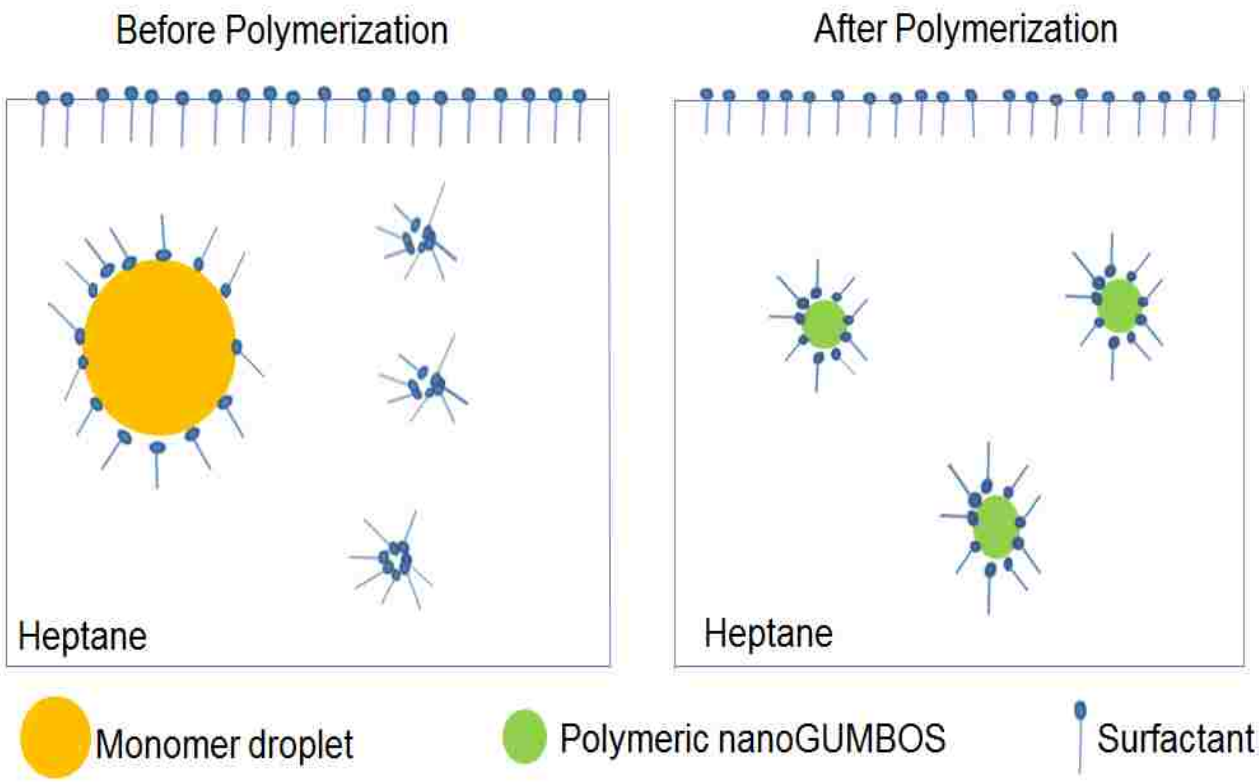

Scheme 4.1. Mechanism of emulsion polymerization: ILs monomers (a) prior and (b) post polymerization.

Moreover, FTIR spectra were collected before and after irradiating for two days the monomer solutions with gamma rays (Figure 4.3). The disappearance or reduction of the peak at 900 cm^{-1} (=C-H bending) and 3110 cm^{-1} (=C-H stretching) confirms the conversion of the carbon double bond into a single bond and the cross-linking of the monomers.[26] Furthermore, the increase in peak intensity at a wavenumber slightly before 3000 cm^{-1} indicates the formation of a new single C-C bond. The intensities of the peaks are compared to that of the standard peak at 1550 cm^{-1}, which is unaffected neither by the polymerization process or the subtraction of the surfactant signal.

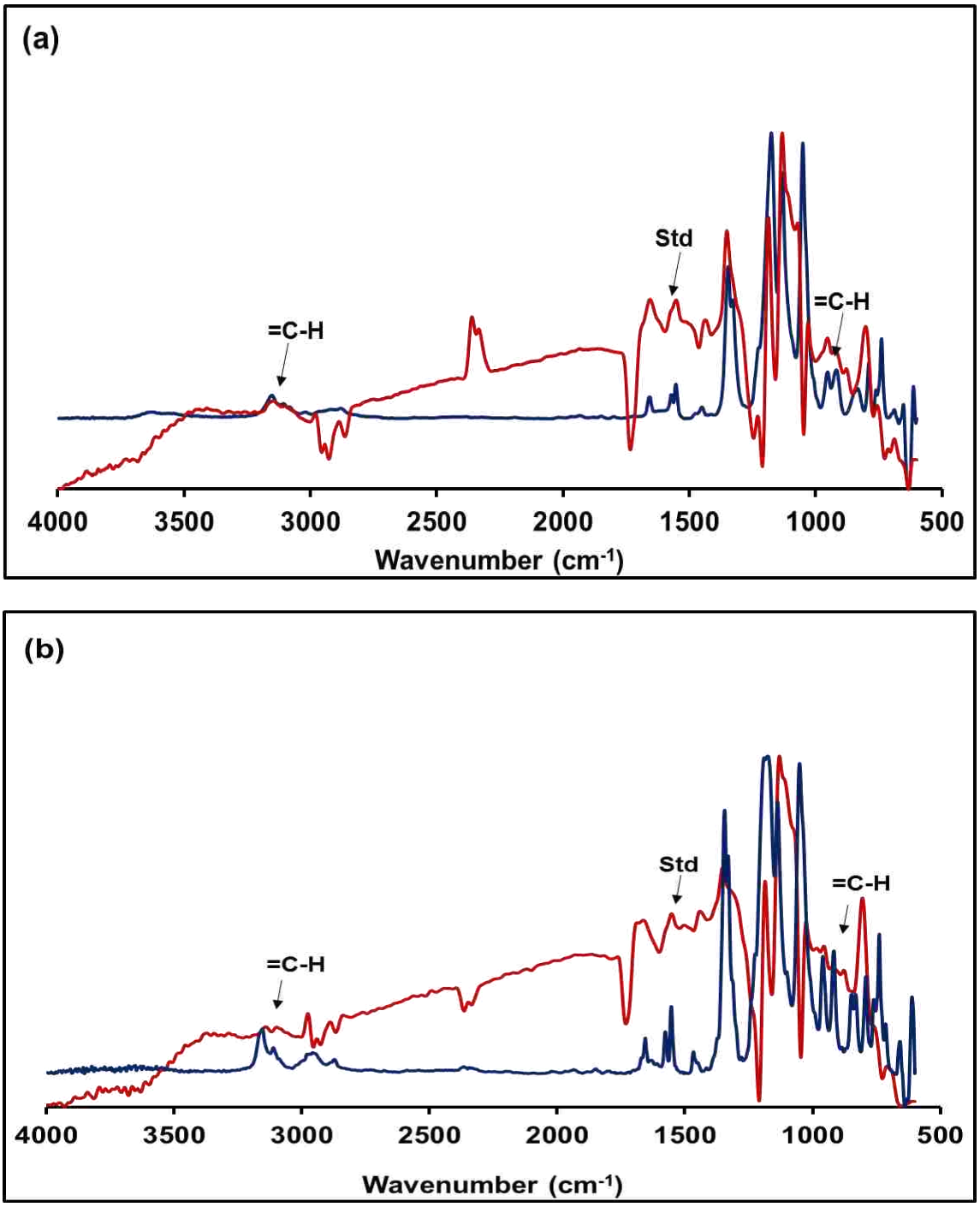

Figure 4.3. FTIR spectra (absorbance mode) of (a) (PEG), (b) alkane, (c) alkyne IL monomers (blue line) and polymeric nanoGUMBOS (red line).

(Figure continued)

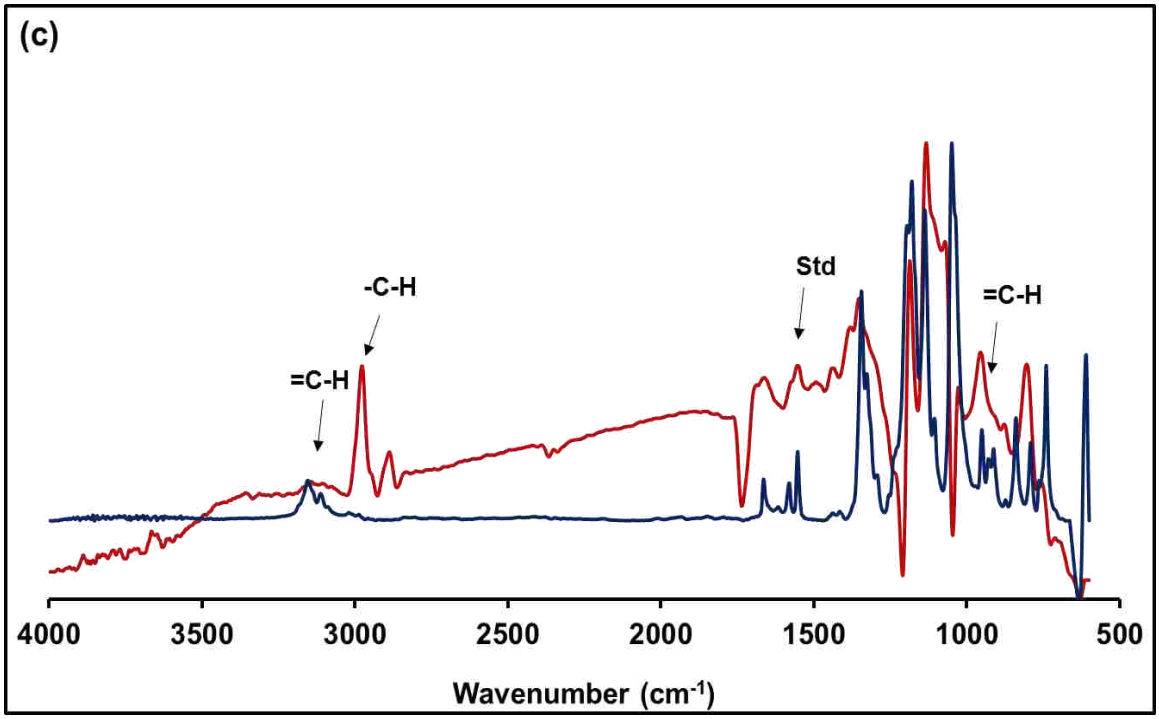

Next, the capacity of the crosslinked polymeric nanoGUMBOS to embrace hydrophilic dyes was evaluated and fluorescein sodium salt was solubilized in the microemulsions prior to irradiation. Dye encapsulation in the quasi-spherical structures was confirmed using fluorescence microscopy (Figure 4.4). The differential interference contrast (DIC) images display the presence of spherical aggregates (*i.e.,* the nanoparticles), whereas fluorescence microscopy images depict the dye encapsulated inside these structures. The three types of polymeric nanoparticles had distinct amounts of encapsulated fluorescein dye, with alkyne nanoparticles showing the lowest level of bound dye as designated by the high background fluorescence in Figure 4.4e.[27] Various kinds of interactions with the dye (ionic, polar, non-polar) were exhibited by the ionic liquids polymers, considering the tunable nature of these compounds. However, for the

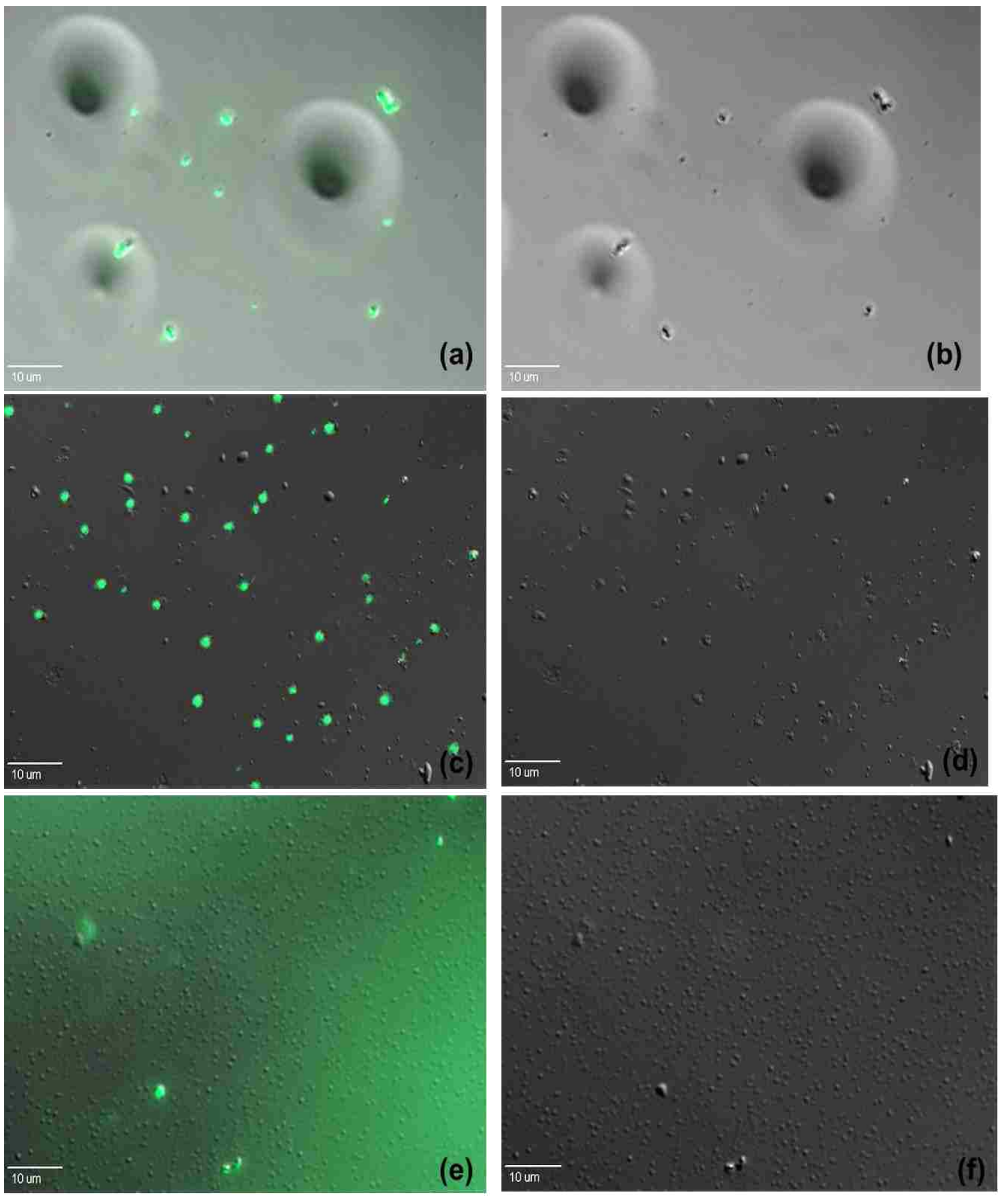

Figure 4.4. Fluorescence and differential interference contrast (DIC) images of (a-b) (PEG), (c-d) alkane, and (e-f) alkyne polymeric nanoparticles encapsulating fluorescein sodium salt (green emission).

alkyne polymers, the presence of the triple bond short spacer limited the accessible interactions with fluorescein sodium salt. This limitation was not encountered in the alkane monomer where the length and flexibility of the hydrocarbon chain increase the points of interactions with the dye and subsequently the encapsulation efficiency.

4.4. Conclusions

(PEG), alkane, and alkyne vinylimidazolium ionic liquids were successfully polymerized at the nanoscale level by gamma irradiation. With different spacer groups between the vinylimidazole, these ionic liquids exhibited distinct tunable properties. The polymeric nanoGUMBOS were formed as a result of an emulsion polymerization mechanism. After two days of gamma irradiation, the average sizes of (PEG), alkane, and alkyne nanoparticles were 283, 239, and 346 respectively. These nanoparticles showed a high propensity to encapsulate the hydrophilic dye fluorescein sodium salt except for alkyne nanoGUMBOS which present a short rigid spacer that restricts the intermolecular interactions with the dye. Overall, polymeric nanoGUMBOS pertains to a new category of tunable polymeric nanomaterials which, according to this study, has shown potential use in drug delivery applications.

4.5. References

1. Plechkova, N. V.; Seddon, K. R. Applications of Ionic Liquids in the Chemical Industry. *Chem. Soc. Rev.* **2008,** *37* (1), 123-150.

2. Welton, T. Room-Temperature Ionic Liquids. Solvents for Synthesis and Catalysis. *Chem. Rev.* **1999,** *99* (8), 2071-2083.

3. Zhang, S. J.; Sun, N.; He, X. Z.; Lu, X. M.; Zhang, X. P. Physical Properties of Ionic Liquids: Database and Evaluation. *J. Phys. Chem. Ref. Data* **2006,** *35* (4), 1475-1517.

4. Green, O.; Grubjesic, S.; Lee, S.; Firestone, M. A. The Design of Polymeric Ionic Liquids for the Preparation of Functional Materials. *Polym. Rev.* **2009,** *49* (4), 339-360.

5. Amarasekara, A. S.; Shanbhag, P. Synthesis and Characterization of Polymeric Ionic Liquid Poly(Imidazolium Chloride-1,3-Diylbutane-1,4-Diyl). *Polym. Bull.* **2011,** *67* (4), 623-629.

6. Yoshizawa, M.; Ohno, H. Molecular Brush Having Molten Salt Domain for Fast Ion Conduction. *Chem. Lett.* **1999,** (9), 889-890.

7. Zhao, Q.; Wajert, J. C.; Anderson, J. L. Polymeric Ionic Liquids as CO_2 Selective Sorbent Coatings for Solid-Phase Microextraction. *Anal. Chem.* **2010,** *82* (2), 707-713.

8. Tang, J. B.; Sun, W. L.; Tang, H. D.; Radosz, M.; Shen, Y. Q. Enhanced CO_2 Absorption of Poly(Ionic Liquid)S. *Macromolecules* **2005,** *38* (6), 2037-2039.

9. Marcilla, R.; Curri, M. L.; Cozzoli, P. D.; Martinez, M. T.; Loinaz, I.; Grande, H.; Pomposo, J. A.; Mecerreyes, D., Nano-Objects on a Round Trip from Water to Organics in a Polymeric Ionic Liquid Vehicle. *Small* **2006,** *2* (4), 507-512.

10. Yuan, J.; Antonietti, M. Poly(Ionic Liquid) Latexes Prepared by Dispersion Polymerization of Ionic Liquid Monomers. *Macromolecules* **2011,** *44* (4), 744-750.

11. Tokuda, M.; Minami, H.; Mizuta, Y.; Yamagami, T. Preparation of Micron-Sized Monodisperse Poly(Ionic Liquid) Particles. *Macromol. Rapid Commun.* **2012,** *33* (13), 1130-1134.

12. Warner, I. M.; El-Zahab, B.; Siraj, N., Perspectives on Moving Ionic Liquid Chemistry into the Solid Phase. *Anal. Chem.* **2014,** *86* (15), 7184-7191.

13. Reis, C. P.; Neufeld, R. J.; Ribeiro, A. J.; Veiga, F. Nanoencapsulation I. Methods for Preparation of Drug-Loaded Polymeric Nanoparticles. *Nanomedicine: Nanotechnology, Biology and Medicine* **2006,** *2* (1), 8-21.

14. von Zamory, J.; Bedu, M.; Fantini, S.; Passerini, S.; Paillard, E. Polymeric Ionic Liquid Nanoparticles as Binder for Composite Li-Ion Electrodes. *J. Power Sources* **2013,** *240*, 745-752.

15. Ulanski, P.; Janik, I.; Rosiak, J. M. Radiation Formation of Polymeric Nanogels. *Radiat. Phys. Chem.* **1998,** *52* (1-6), 289-294.

16. Ortega, A.; Bucio, E.; Burillo, G. New Interpenetrating Polymer Networks of N-Isopropylacrylamide/N-Acryloxysuccinimide: Synthesis and Characterization. *Polym. Bull.* **2008,** *60* (4), 515-524.

17. Rosiak, J. M.; Janik, I.; Kadlubowski, S.; Kozicki, M.; Kujawa, P.; Stasica, P.; Ulanski, P. Nano-, Micro- and Macroscopic Hydrogels Synthesized by Radiation Technique. *Nuclear Instruments & Methods in Physics Research Section B-Beam Interactions with Materials and Atoms* **2003,** *208*, 325-330.

18. Melendez-Ortiz, I.; Flores-Martinez, R.; Bucio, E.; Cortez-Mazatan, G.; Martinez-Gutierrez, H.; Peralta, R. D., Crosslinking of Poly(Vinyl Acetate) Nanolatices by Gamma and UV Radiation. *J. Appl. Polym. Sci.* **2012,** *126* (4), 1328-1336.

19. Chen, Q. D.; Shen, X. H.; Gao, H. C. One-Step Synthesis of Silver-Poly(4-Vinylpyridine) Hybrid Microgels by Gamma-Irradiation and Surfactant-Free Emulsion Polymerization. *Acta Polym. Sin.* **2006,** (5), 722-726.

20. Melendez-Ortiz, H. I.; Peralta, R. D.; Bucio, E.; Zerrweck-Maldonado, L. Preparation of Stimuli-Responsive Nanogels of Poly 2-(Dimethylamino) Ethyl Methacrylate by Heterophase and Microemulsion Polymerization Using Gamma Radiation. *Polym. Eng. Sci.* **2014,** *54* (7), 1625-1631.

21. Abd El-Rehim, H. A.; Hegazy, E. S. A.; Hamed, A. A.; Swilem, A. E., Controlling the Size and Swellability of Stimuli-Responsive Polyvinylpyrrolidone-Poly(Acrylic Acid) Nanogels Synthesized by Gamma Radiation-Induced Template Polymerization. *Eur. Polym. J.* **2013,** *49* (3), 601-612.

22. Huang, Z. H.; Shi, L.; Zhu, Q. R.; Zou, J. T.; Chen, T., Fabrication of Polyaniline/Silver Nanocomposite under Gamma-Ray Irradiation. *Chin. J. Chem. Phys.* **2010,** *23* (6), 701-706.

23. Yoon, S.-K.; Byun, B.-S.; Lee, S.; Choi, S.-H. Radiolytic Synthesis of Poly(Styrene-Co-Divinylbenzene)–Clay Nanocomposite. *J. Ind. Eng. Chem.* **2008,** *14* (4), 417-422.

24. Lu, C. L.; Cheng, Y. R.; Liu, Y. F.; Liu, F.; Yang, B. A Facile Route to Zns-Polymer Nanocomposite Optical Materials with High Nanophase Content Via Gamma-Ray Irradiation Initiated Bulk Polymerization. *Adv. Mat.* **2006,** *18* (9), 1188-1192.

25. Arshady, R. Suspension, Emulsion, and Dispersion Polymerization - a Methodological Survey. *Colloid Polym. Sci.* **1992,** *270* (8), 717-732.

26. Svatos, A.; Attygalle, A. B. Characterization of Vinyl-Substituted, Carbon-Carbon Double Bonds by GC/FT-IR Analysis. *Anal. Chem.* **1997,** *69* (10), 1827-1836.

27. Helwa, Y.; Dave, N.; Liu, J. W. Electrostatically Directed Liposome Adsorption, Internalization and Fusion on Hydrogel Microparticles. *Soft Matter* **2013,** *9* (26), 6151-6158.

CHAPTER FIVE
ENHANCEMENT OF CARBAZOLE-BASED NANOGUMBOS INTRINSIC QUANTUM YIELDS FOR POTENTIAL APPLICATION IN BLUE ORGANIC LIGHT EMITTING DEVICES

5.1. Introduction

Trends in current scientific research focus on the exploration of novel materials which enhance the performance of solid state-based lighting devices.[1-2] These light emitting diodes (LEDs) offer a high efficiency and a decrease in power consumption compared to traditional types of lighting such as fluorescent and incandescent lamps.[1] In this regard, organic light emitting diodes (OLEDs) are particularly promising as these devices are usually less expensive and more environmentally friendly than inorganic light emitting diodes.[3-4] For these reasons, it is expected that OLEDs will become the foundation of the next lighting generation.[5]

OLEDs, emitting primary colors (red, green, blue), are key components for the production of white light. Yet unlike red and green OLEDs, the fabrication of blue OLEDs with high external efficiency was proven difficult.[6] In the past decade, several compounds with enhanced electroluminescence efficiencies were investigated for potential application in blue OLEDs.[6] Fluorine and p-phenylene-based polymers were extensively explored for the use in OLEDs.[7-8] Moreover, organic compounds with π conjugated systems such as polyphenylenevinylenes (PPV) and oligophenylenevinylenes (OVP) were considered excellent materials for blue emission.[9] Carbazole-based compounds, as well as anthracene-based compounds were also synthesized for blue light emission.[10-11] With successful implementation of the primary colors, arrays of OLEDs can generate a full display of colors, and are amenable to applications in electronic devices .[6]

Fluorescent nanomaterials are considered important components for generating highly efficient LEDs. The ease of tuning the optical and physical properties in accordance with the size, morphology, and structure made these nanomaterials desirable for LED fabrication.[12] On this matter, inorganic semiconductor nanoparticles have been the focus of much research.[13] However, unlike inorganic counterparts, organic nanoparticles have been less thoroughly investigated as fluorescent materials in OLEDs.[14] Therefore, the applicability of fluorescent organic nanoparticles (FONs) in OLEDs is highly intriguing, especially organic semiconductors which usually exhibit high luminescence, and are considered useful for optoelectronics applications.[15] In this regard, a new class of materials, *i.e.,* nanoGUMBOS, has been sought as emissive materials in OLEDs. These nanoparticles are derived from a group of uniform materials based on organic salts (GUMBOS) which possess similar properties to those of ionic liquids but have a melting point ranging from 25 to 250 °C. NanoGUMBOS present a flexible design with tunable physical and chemical properties determined by the multiple anion and cation combinations.[16] Hence, the physical, optical, and electronic properties can be easily modified in these organic compounds.[17-23] In addition, nanoGUMBOS have found ground in diverse applications including analytical, biological, and technological fields.[24-27] Luminescent nanoGUMBOS have also been reported by Dumke *et al.,* which afford these nanoparticles as interesting emitting materials to be integrated in OLEDs.[23]

There are several factors that affect the performance of a light emitting device. Luminescence quantum yield is one of the parameters which plays a key role in affecting OLED efficiency.[2, 28] This value is defined as the ratio of the number of photons emitted to the number of photons absorbed per unit time (Equation 4.1).[2]

$$\Phi = \frac{\text{Number of photons emitted}}{\text{Number of photons absorbed}} \quad (1)$$

For application in OLEDs, synthesis of organic nanoparticles with high internal quantum yield is considered challenging.[29] Only a few strategies have been reported to enhance the quantum yield of organic nanomaterials in blue OLEDs. For example, the quantum yield of a poly(2,7-(9,9'-dioctylfluorene)-co-4-diphenylamino-4'-biphenylmethylsulfide) was enhanced up to 86% when this polymer was bound to gold nanoparticles.[30] A plasma-induced technique was used to generate fluorescent carbon dots with a quantum yield of 6%; the fluorescence intensity of these carbon dots was enhanced by increasing the plasma energy.[31]

Herein, we introduce several strategies to synthesize nanoparticles derived from carbazole-based GUMBOS, which were previously reported by Siraj *et al.* as efficient materials for blue OLEDs.[32] Size effects and doping with the transition metal Cu^{2+} were investigated to tune the optical properties and enhance the quantum yield of nanoparticles. The syntheses were also optimized to improve the intrinsic quantum yield of the carbazole-based nanoGUMBOS, which was dependent on the synthesis conditions and the molar ratio of dopant to host.

5.2. Experimental Section

5.2.1. Materials

Carbazole-based GUMBOS were synthesized following the same procedure published by Siraj *et al*.[32] The structures are revealed in Figure 5.1. The GUMBOS are composed of a carbazoleimidazole-based cation and three different anions: iodide ([I]),

trifluoromethanesulfonate ([OTf]), and bis(pentafluoroethylsulfonyl)imide ([BETI]). The compounds 2-hydroxypropyl-β-cyclodextrin (MS = 0.6 and 0.8) as well as copper sulfate were purchased from Sigma Aldrich (St. Louis, MO) and used as received. Ultrapure water (18.2 MΩ cm) was obtained from an ARIES High Purity Water System.

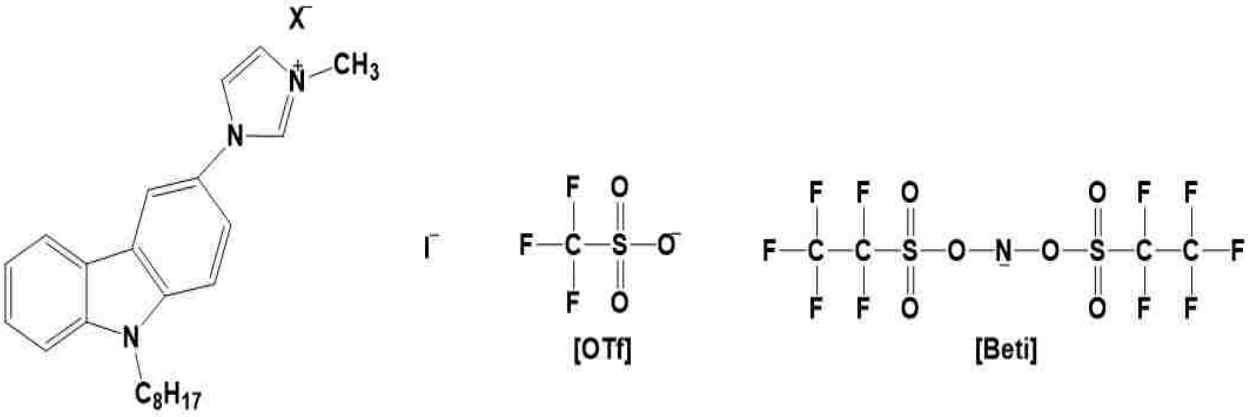

Figure 5.1. Chemical structures of the carbazole-based GUMBOS coupled with different counteranions.

5.2.2. Synthesis of Carbazole-Based NanoGUMBOS

5.2.2.1. Reprecipitation

To a 5 mL of filtered deionized water, 100 µL of ethanolic solution (1 mM) of carbazole compound was added under ultrasonication, produced by an ultrasonic processor, Model VC-750 from SONICS (Newton, CT). The ultrasonication was continuous and lasted for 5 minutes at a 25% amplitude. Nanoparticles suspensions were allowed to stabilize for 30 minutes before any further studies.

5.2.2.2. Reprecipitation in Presence of 2-Hydroxypropyl-β-cyclodextrin

To a mixture of 4.6 mL of filtered distilled water and 400 µL of 2HP-β-CD solution (0.2 mg/mL), a volume of 100 µL ethanolic solution of carbazole compound (1 mM) was

added under ultrasonication. The same experimental conditions were used as described above in the reprecipitation method.

5.2.3. Synthesis of Doped Carbazole-Based NanoGUMBOS

A specific amount of 0.1 mM copper sulphate aqueous solution (100 µL, 200 µL, 300 µL) and a 100 µL volume of carbazole ethanolic solution (1 mM) were added to a filtered deionized water under ultrasonication; the total volume was kept at 5.1 mL. After 5 min of ultrasonication, the doped nanoparticles were allowed to grow and age for 30 minutes.

5.2.4. Characterization of NanoGUMBOS

5.2.4.1. Transmission Electron Microscopy

Transmission electron microscopy was the technique used for measuring the size of nanoGUMBOS. TEM micrographs were obtained using a JEOL JEM-1011 TEM (München, Germany). A volume of 8 µL nanoGUMBOS sample was drop-casted onto ultrathin carbon-coated 400-mesh Ted Pella, Inc TEM grids (Redding, CA). The grids were washed with water to remove any unwanted adsorption of additives.

5.2.4.2. Optical Studies

Absorbance measurements were performed in Varian spectrophotometer cells of 1 cm path length using a UV-Vis-NIR scanning spectrophotometer, (Shimadzu, Columbia, MD). Fluorescence measurements were obtained using a Fluorolog-3 spectrofluorometer (Horiba Scientific, Edison, NJ) and performed in a quartz fluorescence cell (Sterna Cells Atascadero, CA) with 0.4 cm path length. Absolute quantum yields measurements were measured using an integrating sphere, in a Horiba Scientific Quanta φ accessory (150

mm diameter) coupled to the Fluorolog-3 spectrofluorometer (Horiba Scientific, Edison, NJ). For both fluorescence and quantum yields measurements, [Cl][I] and [Cl][OTf] nanoGUMBOS suspensions were diluted by adding a volume of 5 mL of deionized water before analysis. This procedure was implemented to avoid possible inner-filter effects caused by the high absorbance intensity in these samples. [Cl][BETI] nanoGUMBOS were also diluted in a similar procedure prior fluorescence measurements only, for a better illustration and comparison of data.

5.3. Results and Discussion

5.3.1. Syntheses and Optical Properties of Carbazole-Based NanoGUMBOS

Carbazole-based nanoGUMBOS had different average sizes and agglomeration levels, depending on the synthetic approaches (Figure 5.2). For [Cl][I] nanoGUMBOS, the size of nanoparticles significantly decreased in the presence of the template, 2HP-β-CD, from 204 ± 65 nm down to 77 ± 7 nm (2HP-β-CD, MS 0.6) and 101 ± 17 nm (2HP-β-CD, MS 0.8). [Cl][OTf] nanoparticles that were synthesized using a free ultrasonication method, had an average size of 147 ± 17 nm. However, the templated 2HP-β-CD (MS 0.6)-assisted ultrasonication method resulted in the formation of nanoGUMBOS with an average size 49 ± 9 nm, whereas, 2HP-β-CD (MS 0.8)-assisted ultrasonication produced a larger average size of 201 ± 62 nm. In case of [Cl][BETI] compound, the presence of cyclodextrin-derivative template caused an attenuation in the aggregation level. The average sizes of nanoparticles for this compound were 75 ± 15 nm and 86 ± 15 nm in presence of 2HP-β-CD, MS 0.6 and 0.8, respectively. The size-dependence of nanoGUMBOS in the presence of 2HP-β-CD template confirms that the template directs

the assembly of these ionic structures, prior to the nucleation and growth mechanisms. The templating effect of 2HP-β-CD was also reported for other types of nanoparticles, such as silver nanoparticles and copper sulfide nanoparticles.[33-34] Supplementary potential measurements on nanoparticles formed from a reprecipitation method, show that [CI][I] suspensions are the most stable (highest magnitude) and [CI][OTf] the least stable (value closest to zero) in aqueous media (Figure D1 in Appendix D).

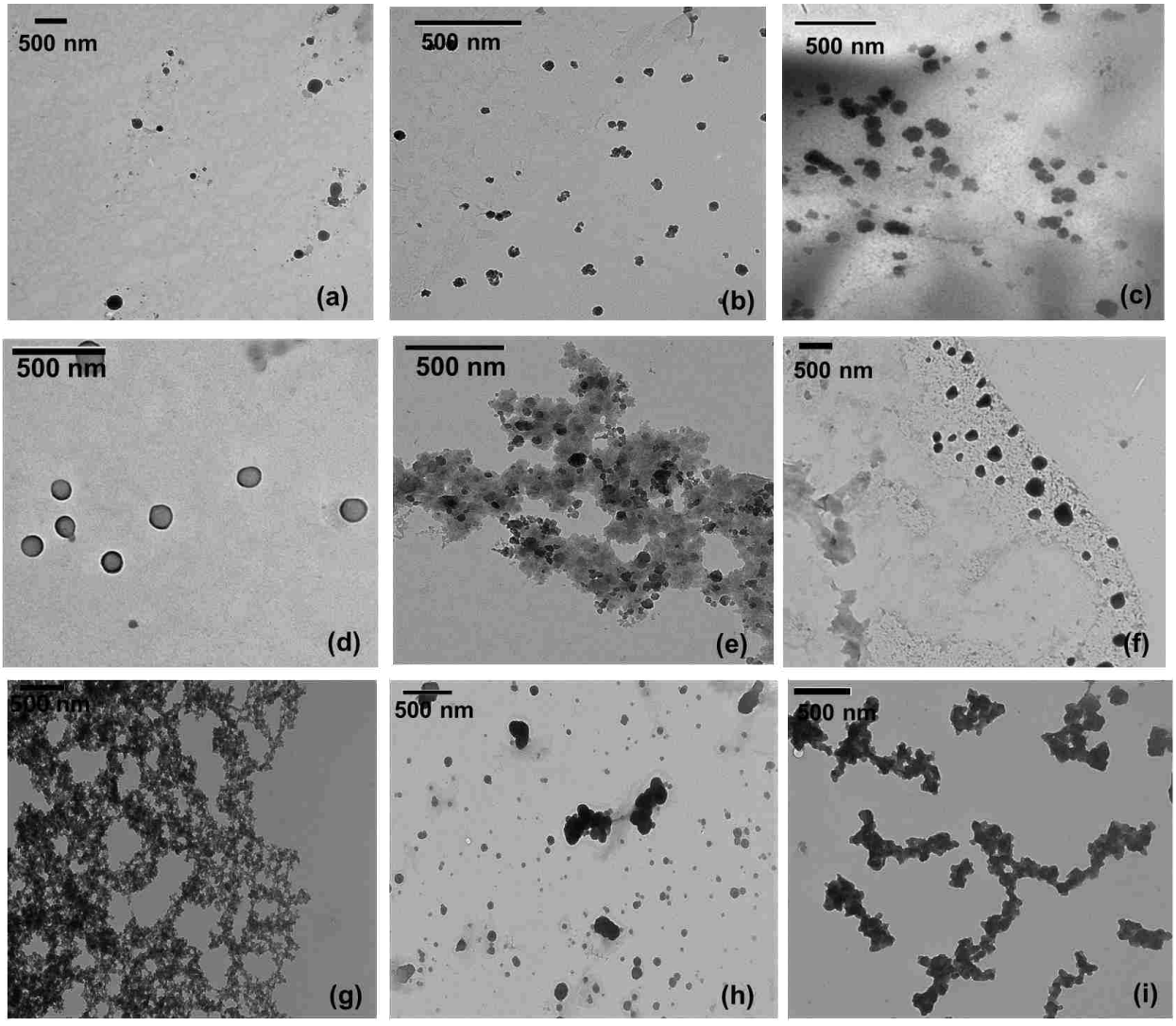

Figure 5.2. TEM micrographs of [CI][I] (a-c), [CI][OTf] (d-f), and [CI][BETI] (g-i) nanoGUMBOS prepared using the free-templated ultrasonication method (a, d, g), the 2HP-β-CD-assisted ultrasonication with molecular substitution 0.6 (b, e, h), and the 2HP-β-CD-assisted ultrasonication with molecular substitution 0.8 (e, f, i).

All nanoGUMBOS suspensions exhibited four distinctive absorbance bands in the spectral region between 220 and 360 nm (Figure 5.3). The distinct values of absorbance wavelengths are reported in Table 4.1. The peaks at wavelengths λ_2 and λ_3 resulted from the absorption transitions of carbazoleimidazolium cation to the second and first excited states, respectively (Table 5.1).[35] All the reported absorbance peaks were due solely to the cation transitions; however, the relative intensities of these peaks varied with the type of anion. This effect was mainly proved in the case of [CI][BETI], where a significant decrease in absorbance intensity was observed when compared to [CI][I] and [CI][OTf] nanoGUMBOS measurements. The decrease in absorbance suggests a difference in correlation between the associated species (anion-cation and cation-cation pairs).

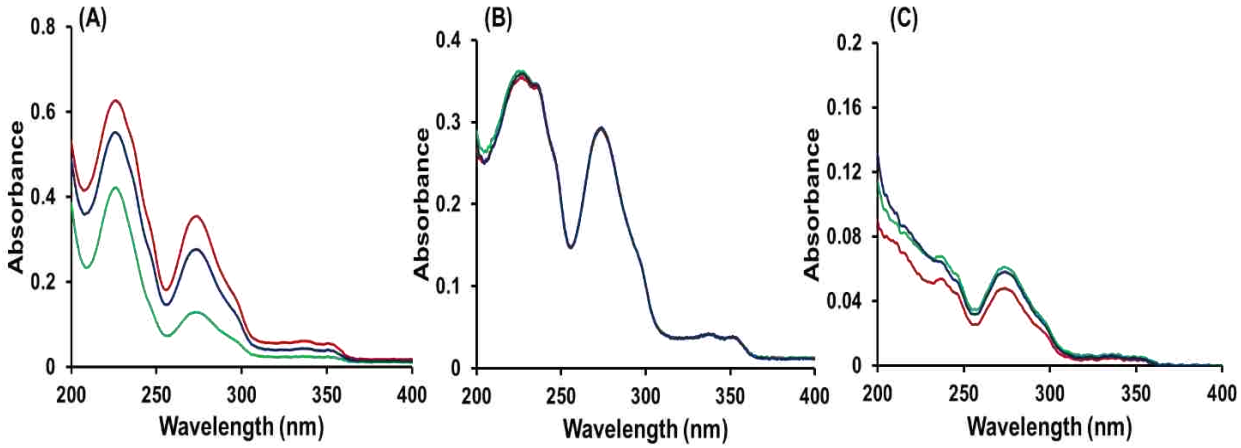

Figure 5.3. Absorbance Spectra of (A) [CI][I], (B) [CI][OTf], (C) [CI][BETI] nanoGUMBOS synthesized using three different procedures: ultrasonication probe (red line); ultrasonication probe with the template 2HP-β-CD (MS:0.6) (green line) and the template 2HP-β-CD (MS:0.8) (blue line). The final concentration of nanoGUMBOS suspension was equal to 0.02 mM.

In addition, as depicted in the absorbance spectra of the nanoGUMBOS, a shoulder appeared at 297 nm suggesting the presence of multiple excited states.[32] Furthermore, the absorbance of the nanomaterials suspensions was affected by the size of

nanoGUMBOS. An increase in the absorbance value was associated with large sized [CI][I] nanoGUMBOS, which can be explained by the expansion of the nanoparticle cross-section exposed to the light upon increasing the size of nanoGUMBOS. For [CI][OTf] nanoGUMBOS, the absorbance was size-independent as a possible result of the structural orientation (*i.e.,* conformation) of the anion around the cation. This independence was not observed in the case of [CI][BETI] where the agglomeration level of nanoparticles was the main factor affecting the molar extinction which decreased with increasing the intermolecular electronic interactions upon aggregation.[36]

Table 5.1. Absorbance wavelengths for [CI][I], [CI][OTf], and [CI][BETI] nanoGUMBOS synthesized using three different approaches.

	Ultrasonication				Ultrasonication with 2-HP-β-CD MS 0.6				Ultrasonication with 2-HP-β-CD MS 0.8			
	λ_1	λ_2	λ_3	λ_4	λ_1	λ_2	λ_3	λ_4	λ_1	λ_2	λ_3	λ_4
[CI][I]	226	273.5	335	350.5	226	274	335	350	226	273	335.5	350.5
[CI][OTf]	227	273.5	339	350	227.5	273.5	337	351.5	227.5	274	337.5	351.5
[CI][BETI]	237	274	336	349	237	274	336	349	236	274	336	349

The fluorescence studies of nanoGUMBOS suspensions showed an emission at two different wavelengths when excited at 275 nm (Figure 5.4). The strong fluorescence at the longer wavelength is due to the emission from first excited singlet state while the less intense fluorescence emission at shorter wavelength resulted from second excited singlet state. All the nanoGUMBOS coupled with different anions presented emissions at

the same wavelengths as shown in Table 5.2. However, the suspensions showed almost a twofold enhancement of fluorescence whenever the nanoGUMBOS were synthesized in the presence of 2HP-β-CD template. This enhancement is related to the presence of 2HP-β-CD which stabilizes the suspensions and eventually decreases the non-radiative decays caused by environmental quenching.[37] Moreover, the modification of the synthetic approach might have caused the formation of nanoaggregates with an intramolecular planarization conformation state causing eventually an increase in fluorescence intensity.[38]

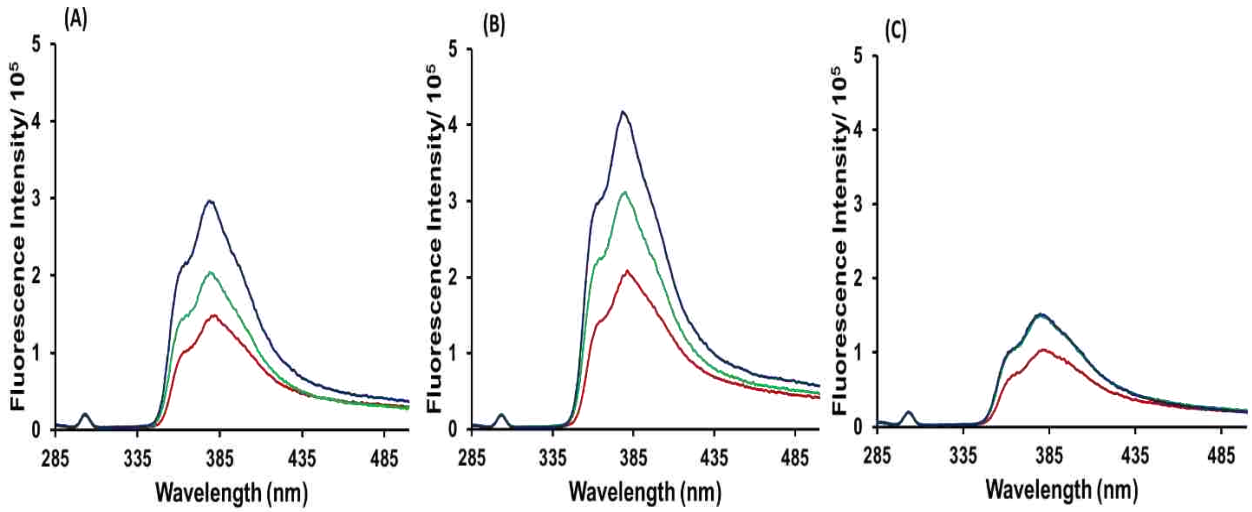

Figure 5.4. Fluorescence Spectra of (A) [CI][I], (B) [CI][OTf], (C) [CI][BETI] nanoGUMBOS synthesized using three different procedures: ultrasonication probe (red line); ultrasonication probe with the template 2HP-β-CD (MS:0.6) (green line) and the template 2HP-β-CD (MS:0.8) (blue line). The final concentration of nanoGUMBOS suspension (after dilution) was equal to 0.01 mM.

As previously mentioned, luminescence quantum yield (Φ) is a major parameter that affects the performance of an OLED. Therefore, absolute quantum yields were measured for the three types of nanoparticles, synthesized using different synthetic

approaches. The results are presented in Table 5.3. The absolute quantum yields of carbazole-based nanoGUMBOS were significantly lower than those of bulk materials which had the quantum yields around 100% as reported by Siraj *et al.*[32] This decrease in

Table 5.2. Emission wavelengths for [CI][I], [CI][OTf], and [CI][BETI] nanoGUMBOS synthesized using three different approaches.

	Ultrasonication		Ultrasonication with 2-HP-β-CD MS 0.6		Ultrasonication with 2-HP-β-CD MS 0.8	
	λ_1	λ_2	λ_1	λ_2	λ_1	λ_2
[CI][I]	303	382	303	379	303	379
[CI][OTf]	304	381	303	377	303	378
[CI][BETI]	303	381	303	380	303	380

quantum yields is due to the formation of excimers which promote intermolecular vibronic relaxation and non-radiational transitions at solid phase.[29] Nonetheless, [CI][BETI] nanoGUMBOS showed the highest quantum yields as compared to [CI][I] and [CI][OTf] nanoGUMBOS, while the presence of the template 2HP-β-CD increased the quantum yields for all nanoGUMBOS. The quantum yield increase was the most noticeable for [CI][BETI] nanoGUMBOS which were prepared in presence of 2HP-β-CD MS 0.6. Around 6% increase in quantum yield (*i.e.,* 14%) was observed for these nanoparticles in comparison to the nanoparticles synthesized without a template (*i.e.,* 8%). This enhancement in quantum yield correlates with a decrease in agglomeration level probably due to self-quenching via intermolecular contacts.[39]

Table 5.3. Absolute quantum yields (Φ) of [Cl][I], [Cl][OTf], and [Cl][BETI] synthesized using free ultrasonication, ultrasonication with the template 2HP-β-CD (MS:0.6), and ultrasonication with the template 2HP-β-CD (MS:0.8).

	Ultrasonication	**Ultrasonication with 2HP-β-CD MS 0.6**	**Ultrasonication with 2HP-β-CD MS 0.8**
QY ([Cl][I]) %	1.9	2.2	3.6
QY ([Cl][OTf]) %	2.1	2.7	3.2
QY ([Cl][BETI]) %	8.2	13.8	12.0

5.3.2. Doping Carbazole-Based NanoGUMBOS

The carbazole-based nanoGUMBOS were doped with the transition metal Cu^{2+} to study the effect of doping on the nanoparticles optical properties. The variations in absorbance and fluorescence intensities of nanoGUMBOS aqueous suspensions are shown in Figure 5.5. The presence of Cu^{2+} in the vicinity of nanoGUMBOS caused an increase in the absorbance of [Cl][OTf] while an opposite response was observed in the case of [Cl][BETI] where a low absorbance value was observed at 20% Cu^{2+}. However, there was no effect of Cu^{2+} dopant on the absorbance of [Cl][I]. The adsorption of Cu^{2+} ions at the core or the surface of nanoGUMBOS determines the measured absorbance. This phenomenon is related to the doping strategy (*i.e.,* nucleation or growth doping) and the amount of dopant added.[40] Additionally, the type, size, and valence of the dopant need to be taken into consideration.[41] These systems could undergo a “self-purification”

mechanism that can prevent in some cases an effective doping of nanoparticles.[42] The three types of nanoGUMBOS suspensions displayed different fluorescence behaviors. [CI][I] nanoGUMBOS had an increase in fluorescence when doped with Cu^{2+}, the maximum fluorescence was observed at 10% Cu^{2+}. At higher amounts of Cu^{2+}, the fluorescence intensity starts to decrease and exhibited equivalent intensity for 20% and 30% doping. [CI][OTf] nanoGUMBOS showed a decrease in fluorescence intensity at 10% Cu^{2+}, followed by an increase back to the original intensity upon increasing the amount of Cu^{2+}. Lastly, [CI][BETI] nanoGUMBOS exhibited a slight increase in fluorescence intensity in presence of Cu^{2+}. It is expected that the presence of Cu^{2+} causes a population of electrons in the surface trap states from where the emission takes place. The electron-hole recombination can happen at the d orbitals of Cu^{2+} which lie between the valence and conduction bands of the host, causing an alteration in the fluorescence signal of nanoGUMBOS.[40] Moreover, doping [CI][I], [CI][OTf], and [CI][BETI] nanoGUMBOS with different amounts of Cu^{2+} caused an increase in quantum yield up to 2.5%, 3.9%, and 11.6%, respectively (Table 5.4). The variation in absolute quantum yield is related to structural effects which affected the spectroscopic properties of the nanoGUMBOS. The decrease in quantum yield at 30% Cu^{2+} was common among all nanoGUMBOS. The excess amount of dopant causes the appearance of surface defects, which is in favor of non-radiative decays.[40] However, quantum yield values which are tabulated in Table 5.4 did not reflect the data reported in Figure 5.5, especially for [CI][OTf] nanoGUMBOS which showed a slight increase in fluorescence at 30% Cu^{2+} for 0.1 mM concentration of nanoGUMBOS. Parameters such as the long lifetime of

nanoGUMBOS in the excited state and the high concentration of nanoparticles suspension might promote the occurrence of quenching mechanisms; hence, further analysis is required in this regard.

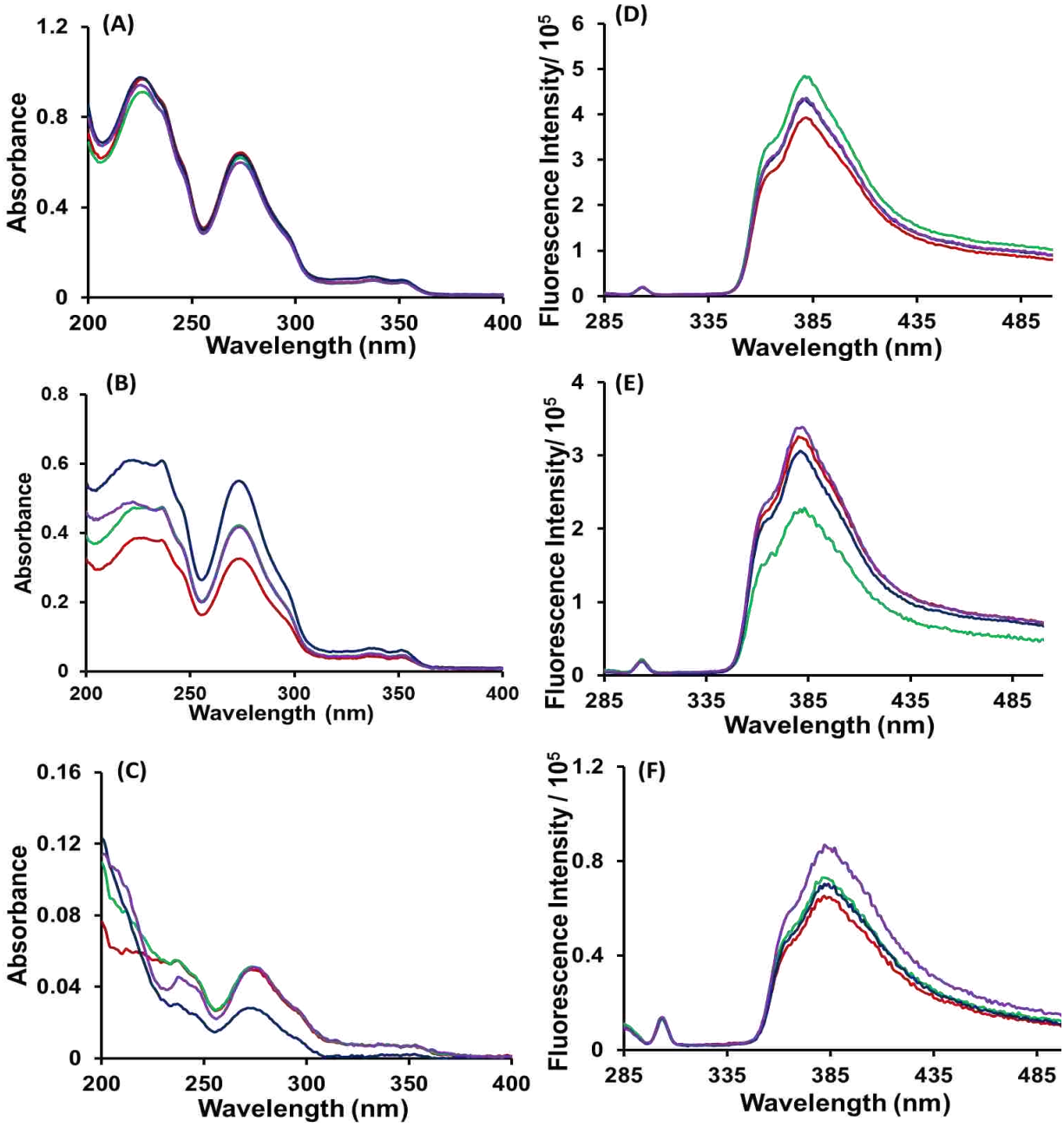

Figure 5.5. Absorbance and fluorescence spectra of (A,D) [Cl][I], (B,E) [Cl][OTf], and (C,F) [Cl][BETI] nanoGUMBOS doped with different molar percentages of Cu^{2+}: 0% (red line), 10% (green line), 20% (blue line), and 30% (purple line). The concentration of nanoGUMBOS was 0.02 mM (absorbance data) and 0.01 mM (fluorescence data).

Table 5.4. Quantum yields of [CI][I], [CI][OTf], and [CI][BETI] nanoGUMBOS doped with different percentages of Cu^{2+}: 0%, 10%, 20%, and 30%.

	Ultrasonication	**Ultrasonication with 10% Cu^{2+}**	**Ultrasonication with 20% Cu^{2+}**	**Ultrasonication with 30% Cu^{2+}**
QY [CI][I] %	1.8	2.5	2.0	1.7
QY [CI][OTf] %	2.1	2.3	3.9	1.8
QY [CI][BETI] %	10.0	11.0	11.6	6.9

Size studies were also performed on doped carbazole-based nanoGUMBOS to validate any effect of doping on the size of nanoGUMBOS (Figure 5.6). The analysis of TEM micrographs reveals that the sizes of nanoGUMBOS were varying with the amount of doping; yet, there is no direct relationship between the size and absorbance or fluorescence spectra. This is partially due to the presence of other factors related to the doping mechanism such as conformational changes and quenching mechanisms. Nonetheless, an obvious change in quantum yield was associated with the abrupt change in size. For example, [CI][I] nanoGUMBOS showed a decrease in size down to 74 nm associated with an increase in quantum yield (2.5%), when these nanoparticles were doped with 10% Cu^{2+}. [CI][OTf] nanoGUMBOS had a concurrent increase in size (312 nm) and quantum yield (3.9%) at 20% doping. However, [CI][BETI] showed a decrease in agglomeration level at 10% level of dopant to result in distinct nanoparticles with a moderate level of agglomeration at 20% and 30% (Figure 5.6). The quantum yield for these nanoparticles was the highest at 20% (11.6%), which is in accordance with the formation of defined shape nanoparticles.

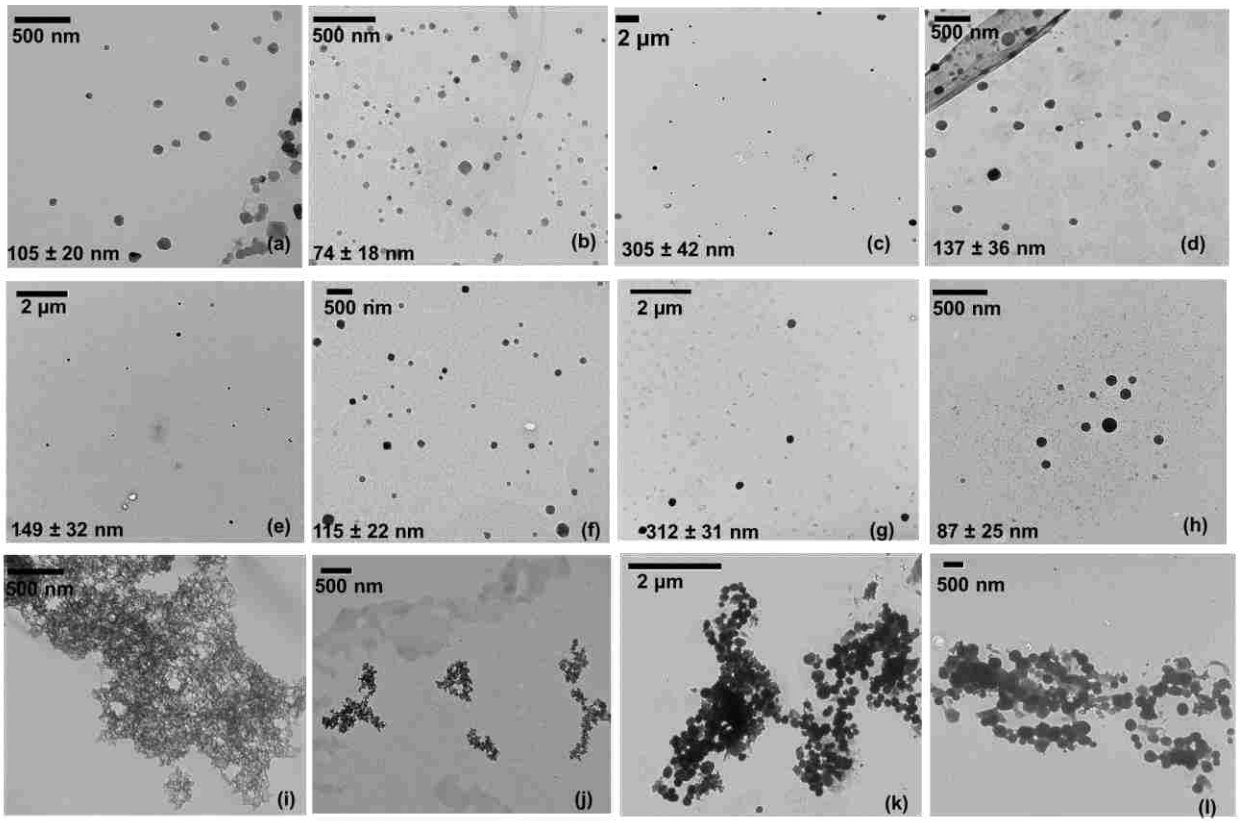

Figure 5.6. TEM micrographs of [Cl][I] (a-d), [Cl][OTf] (e-h), and [Cl][BETI] (i-l) nanoGUMBOS doped with Cu^{2+} at different molar percentages: 0%, 10%, 20%, 30% (from left to right). The average sizes were not accurately determined in Figures i-l due to the agglomeration of nanoparticles.

5.4. Conclusions

Carbazole-based nanoGUMBOS have proven to be interesting FONs with potential to be applied as emitting materials for OLEDs. The quantum yield of these nanoparticles can be efficiently tuned by changing the type of counteranion and the synthetic approaches. Several techniques have been presented for tuning the optical properties of these compounds as well as quantum yields. The presence of 2HP-β-CD template during the synthesis of these nanoparticles enhanced the fluorescence and increased the quantum yield of the suspensions. [Cl][BETI] had the highest quantum yield (*i.e.,* 14%) among the carbazole-based nanoGUMBOS. A doping method was also

explored for the purpose of increasing the nanomaterials quantum yield. Carbazole-based nanoGUMBOS showed different responses upon doping with the transition metal Cu^{2+}. Each type of nanoGUMBOS had a distinct optimal amount of dopant at which the quantum yield is the highest. The ultimate quantum yields were 2.5%, 3.9% and 11.6% for [Cl][I], [Cl][OTf], and [Cl][BETI] nanoGUMBOS respectively. It is noted that the structural and size effects were the major factors in determining the quantum yield of doped nanoGUMBOS.

5.5. References

1. De Almeida, A.; Santos, B.; Paolo, B.; Quicheron, M. Solid State Lighting Review - Potential and Challenges in Europe. *Renewable Sustainable Energy Rev.* **2014,** *34*, 30-48.

2. Thejokalyani, N.; Dhoble, S. J. Novel Approaches for Energy Efficient Solid State Lighting by Rgb Organic Light Emitting Diodes - a Review. *Renewable Sustainable Energy Rev.* **2014,** *32*, 448-467.

3. Mukherjee, S.; Thilagar, P. Organic White-Light Emitting Materials. *Dyes Pigm.* **2014,** *110*, 2-27.

4. Sasabe, H.; Kido, J. Recent Progress in Phosphorescent Organic Light-Emitting Devices. *Eur. J. Org. Chem.* **2013,** *2013* (34), 7653-7663.

5. Hu, J. Y.; Pu, Y. J.; Satoh, F.; Kawata, S.; Katagiri, H.; Sasabe, H.; Kido, J. Bisanthracene- Based Donor- Acceptor- Type Light- Emitting Dopants: Highly Efficient Deep- Blue Emission in Organic Light- Emitting Devices. *Adv. Funct. Mater.* **2014,** *24* (14), 2064-2071.

6. Zhu, M. R.; Yang, C. L., Blue Fluorescent Emitters: Design Tactics and Applications in Organic Light-Emitting Diodes. *Chem. Soc. Rev.* **2013,** *42* (12), 4963-4976.

7. Grem, G.; Leditzky, G.; Ullrich, B.; Leising, G. Realization of a Blue-Light-Emitting Device Using Poly(Para-Phenylene). *Adv. Mater.* **1992,** *4* (1), 36-37.

8. Miteva, T.; Meisel, A.; Knoll, W.; Nothofer, H. G.; Scherf, U.; Muller, D. C.; Meerholz, K.; Yasuda, A.; Neher, D. Improving the Performance of Polyfluorene-Based Organic Light-Emitting Diodes Via End-Capping. *Adv. Mater.* **2001,** *13* (8), 565-570.

9. Oelkrug, D.; Tompert, A.; Egelhaaf, H. J.; Hanack, M.; Steinhuber, E.; Hohloch, M.; Meier, H.; Stalmach, U. Towards Highly Luminescent Phenylene Vinylene Films. *Synth. Met.* **1996,** *83* (3), 231-237.

10. Lee, S. J.; Park, J. S.; Yoon, K. J.; Kim, Y. I.; Jin, S. H.; Kang, S. K.; Gal, Y. S.; Kang, S.; Lee, J. Y.; Kang, J. W.; Lee, S. H.; Park, H. D.; Kim, J. J. High-Efficiency Deep-Blue Light-Emitting Diodes Based on Phenylquinoline/Carbazole-Based Compounds. *Adv. Funct. Mater.* **2008,** *18* (24), 3922-3930.

11. Ding, B. D.; Zhu, W. Q.; Jiang, X. Y.; Zhang, Z. L. Pure Blue Emission from Undoped Organic Light Emitting Diode Based on Anthracene Derivative. *Curr. Appl. Phys.* **2008,** *8* (5), 523-526.

12. Zhang, Q.; Wang, C. F.; Ling, L. T.; Chen, S. Fluorescent Nanomaterial-Derived White Light-Emitting Diodes: What's Going On. *J. Mater. Chem. C* **2014,** *2* (22), 4358-4373.

13. Lee, K. H.; Lee, J. H.; Song, W. S.; Ko, H.; Lee, C.; Lee, J. H.; Yang, H. Highly Efficient, Color-Pure, Color-Stable Blue Quantum Dot Light-Emitting Devices. *ACS Nano* **2013,** *7* (8), 7295-7302.

14. Sharma, P. K.; Kumar, M.; Pandey, A. C. Green Luminescent ZnO:Cu^{2+} Nanoparticles for Their Applications in White-Light Generation from UV LEDS. *J. Nanopart. Res.* **2011,** *13* (4), 1629-1637.

15. Salah, N.; Habib, S. S.; Khan, Z. H.; Alharbi, N. D. Synthesis and Characterization of Pure and Tb/Cu Doped Alq(3) Nanostructures. *J. Lumin*. **2013,** *143*, 640-644.

16. Tesfai, A.; El-Zahab, B.; Kelley, A. T.; Li, M.; Garno, J. C.; Baker, G. A.; Warner, I. M. Magnetic and Nonmagnetic Nanoparticles from a Group of Uniform Materials Based on Organic Salts. *ACS Nano* **2009,** *3* (10), 3244-3250.

17. Jordan, A. N.; Siraj, N.; Das, S.; Warner, I. M. Tunable near-Infrared Emission of Binary Nano- and Mesoscale GUMBOS. *RSC Adv.* **2014,** *4* (54), 28471-28480.

18. Sarkar, A.; Kanakamedala, K.; Jagadish, N. N.; Jordan, A.; Das, S.; Siraj, N.; Warner, I. M.; Daniels-Race, T. Electro-Optical Characterization of Cyanine-Based GUMBOS and NanoGUMBOS. *Electron. Mater. Lett.* **2014,** *10* (5), 879-885.

19. Dumke, J. C.; Oureshi, A.; Hamdan, S.; El-Zahab, B.; Das, S.; Hayes, D. J.; Boldor, D.; Rupnik, K.; Warner, I. M. Photothermal Response of near-Infrared-Absorbing NanoGUMBOS. *Appl. Spectrosc.* **2014,** *68* (3), 340-352.

20. de Rooy, S. L.; Das, S.; Li, M.; El-Zahab, B.; Jordan, A.; Lodes, R.; Weber, A.; Chandler, L.; Baker, G. A.; Warner, I. M. Ionically Self-Assembled, Multi-Luminophore One-Dimensional Micro- and Nanoscale Aggregates of Thiacarbocyanine GUMBOS. *J. Phys. Chem. C* **2012,** *116* (14), 8251-8260.

21. Lu, C. F.; Das, S.; Magut, P. K. S.; Li, M.; El-Zahab, B.; Warner, I. M. Irradiation Induced Fluorescence Enhancement in Pegylated Cyanine-Based NIR Nano- and Mesoscale GUMBOS. *Langmuir* **2012,** *28* (40), 14415-14423.

22. Das, S.; Bwambok, D.; El-Zahab, B.; Monk, J.; de Rooy, S. L.; Challa, S.; Li, M.; Hung, F. R.; Baker, G. A.; Warner, I. M. Nontemplated Approach to Tuning the Spectral Properties of Cyanine-Based Fluorescent NanoGUMBOS. *Langmuir* **2010,** *26* (15), 12867-12876.

23. Dumke, J. C.; El-Zahab, B.; Challa, S.; Das, S.; Chandler, L.; Tolocka, M.; Hayes, D. J.; Warner, I. M. Lanthanide-Based Luminescent NanoGUMBOS. *Langmuir* **2010,** *26* (19), 15599-15603.

24. Dumke, J. C.; Qureshi, A.; Hamdan, S.; Rupnik, K.; El-Zahab, B.; Hayes, D. J.; Warner, I. M. In Vitro Activity Studies of Hyperthermal near-Infrared NanoGUMBOS in Mda-Mb-231 Breast Cancer Cells. *Photochem. Photobiol. Sci.* **2014,** *13* (9), 1270-1280.

25. Jordan, A. N.; Das, S.; Siraj, N.; de Rooy, S. L.; Li, M.; El-Zahab, B.; Chandler, L.; Baker, G. A.; Warner, I. M. Anion-Controlled Morphologies and Spectral Features of Cyanine-Based NanoGUMBOS - an Improved Photosensitizer. *Nanoscale* **2012,** *4* (16), 5031-5038.

26. Bwambok, D. K.; El-Zahab, B.; Challa, S. K.; Li, M.; Chandler, L.; Baker, G. A.; Warner, I. M. Near-Infrared Fluorescent NanoGUMBOS for Biomedical Imaging. *ACS Nano* **2009,** *3* (12), 3854-3860.

27. Das, S.; Magut, P. K. S.; de Rooy, S. L.; Hasan, F.; Warner, I. M. Ionic Liquid-Based Fluorescein Colorimetric pH Nanosensors. *RSC Adv.* **2013,** *3* (43), 21054-21061.

28. Sasabe, H.; Kido, J. Recent Progress in Phosphorescent Organic Light-Emitting Devices. *Eur. J. Org. Chem.* **2013,** *2013* (34), 7653-7663.

29. Jenekhe, S. A.; Osaheni, J. A. Excimers and Exciplexes of Conjugated Polymers. *Science* **1994,** *265* (5173), 765-768.

30. Hsu, S. L.; Chou, C. H.; Chen, C. P.; Wei, K. H. Blue Electroluminescence Enhancement of Poly{2,7-(9,9'-Dioctylfluorene)-Co-4-Diphenylamino-4'-Bipenylmethylsulfide} Incorporating Side-Chain-Tethered Gold Nanoparticles. *Adv. Funct. Mater.* **2007,** *17* (14), 2534-2541.

31. Li, C. X.; Yu, C.; Wang, C. F.; Chen, S. Facile Plasma-Induced Fabrication of Fluorescent Carbon Dots toward High-Performance White Leds. *J. Mater. Sci.* **2013,** *48* (18), 6307-6311.

32. Siraj, N.; Hasan, F.; Das, S.; Kiruri, L. W.; Gall, K. E. S.; Baker, G. A.; Warner, I. M. Carbazole-Derived Group of Uniform Materials Based on Organic Salts: Solid State Fluorescent Analogues of Ionic Liquids for Potential Applications in Organic-Based Blue Light-Emitting Diodes. *J. Phys. Chem. C* **2014,** *118* (5), 2312-2320.

33. Devi, L. B.; Mandal, A. B. Self-Assembly of Ag Nanoparticles Using Hydroxypropyl Cyclodextrin: Synthesis, Characterisation and Application for the Catalytic Reduction of P-Nitrophenol. *RSC Adv.* **2013,** *3* (15), 5238-5253.

34. Xu, J. Z.; Xu, S.; Geng, J.; Li, G. X.; Zhu, J. J. The Fabrication of Hollow Spherical Copper Sulfide Nanoparticle Assemblies with 2-Hydroxypropyl-Beta-Cyclodextrin as a Template under Sonication. *Ultrason. Sonochem.* **2006,** *13* (5), 451-454.

35. Bonesi, S. M.; Erra-Balsells, R., Electronic Spectroscopy of Carbazole and N- and C-Substituted Carbazoles in Homogeneous Media and in Solid Matrix. *J. Lumin.* **2001,** *93* (1), 51-74.

36. Fu, H. B.; Yao, J. N. Size Effects on the Optical Properties of Organic Nanoparticles. *J. Am. Chem. Soc.* **2001,** *123* (7), 1434-1439.

37. Paau, M. C.; Lo, C. K.; Yang, X. P.; Choi, M. M. F. Synthesis of 1.4 Nm Alpha-Cyclodextrin-Protected Gold Nanoparticles for Luminescence Sensing of Mercury(Ii) with Picomolar Detection Limit. *J. Phys. Chem. C* **2010,** *114* (38), 15995-16003.

38. Sun, Y. Y.; Liao, J. H.; Fang, J. M.; Chou, P. T.; Shen, C. H.; Hsu, C. W.; Chen, L. C. Fluorescent Organic Nanoparticles of Benzofuran-Naphthyridine Linked Molecules: Formation and Fluorescence Enhancement in Aqueous Media. *Org. Lett.* **2006,** *8* (17), 3713-3716.

39. Bernards, D. A.; Owens, R. M.; Malliaras, G. G., *Organic Semiconductors in Sensor Applications*. Springer: 2008.

40. Panda, S. K.; Hickey, S. G.; Demir, H. V.; Eychmuller, A. Bright White-Light Emitting Manganese and Copper Co-Doped Znse Quantum Dots. *Angew. Chem. Int. Ed.* **2011,** *50* (19), 4432-4436.

41. Wu, P.; Yan, X.-P. Doped Quantum Dots for Chemo/Biosensing and Bioimaging. *Chem. Soc. Rev.* **2013,** *42* (12), 5489-5521.

42. Dalpian, G. M.; Chelikowsky, J. R. Self-Purification in Semiconductor Nanocrystals. *Phys. Rev. Lett.* **2006,** *96* (22).

CHAPTER SIX
CONCLUSIONS AND FUTURE WORK

6.1. Conclusions

A new class of organic nanoparticles (nanoGUMBOS), which drives the chemistry of ionic liquids to the nanoscale level, was introduced in this work. Interestingly, these nanomaterials have exhibited tunable physical and chemical properties, allowing for use in a wide range of applications. The diversity and flexibility of these nanoparticles have thus far permitted implementation of nanoGUMBOS in diverse fields of research, such as polymer chemistry and optoelectronics. Throughout the research chapters of this dissertation, size-control of nanoGUMBOS (Chapter Two), design of MIP nanoGUMBOS for chiral recognition (Chapter Three), preparation of polymeric nanoGUMBOS using gamma irradiation (Chapter Four), and synthesis of semiconductive nanoGUMBOS for use in OLEDs (Chapter Five) were discussed.

The introductory chapter revealed the fundamentals of nanotechnology. The history of nanotechnology is highly associated with the chemistry field. In this regard, ionic liquids and polymeric ionic liquids materials were applied in nanotechnology. Nanoparticles derived from these organic materials (nanoGUMBOS and polymeric nanoGUMBOS) were synthesized. Synthesis approaches and theories of nanoparticle formation were deliberated. The last part of the chapter included the characterization techniques used to study the size, morphology, surface charge, and optical properties of nanoGUMBOS.

Next, in the second chapter, strategies which have been investigated for the synthesis- and size-control of nanoGUMBOS were elaborated. The compound under

investigation was derived from an imidazolium-based ionic liquid, commonly used for metal ion extraction and lignocellulose processing. The syntheses, performed in aqueous medium, were facile and reliable bottom-up approaches. Systems based on ultrasound and microwaves were employed to synthesize uniform nanoparticles. Furthermore, soft templates including surfactants and cyclodextrin derivatives enabled the fabrication of reduced size nanoGUMBOS. Results from the studies revealed that the templated procedures delivered quasi-spherical nanoGUMBOS with controlled average sizes from 12 to 99 nm and standard deviations between 2 and 12 nm. The size-control study permits a better regulation of the properties and a reliable performance of nanoparticles in various applications.

Chapter Three covered the synthesis of chiral imprinted polymeric nanoGUMBOS using a molecular imprinting strategy under aqueous conditions. Four crosslinking ionic liquid monomers, with different spacers (moieties) between two vinylimidazole groups in the cationic structure, were investigated. The successful imprinting of these compounds in aqueous conditions was related primarily to the high interactions between the imidazolium moiety and the template L-tryptophan. The polymeric nanoGUMBOS showed high degree of recognition for L-tryptophan; however, the enantiorecognition was distinctive among the polymers due to the presence of unique interactions between each type of nanoGUMBOS and the imprint molecule. These materials were the first example of molecularly imprinted ionic liquid-based polymeric nanomaterials used for chiral recognition studies, while implementing the imprinting procedure in aqueous medium.

The fourth chapter dealt with the use of gamma irradiation to initiate the polymerization of vinylimidazoles ionic liquids at the nanoscale level. This method

provokes a polymerization process in absence of an initiator; concurrently, the high energy of gamma rays allows a homogeneous irradiation of large samples, which is beneficial for the formation of uniform nanoparticles. The synthesized (PEG), alkane, and alkyne polymeric nanoGUMBOS were evaluated as potential drug nanocarriers by encapsulating these nanoparticles with the hydrophilic dye, fluorescein sodium salt. As preliminary assessment, the nanoGUMBOS exhibited the ability to carry the dye; however, alkyne nanoGUMBOS showed the lesser encapsulation efficiency. The short distance of the spacer group between the vinylimidazoles in alkyne nanoGUMBOS, may have led to a decrease in possible interactions with fluorescein sodium salt.

Finally, Chapter Five focused on the investigation of semiconductive nanoGUMBOS as emitting nanomaterials in blue organic light-emitting devices. Studies were conducted to improve the quantum yield of these materials using several procedures. In this regard, the carbazoleimidazole cations in these nanoGUMBOS were coupled with various counteranions to examine any resulting effect on optical properties (*i.e.,* absorbance and fluorescence). Tunable optical properties were achieved by varying the synthesis approaches and the experimental conditions. A Cyclodextrin-assisted reprecipitation method was selected to control the size of nanoGUMBOS. The presence of this template caused an enhancement in fluorescence and quantum yield. Doping with the transition metal Cu^{2+} was also successful in enhancing the quantum yield of the nanoGUMBOS suspensions. The excess in the amount of dopant caused a decrease in quantum yield attributed to the formation of surface defects.

6.2. Future Work

Future work in the area of nanoGUMBOS includes the application of chemometric studies on the synthesis of these nanoparticles. A mathematical model will be designed to explore the optimal experimental conditions for the formation of nanoGUMBOS. The use of a mathematical model to predict the size of nanoparticles synthesized under fixed conditions has been reported for spinel ferrite nanoparticles.[1] A factorial design based on the chemometrics science offers the possibility to relate the synthesis conditions and size of nanoGUMBOS, once an accurate correlation model is applied. A statistical method based on a two-level-six-factor partial factorial design was performed on the synthesis of [Hmim][TPB] nanoGUMBOS (Table E1 in Appendix E). These initial studies can be used to determine statistically the factors that affect the size of nanoparticles. Further experiments will be required, before the determination of a chemometric model, to correlate between the experimental conditions and the size of nanoGUMBOS.

Moreover, novel separation techniques such as asymmetric-flow field flow fractionation (AF_4) will be investigated and optimized for size-selection of nanoGUMBOS. AF4 is a chromatography-based technique that separates analytes based on relative physicochemical properties (*e.g.,* molecular weight, size, shape).[2] The uniformity of nanoGUMBOS is necessary to have control over optical, electrical, and even physical properties. In addition, monodisperse nanoGUMBOS may offer enhanced properties and performance in various applications. Preliminary data were obtained for size-selection of [Hmim][TPB] nanoGUMBOS using AF4 (Figure E2 in Appendix E). The nanoparticles with average size of 50 nm were well discerned from the nanoparticles with 100 nm size;

however, a high level of agglomeration was observed after the collection of nanoparticles aliquots. The samples were also diluted for the detector, which is based on static scattering, to accurately sort different size nanoparticles. Optimization procedures will be needed to provide more uniform and non-agglomerated nanoGUMBOS.

Surface modification of nanoGUMBOS will be implemented to improve the performance of nanoparticles. This strategy allows the introduction of further intrinsic properties into these nanoparticles and provides active interacting surfaces.[3] The study will promote the use of nanoGUMBOS in diverse applications by creating multifunctional systems. For example, trihexyltetradecylphosphonium fluorescein $[(TTP)_2][FL]$ nanoGUMBOS which are fluorescent, pH sensitive, and can be used for biomedical applications,[4] were initially surface modified by folate ion (Figure E3 in Appendix E). Herein, the surface modification of nanoGUMBOS will mediate targeting cancer cells which overexpress the folate receptor. This investigation needs to be thoroughly developed to increase the adsorption of folate onto the surface of nanoparticles by optimizing experimental conditions such as the pH, the amount of folate added, and the incubation time. Other modifiers can be used as well in the surface modification strategy; polymer-modified nanoGUMBOS will increase for instance the biocompatibility and efficiency of these nanomaterials for in vivo studies.

The imprinted polymeric nanoGUMBOS show potential application in chiral separation. Therefore, future work in this field will include imprinting polymeric nanoGUMBOS with enantiomeric drugs which show chirality-dependent activity. The nanoparticles will be used as stationary phases in capillary electrochromatography (CEC)

for separation of these chiral drugs.[5] In addition, novel imprinted polymeric nanoGUMBOS which show a signal change upon recognition of a target molecule will be investigated. These stimuli-responsive polymeric nanomaterials will be made fluorescent, magnetic, or light sensitive by changing the type of anion or cation. The imprinted nanoGUMBOS will be applied as nanosensors for the target molecule in interest.[6]

The synthesis of polymeric nanoGUMBOS via gamma irradiation will be further controlled by studying the effect of monomeric solution, volume and concentration, on the size of nanoparticles. The minimum required dosage of gamma rays will be monitored by tracking the degree of polymerization. Furthermore, drug encapsulation studies on the polymeric nanoGUMBOS will be implemented using quantitative methods such as absorbance or fluorescence spectroscopy to accurately measure the encapsulation efficiency. Release studies of fluorescein sodium salt over time will also be performed using dialysis method. Other dyes such as Rhodamines will be investigated to elaborate on the interactions involved in drug encapsulation and release processes.

Lastly, carbazole-based nanoGUMBOS will be doped with different transition metals such as Mn^{2+} and Zn^{2+}. The ultimate goal of doping will be to achieve white light emission at high quantum yield, which is extremely significant in OLEDs.[7] Moreover, an OLED device will be fabricated using the nanoGUMBOS as emitting materials. The operation of the device will be evaluated based on its external quantum efficiency. This value is typically affected by several parameters including light extraction efficiency, power efficiency, electron-hole recombination efficiency, and internal quantum efficiency.[8]

In the end, the field of nanoGUMBOS holds a plethora of potential studies that can be performed to further clarify the fundamentals of nanoparticles formation for a better control over potential applications. The tunability of nanoGUMBOS raises the opportunities to perform several projects related to the synthesis, characterization, and application of these nanomaterials. The proposed studies will promote the use of nanoGUMBOS in analytical, biological, and technological arenas.

6.3. References

1. Rondinone, A. J.; Samia, A. C. S.; Zhang, Z. J. A Chemometric Approach for Predicting the Size of Magnetic Spinel Ferrite Nanoparticles from the Synthesis Conditions *J. Phys. Chem. B* **2000,** *104* (33), 7919-7922.

2. Williams, S. K. R.; Runyon, J. R.; Ashames, A. A. Field-Flow Fractionation: Addressing the Nano Challenge. *Anal. Chem.* **2011,** *83* (3), 634-642.

3. Verma, A.; Stellacci, F. Effect of Surface Properties on Nanoparticle-Cell Interactions. *Small* **2010,** *6* (1), 12-21.

4. Das, S.; Magut, P. K. S.; de Rooy, S. L.; Hasan, F.; Warner, I. M., Ionic Liquid-Based Fluorescein Colorimetric pH Nanosensors. *RSC Adv.* **2013**, *3* (43), 21054-21061.

5. Haupt, K. Molecularly Imprinted Polymers in Analytical Chemistry. *Analyst* **2001,** *126* (6), 747-756.

6. Takeuchi, T.; Mukawa, T.; Shinmori, H. Signaling Molecularly Imprinted Polymers: Molecular Recognition-Based Sensing Materials. *Chem. Rec.* **2005,** *5* (5), 263-275.

7. Zhang, Q.; Wang, C. F.; Ling, L. T.; Chen, S. Fluorescent Nanomaterial-Derived White Light-Emitting Diodes: What's Going On. *J. Mater. Chem. C* **2014,** *2* (22), 4358-4373.

8. Thejokalyani, N.; Dhoble, S. J. Novel Approaches for Energy Efficient Solid State Lighting by RGB Organic Light Emitting Diodes - a Review. *Renewable Sustainable Energy Rev.* **2014,** *32*, 448-467.

APPENDIX A. SUPPORTING INFORMATION FOR CHAPTER TWO: FIGURES

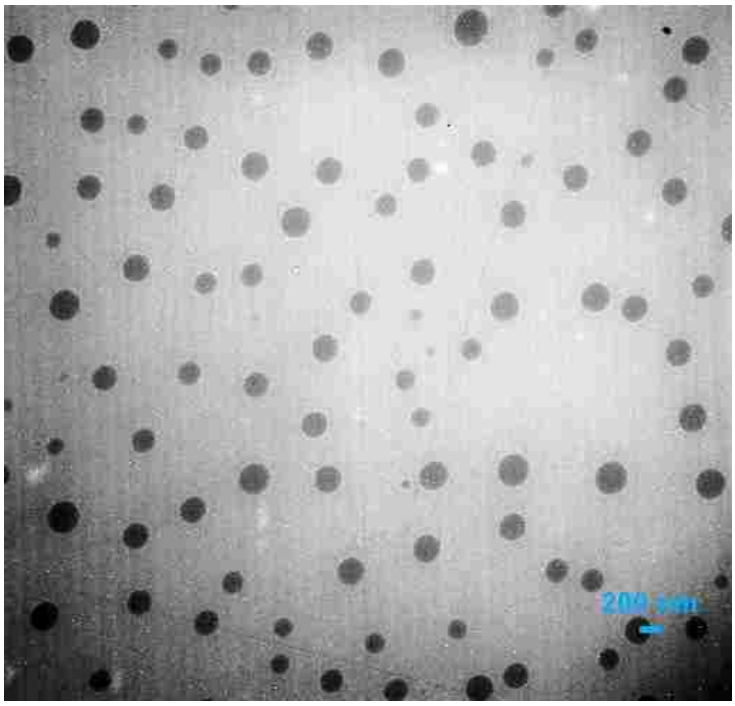

Figure A1. TEM micrograph of [Hmim][TPB] nanoGUMBOS synthesized under ultrasonication.

In this procedure, 100 μL of an aqueous solution of [Hmim][TPB] was added to a 10 mL total volume of water and acetonitrile (50:50 volume composition), mixed in a bath sonicator. [Hmim][Cl] aqueous solution (100 μL) was then added gradually (5 μL/minute) to the mixture. After adding all the amount of [Hmim][Cl], the sonication was stopped and the solutions were allowed to react for 16 hours, which is a sufficient time for the acetonitrile to evaporate from the medium. The experimental conditions were as follow: concentration of reactants: 0.025 M, volume ratio: water/acetonitrile 50:50, and the growth time of nanoparticles: 16 hours. The above TEM micrograph was taken using an LVEM5-TEM (Delong America, Montreal, Canada). The average size of nanoparticles was 210 ± 43 nm.

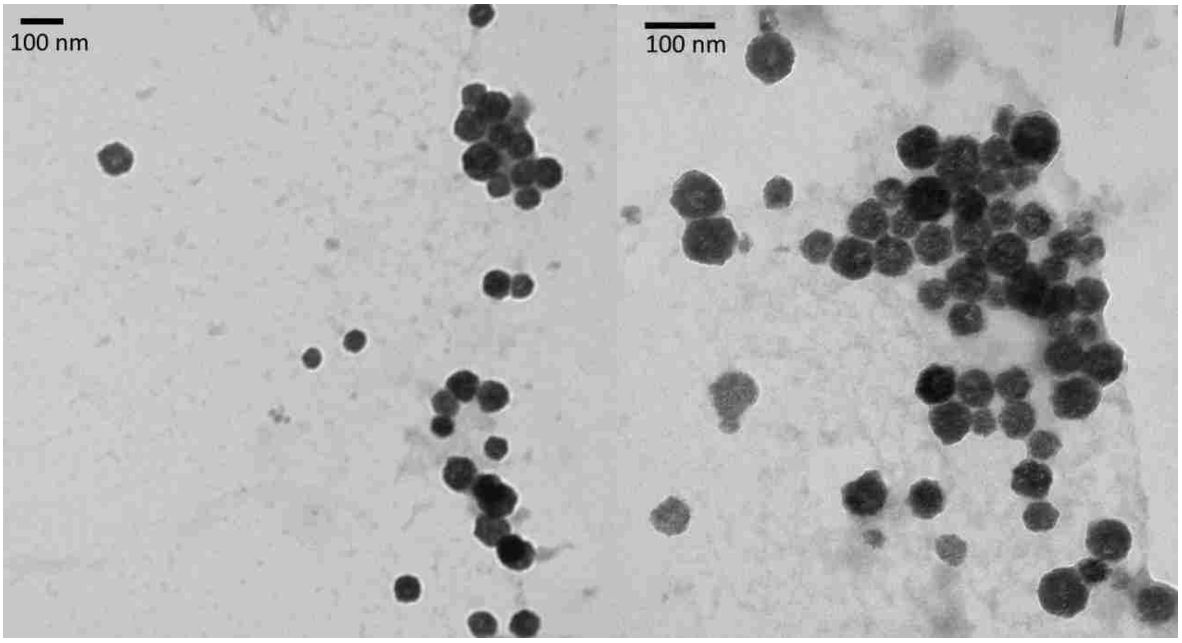

Figure A2. TEM micrographs of [Hmim][TPB] nanoGUMBOS synthesized in presence of 2-hydroxypropyl-α-CD and the probe ultrasonication (size of nanoparticles: 70 ±10 nm).

Experimental conditions were as follow: concentration of reactants: 4 mM, amount of 2HP-α-CD: 8 mg, total volume of mixture: 10 mL, amplitude of ultrasonication: 25%, time of ultrasonication: 10 min.

APPENDIX B. SUPPORTING INFORMATION FOR CHAPTER THREE: FIGURES

(a)

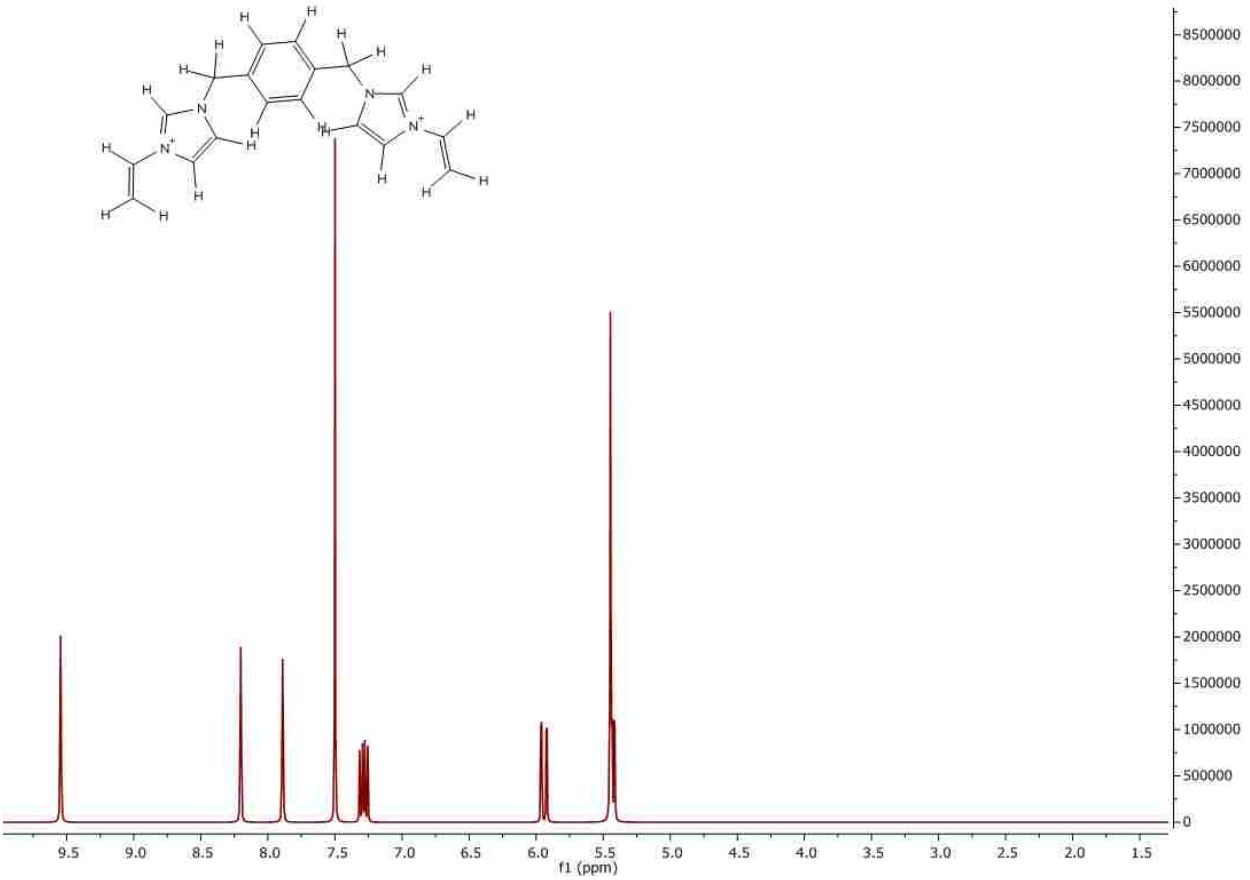

Figure B1a. ^{1}H NMR data reported for benzene ionic liquid monomer coupled with NTf_2 anion.

^{1}H-NMR, benzene-based monomer: (400 MHz, DMSO-d_6, δ): 9.55 (t, J_1=1.96, J_2= 1.44 Hz, 2H), 8.20 (t, J_1=1.8 Hz, J_2= 2Hz, 2H) 7.89 (t, J_1= 2Hz, J_2= 1.8 Hz, 2H),7.5 (s, 4H), 7.29 (dd, J_1= 8.8Hz, J_2 = 15.6Hz, 2H), 5.95 (dd, J_1= 2.4Hz, J_2= 15.6Hz, 2H),5.45 (s, 4H), 5.43 (dd, J_1= 2.4Hz, J_2= 8.8Hz, 2H)

(b)

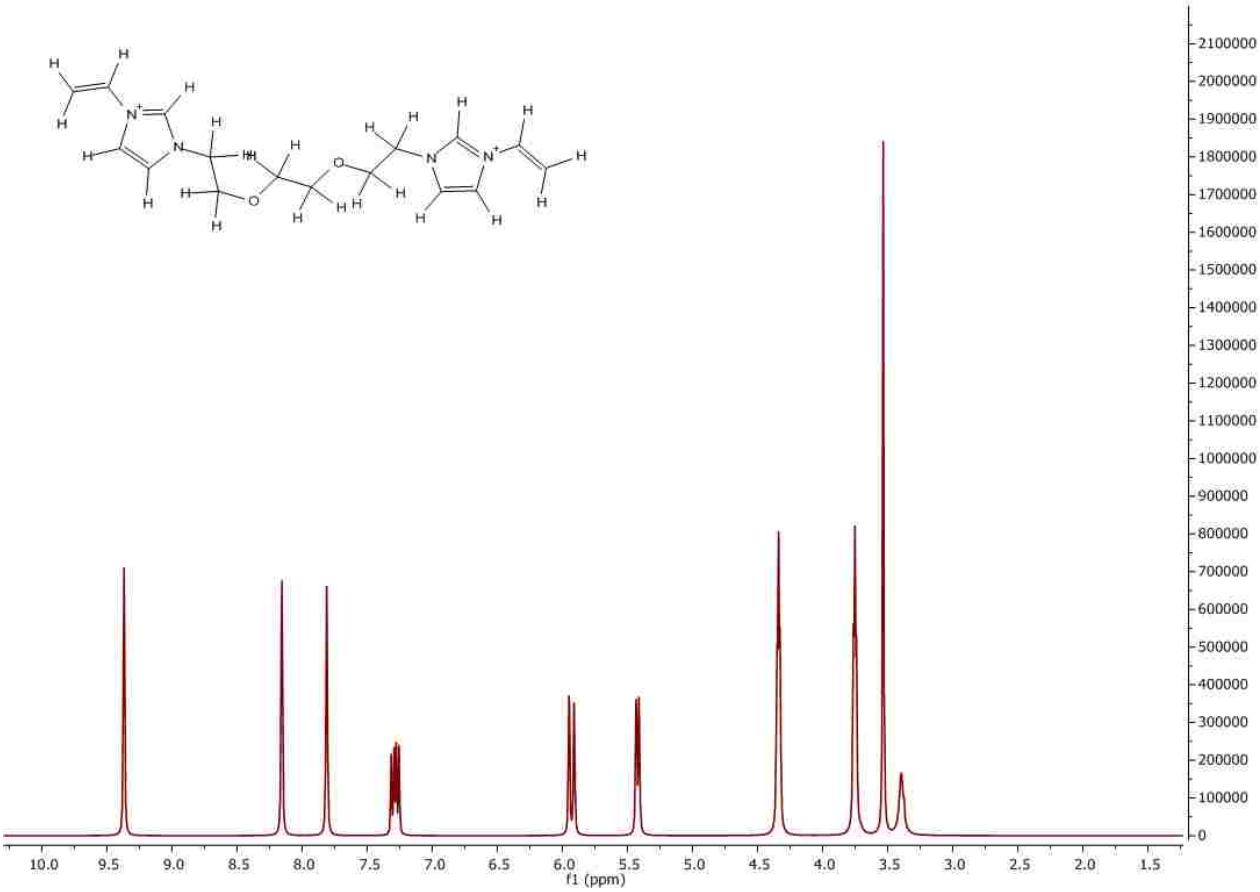

Figure B1b. ^{1}H NMR data reported for (PEG) ionic liquid monomer coupled with NTf_2 anion.

^{1}H-NMR, (PEG)-based monomer: (400 MHz, DMSO-d_6, δ): 9.37 (s, 2H), 8.15 (t, J= 1.6 Hz, 2H), 7.81 (t, J= 1 Hz, 2H), 7.29 (dd, J_1= 8.8 Hz, J_2= 16 Hz, 2H), 5.93 (dd, J_1=3 Hz, J_2=16 Hz, 2H), 5.42 (dd, J_1=8.8 Hz, J_2 = 2.4 Hz, 2H), 4.34 (t, J=5 Hz , 4H), 3.75 (t, J= 5 Hz, 4H), 3.6 (s, 4H), 3.39 (water).

(c)

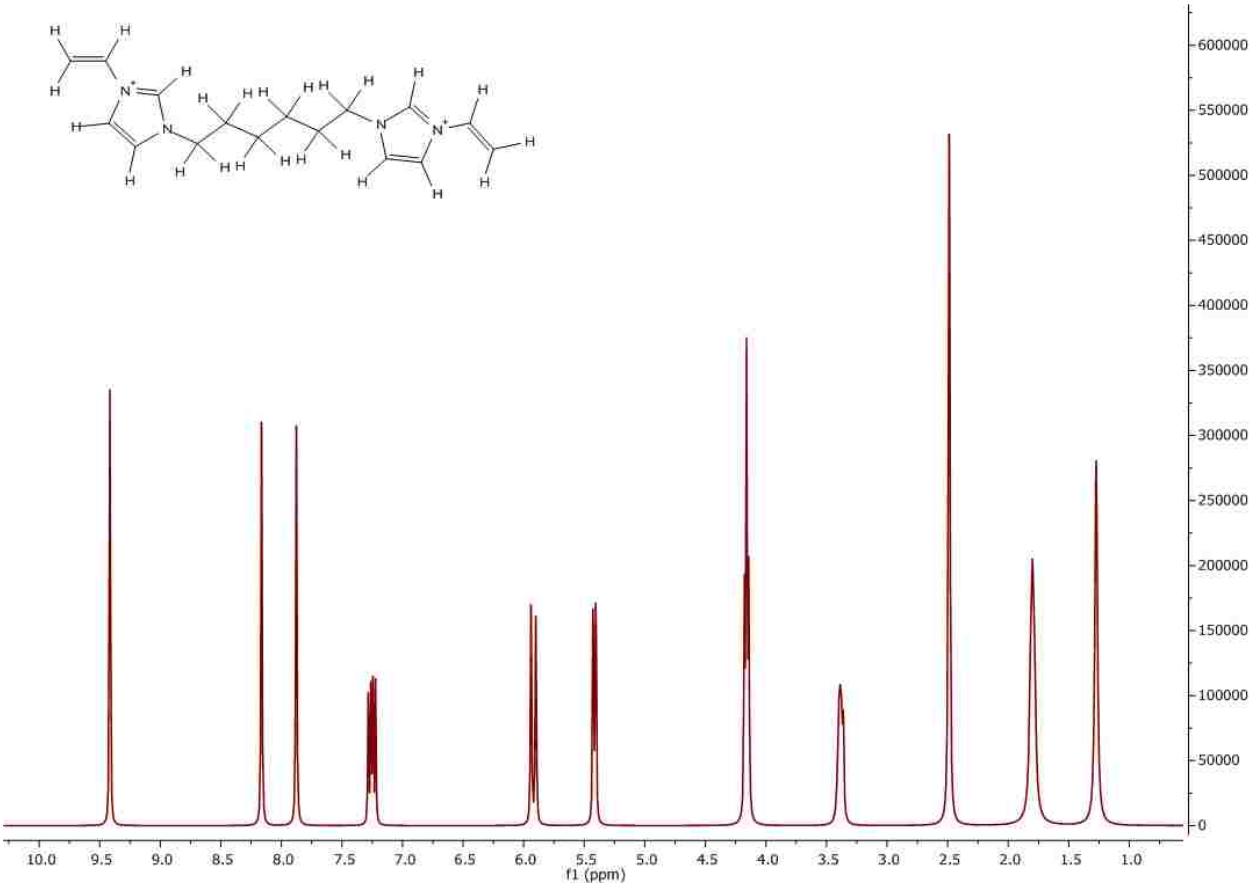

Figure B1c. ^{1}H NMR data reported for alkane ionic liquid monomer coupled with NTf_2 anion.

^{1}H-NMR, alkane-based monomer: (400 MHz, DMSO- d_6, δ): 9.42 (s, 2H), 8.16 (d, J= 2.2 Hz, 2H), 7.88 (broad s, 2H), 7.25 (dd, J_1= 9 Hz, J_2 =16 Hz, 2H), 5.92(dd, J_1= 4 Hz, J_2= 16 Hz, 2H), 5.41 (dd, J_1= 2.4Hz, J_2= 8.8Hz, 2H), 4.28 (t, J= 7 Hz, 4H), 2.49 (s, DMSO-d_6 solvent), 1.8 (t, J= 7 Hz, 4H), 1.27 (t, J=7 Hz, 4 H).

(d)

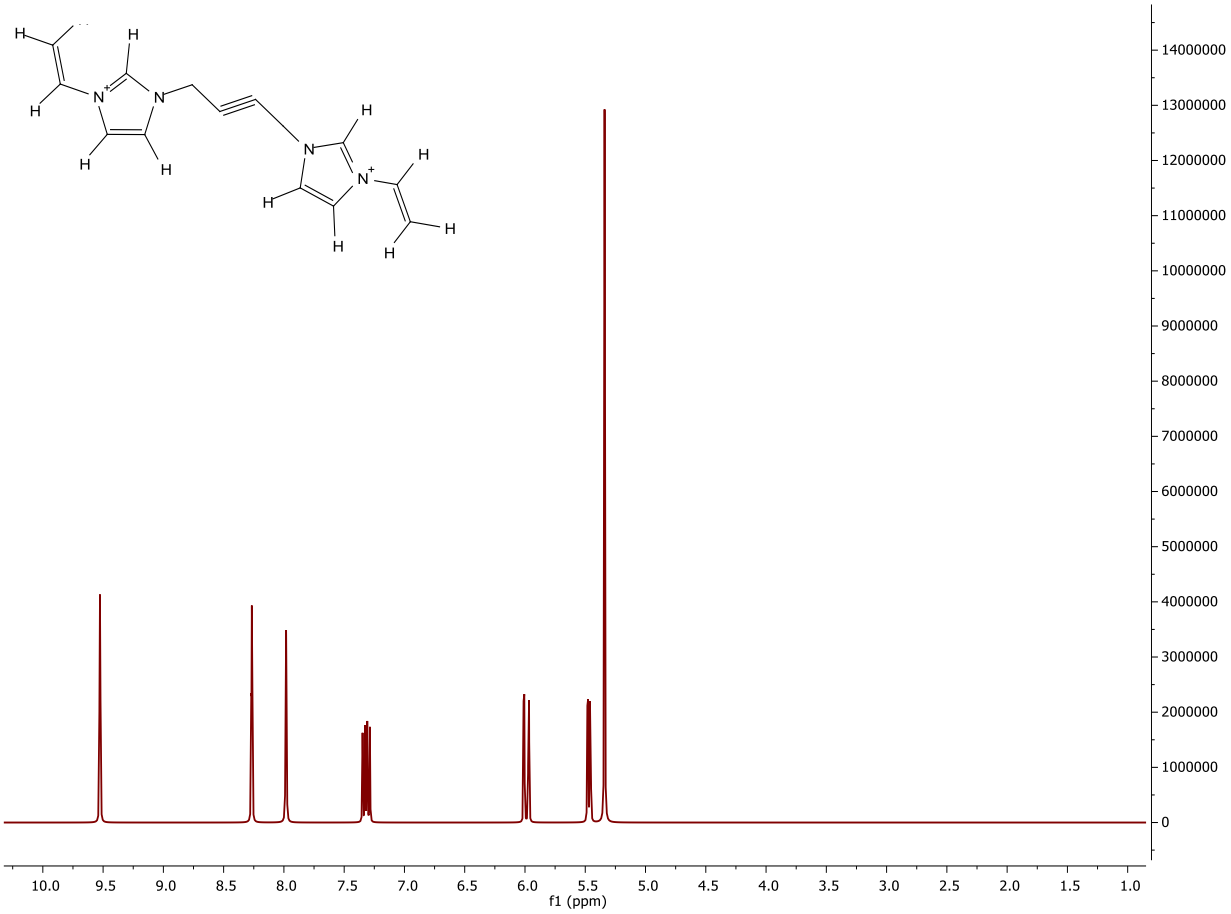

Figure B1d. ^{1}H NMR data reported for alkyne ionic liquid monomer coupled with NTf_2 anion.

^{1}H-NMR, alkyne-based monomer: (400 MHz, DMSO-d_6, δ): 9.52 (t,J_1=1.56, J_2= 1.64Hz, 2H), 8.25 (t, J_1=1.4 Hz, J_2= 2.2 Hz , 2H), 7.97 (t, J_1= 1Hz, J_2= 2Hz, 2H), 7.32 (dd, J_1= 8.4Hz, J_2 = 15.6Hz, 2H), 5.97 (dd, J_1= 2.4Hz, J_2= 15.6Hz, 2H), 5.47 (dd, J_1= 2.8Hz, J_2= 9 Hz, 2H), 5.34 (s, 4H).

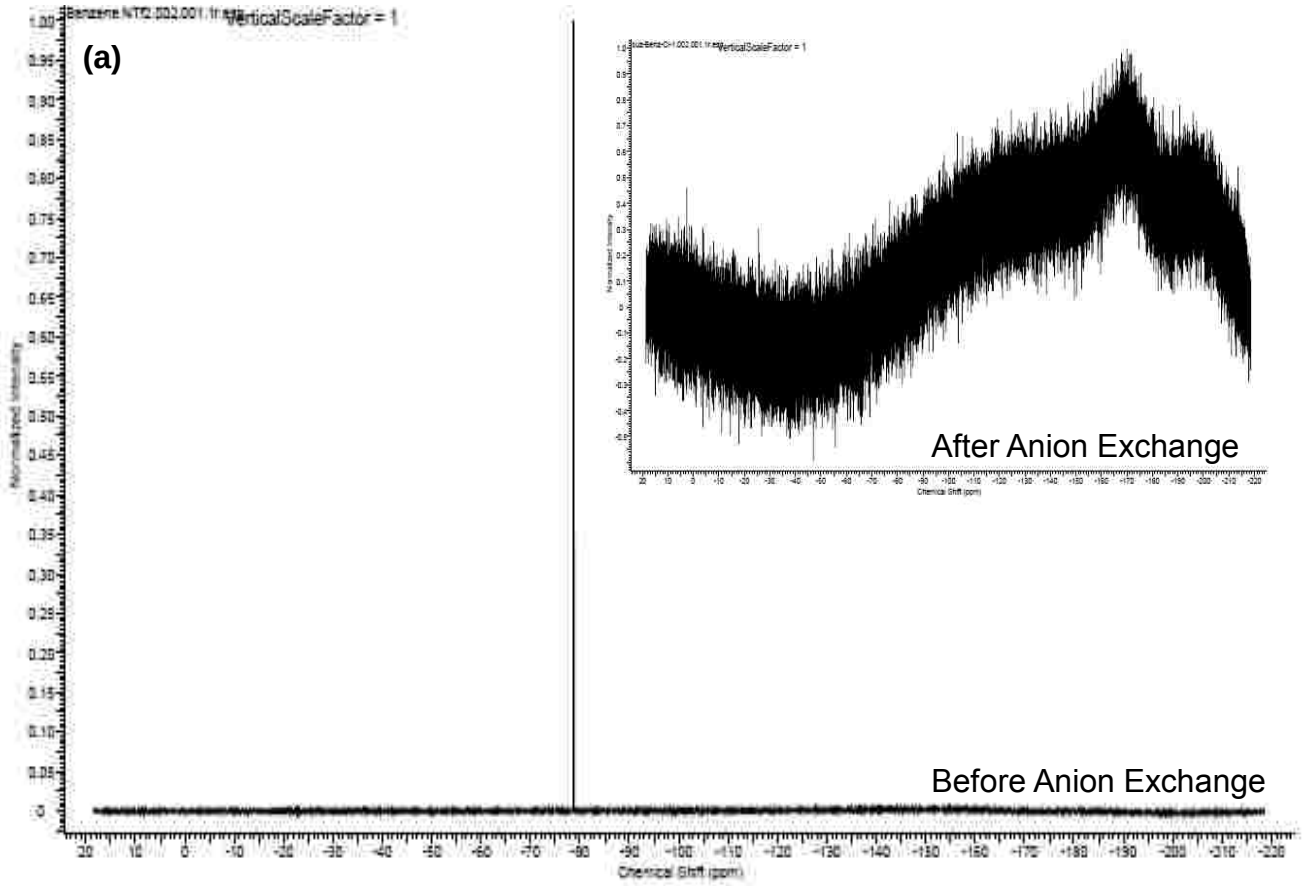

Figure B2a. ^{19}F-NMR for benzene ionic liquid monomer before and after anion exchange.

Before anion exchange, ^{19}F-NMR (DMSO, 400 MHz): δ -78.7 ppm

After anion exchange, ^{19}F-NMR (DMSO, 400 MHz): no peak

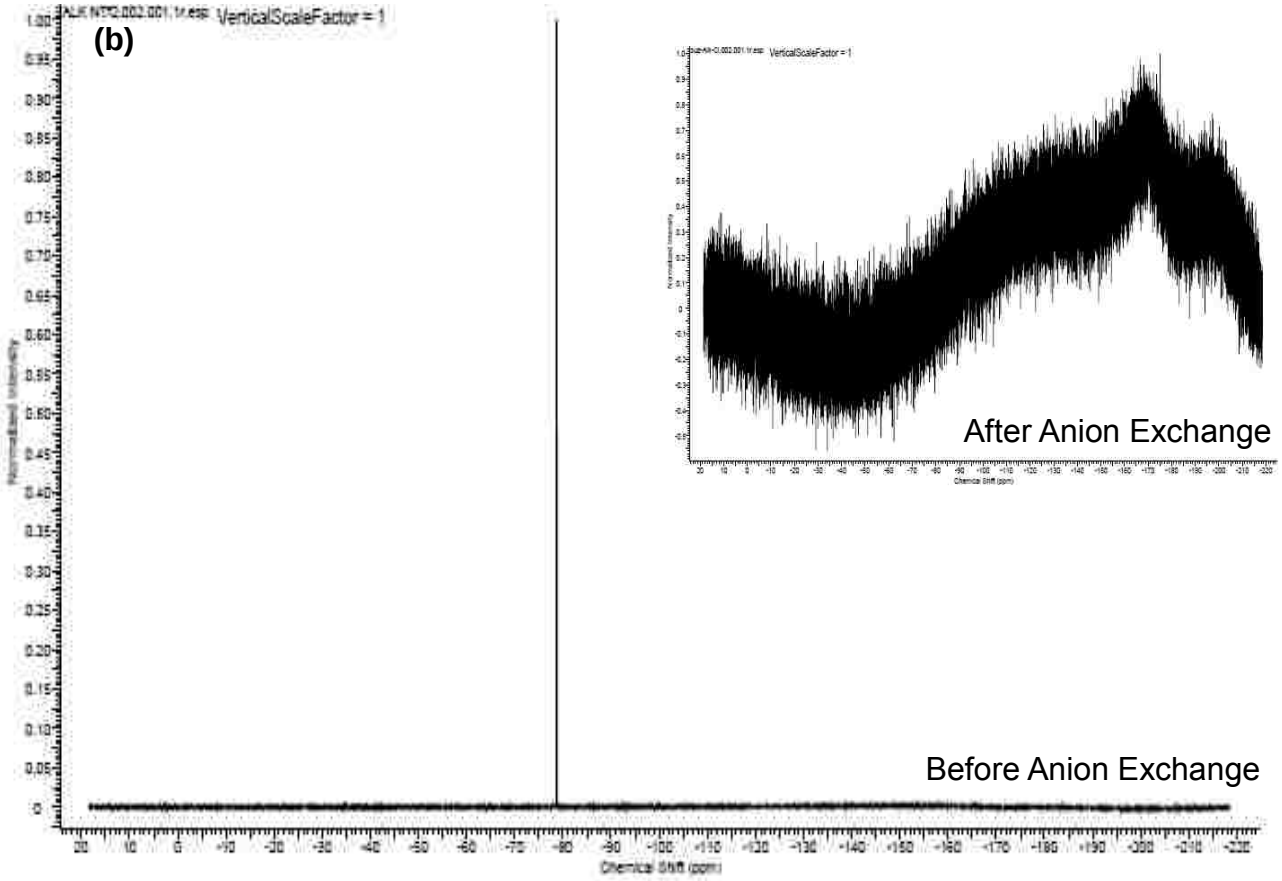

Figure B2b. ^{19}F-NMR for alkane ionic liquid monomer before and after anion exchange.

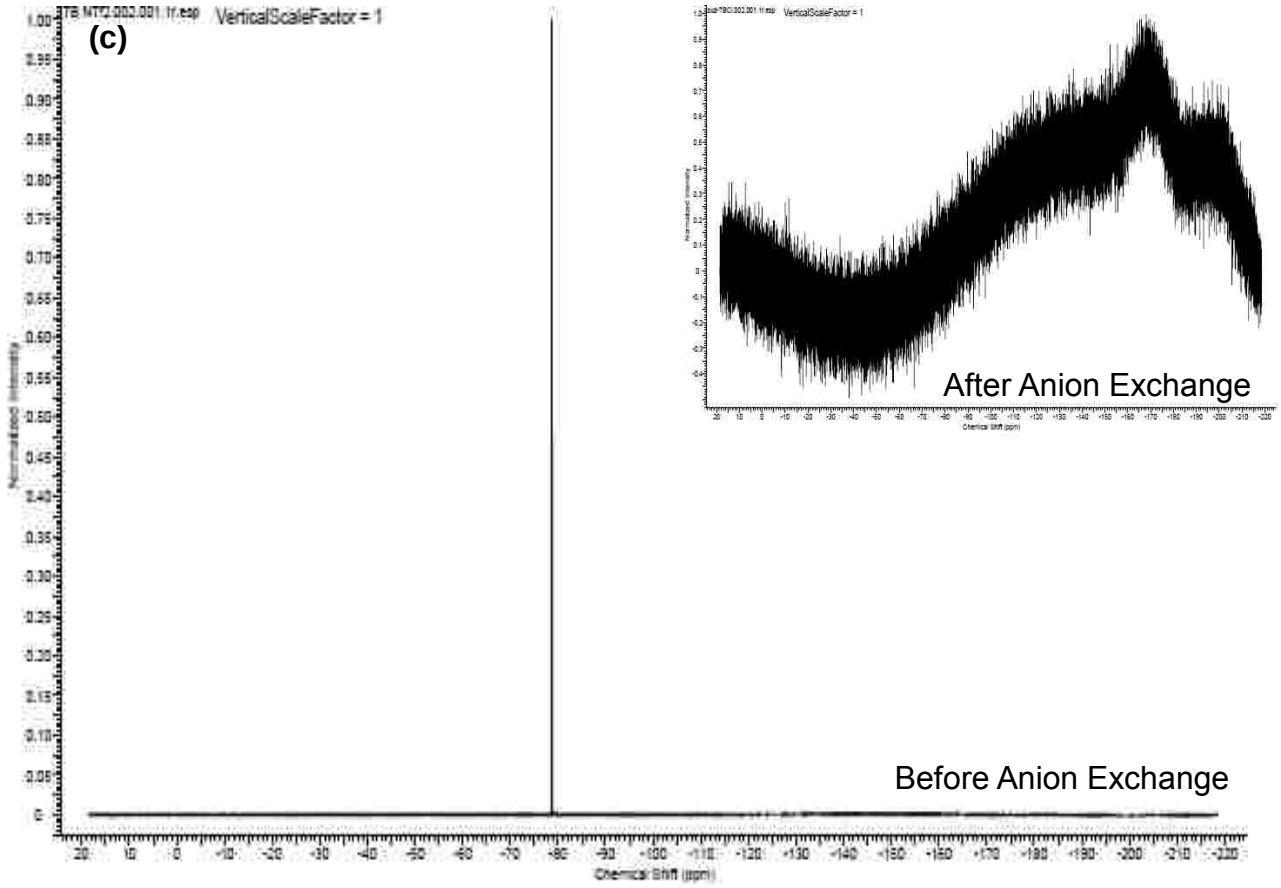

Figure B2c. ^{19}F-NMR for alkyne ionic liquid monomer before and after anion exchange.

APPENDIX C. SUPPORTING INFORMATION FOR CHAPTER FOUR: FIGURES AND TABLE

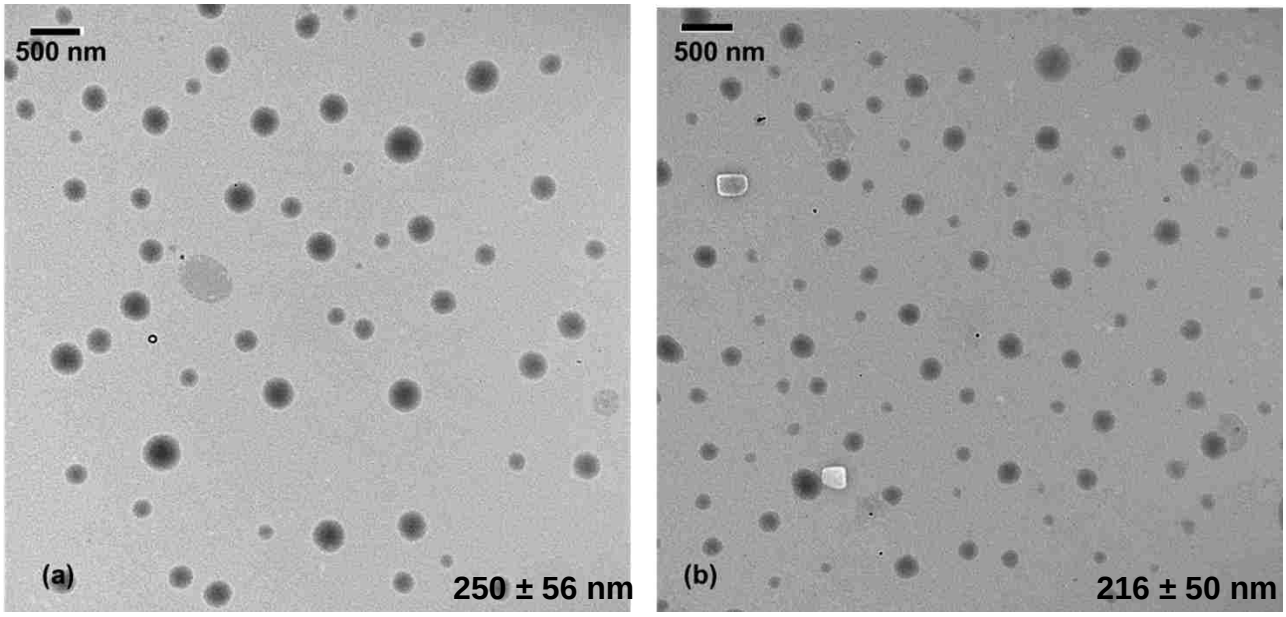

Figure C1. TEM micrographs of (a) (PEG) and (b) alkane polymeric nanoGUMBOS after five days of gamma irradiation.

Table C2. Average sizes of ionic liquids micro/nanomaterials before and after one day/two days irradiation.

	Before irradiation	**One Day irradiation**	**Two Days irradiation**
(PEG) ionic liquid Diameter (Average ± SD)	682 ± 128 nm	244 ± 60 nm	283 ± 58 nm
Alkane ionic liquid Diameter (Average ± SD)	766 ± 114 nm	171 ± 47 nm	239 ± 19 nm
Alkyne ionic liquid Diameter (Average ± SD)	2287 ± 290 nm	340 ± 113 nm	346 ± 66 nm

APPENDIX D. SUPPORTING INFORMATION FOR CHAPTER FIVE: FIGURES AND DATA

(a)

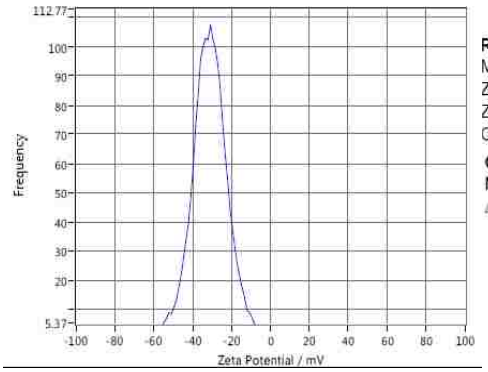

Result
Mobility: -2.48 FWHM 1.44 µm/sec/V/cm, @ 25°C: -2.44 µm/sec/V/cm
ZP Factor 12.6 (Smoluchowski):
Zeta Potential @ 25 °C: -31.21 FWHM 9.91 mV
Concentration 36.71E+6 Particles / mL

Quality
Number of Traced Particles: 1807
ΔSL: 8.20 mV

(b)

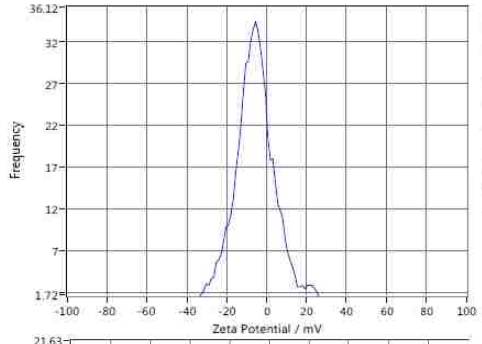

Result
Mobility: -0.46 FWHM 1.45 µm/sec/V/cm, @ 25°C: -0.45 µm/sec/V/cm
ZP Factor 12.3 (Smoluchowski):
Zeta Potential @ 25 °C: -5.70 FWHM 11.91 mV
Concentration 17.37E+6 Particles / mL

Quality
Number of Traced Particles: 624
ΔSL: 9.32 mV

(c)

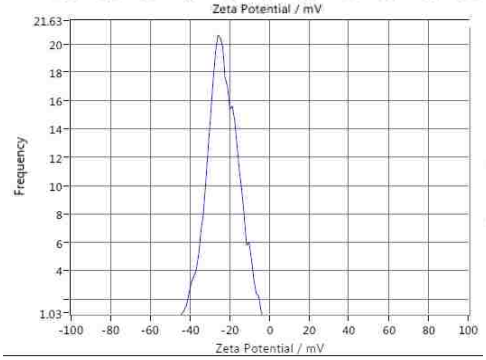

Result
Mobility: -1.93 FWHM 1.38 µm/sec/V/cm, @ 25°C: -1.83 µm/sec/V/cm
ZP Factor 12.1 (Smoluchowski):
Zeta Potential @ 25 °C: -23.39 FWHM 8.67 mV
Concentration 8.41E+6 Particles / mL

Quality
Number of Traced Particles: 329
ΔSL: 1.79 mV

Figure D1. Zeta potential data for (a) [Cl][I] (pH:7.72), (b) [Cl][OTf] (pH: 7.57), and (c) [Cl][BETI] (pH: 8.07) nanoGUMBOS synthesized using a reprecipitation method. The measurements were performed on a zetaview, particle tracking, instrument (Microtrac, PA, US).

APPENDIX E. SUPPORTING INFORMATION FOR CHAPTER SIX: TABLE AND FIGURES

Table E1. Chemometrics studies (partial factorial design) on [Hmim][TPB] nanoGUMBOS synthesized using different experimental conditions and the reported average sizes for each experiment.

Expt	X_1	X_2	X_3	X_4	X_5	X_6	TEM Results
1	MS:0.6	0.5 mg	0.05 mM	tertbutanol	50 uL	Low T°	274 ± 38 nm
2	MS:0.8	0.5 mg	0.05 mM	tertbutanol	250 uL	Low T°	83 ± 23 nm
3	MS:0.6	1.5 mg	0.05 mM	tertbutanol	250 uL	High T°	118 ± 21 nm
4	MS:0.8	1.5 mg	0.05 mM	tertbutanol	50 uL	High T°	104 ± 24 nm
5	MS:0.6	0.5 mg	1 mM	tertbutanol	250 uL	High T°	140 ± 22 nm
6	MS:0.8	0.5 mg	1 mM	tertbutanol	50 uL	High T°	1345 ± 399 nm
7	MS:0.6	1.5 mg	1 mM	tertbutanol	50 uL	Low T°	103 ± 15 nm
8	MS:0.8	1.5 mg	1 mM	tertbutanol	250 uL	Low T°	141 ± 28 nm
9	MS:0.6	0.5 mg	0.05 mM	1-butanol	50 uL	High T°	105 ± 15 nm
10	MS:0.8	0.5 mg	0.05 mM	1-butanol	250 uL	High T°	127 ± 23 nm
11	MS:0.6	1.5 mg	0.05 mM	1-butanol	250 uL	Low T°	71 ± 10 nm
12	MS:0.8	1.5 mg	0.05 mM	1-butanol	50 uL	Low T°	176 ± 44 nm
13	MS:0.6	0.5 mg	1 mM	1-butanol	250 uL	Low T°	43 ± 6 nm
14	MS:0.8	0.5 mg	1 mM	1-butanol	50 uL	Low T°	254 ±29 nm
15	MS:0.6	1.5 mg	1 mM	1-butanol	50 uL	High T°	77 ± 18 nm
16	MS:0.8	1.5 mg	1 mM	1-butanol	250 uL	High T°	1087 ± 208 nm

X_1 = Type of cyclodextrin: 2HP-β-CD MS 0.6 or MS 0.8
X_2 = Amount of cyclodextrin used
X_3 = Concentration of reactants: [Hmim][Cl] and [Na][TPB]
X_4 = Type of alcohol: tert-butanol and 1-butanol
X_5 = Total amount of alcohol used
X_6 = Temperature of synthesis: low temperature signifies presence of ice around the reaction container and high temperature signifies absence of ice around the container

The reactants [Hmim][Cl] and [Na][TPB] were mixed under ultrasonication (25% amplitude and 3 minutes), then the mixture was left for 7 minutes before spotting a volume of 8 μL on the TEM grids; the total volume of mixture was kept constant at 10 mL.

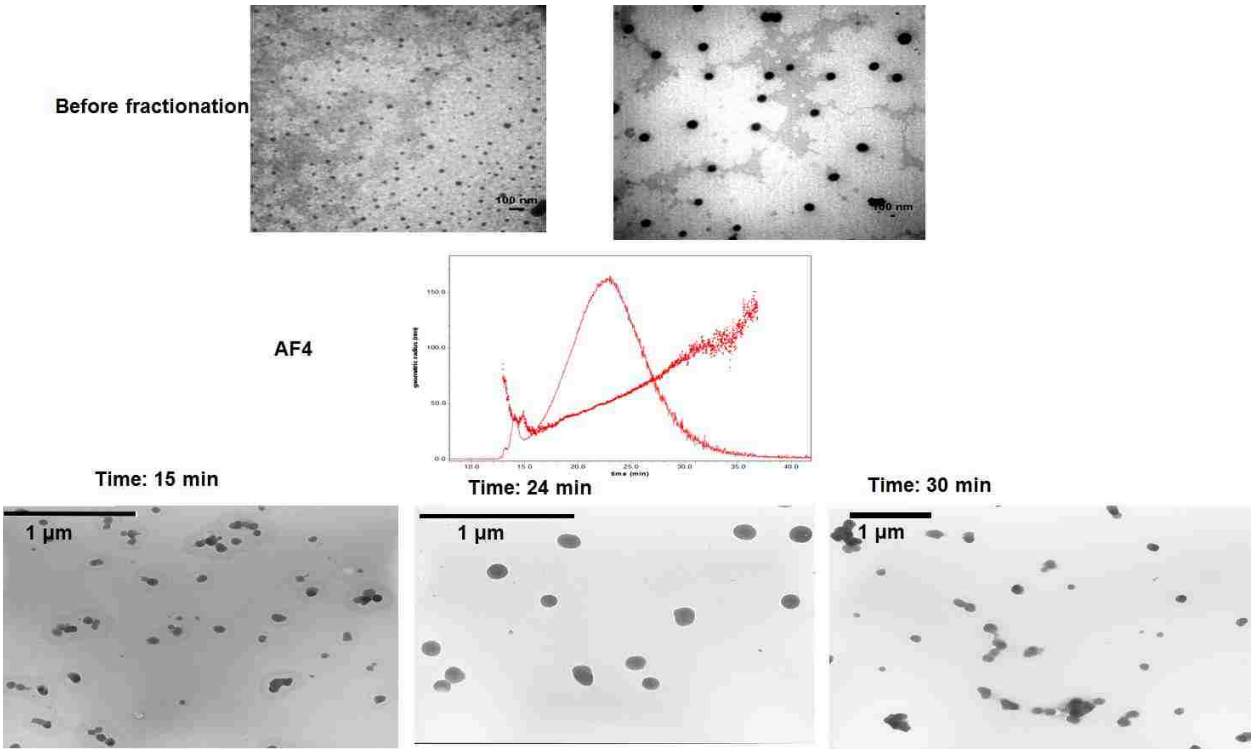

Figure E2. AF4 applied on [Hmim][TPB] nanoGUMBOS; the samples were collected at 15 min, 24 min, and 30 min elution time.

Before fractionation, [Hmim][TPB] nanoGUMBOS were synthesized using the probe ultrasonication in presence of 2HP-β-CD at the following conditions: reactants [Hmim][Cl] and [Na][TPB] (0.7 M; 50 µL each), 2HP-β-CD (0.1 g/ 8 mL water). The sizes of nanoGUMBOS were: 28 ± 5 nm and 211 ± 25 nm (in one sample). The TEM microscope used for data analysis before fractionation was an LVEM5-TEM (Delong America, Montreal, Canada).

After fractionation, the average sizes of nanoGUMBOS collected at 15, 24, and 30 min were 60 ± 13 nm, 128 ±15 nm, and 113 ± 22 nm, respectively. The TEM micrographs in this case were obtained using a JEOL 100CX TEM (Peabody, MA).

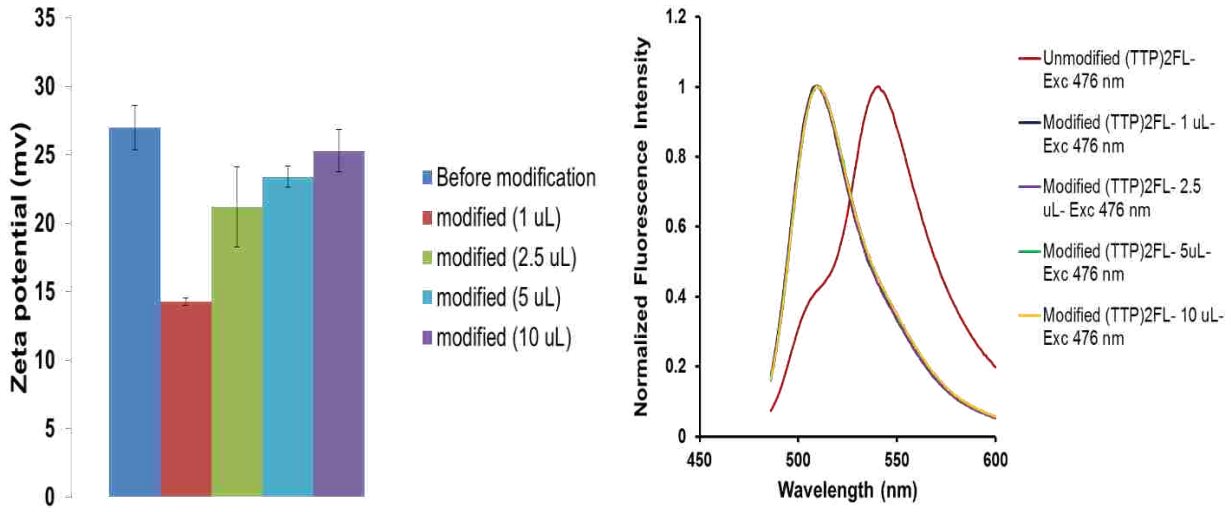

Figure E3. (a) Zeta potential measurements and (b) normalized fluorescence data of $[(TTP)_2][FL]$ nanodroplets before and after surface modification with different amounts of sodium folate (1, 2.5, 5, and 10 µL).

In this procedure, 100 µL of $[TTP]_2[FL]$ ethanolic solution (1 mM) was added to a 5 mL deionized water under ultrasonication. After 5 min sonication followed by 30 minutes of nanomaterials aging, sodium folate (0.1 M) was added to 1 mL volume of the suspension and the mixture was incubated for 30 min before analysis. Upon centrifugation, washing, and suspension in fresh water, zeta potential measurements on the suspensions showed a decrease in value following surface modification with 1 µL of sodium folate, which confirm the physical adsorption of the folate ion onto the surface of the nanomaterials. Fluorescence data show blue shifting after surface modification suggesting possible aggregation of the nanomaterials.

APPENDIX F. LETTER OF PERMISSION

RightsLink | Copyright Clearance Center

Thank You For Your Order!

Dear Dr. Isiah Warner,

Thank you for placing your order through Copyright Clearance Center's RightsLink service. Elsevier has partnered with RightsLink to license its content. This notice is a confirmation that your order was successful.

Your order details and publisher terms and conditions are available by clicking the link below:
http://s100.copyright.com/CustomerAdmin/PLF.jsp?ref=4783e6b1-ba67-4ae9-b515-c3600cdf668c

Order Details
Licensee: Isiah M Warner
License Date: Mar 23, 2015
License Number: 3594860528454
Publication: Journal of Colloid and Interface Science
Title: Strategies for controlled synthesis of nanoparticles derived from a group of uniform materials based on organic salts
Type Of Use: reuse in a thesis/dissertation
Total: 0.00 USD

To access your account, please visit https://myaccount.copyright.com.

Please note: Online payments are charged immediately after order confirmation; invoices are issued daily and are payable immediately upon receipt.

To ensure that we are continuously improving our services, please take a moment to complete our customer satisfaction survey.

B.1:v4.2

VITA

Suzana Hamdan is from Lebanon and was born in Lvov, Moscow to Hamdan Hamdan and Wahibe Abi Chahine. Suzana attended High School at “Saintes Familles Maronites” private school in Chekka, Lebanon. She went for college in Beirut, Lebanon where she pursued her undergraduate studies in general chemistry at Lebanese University and graduated in 2006. Suzana was awarded the Master of Science degree in analytical chemistry from East Tennessee State University under the supervision of Professor Chu-Ngi Ho. In the Fall of 2009, Suzana started her Ph.D. studies in analytical chemistry at Louisiana State University (LSU) under the guidance of Professor Isiah M. Warner. During her graduate studies, she received two Coates Travel Awards from LSU and an Advancing Science Travel Award from NOBCChE organization. She attended ten conferences including three international conferences where she presented oral talks and posters. She also presided two sessions about nanotechnology in the 245th ACS National Meeting. Suzana is currently a member of many professional affiliations such as American Chemical Society (ACS), American Association of University Women (AAUW), and National Association of Professional Women (NAPW). She is also a member of honor societies like Phi Kappa Phi and The National Scholars Honor Society. Suzana has currently two first author and three coauthor papers in publication. She is planning on graduating with the degree of Doctor of Philosophy in chemistry from Louisiana State University in May 2015.

PROFESSIONAL PRESENTATIONS

Hamdan, S.; Alammar, N.; Siraj, N.; Warner, I.M.*; “Control of NanoGUMBOS: Strategies for Size and Optical Properties”, PITTCON, New Orleans, LA, March 2015.

Hamdan, S.; Moore, L.; Hasan, F.; Gin, D.; LaFrate, A.; Noble, R. D.; Spivak, D.; Warner, I.M.*; “Molecularly Imprinted Polymeric NanoGUMBOS for Enantioselective Recognition of Amino Acids”, NOBCChE, New Orleans, LA, September 2014.

Hamdan, S.; El-Zahab, B.; Das, S.; Warner, I. M.*; “Size-Control of NanoGUMBOS and Importance for Analytical Applications”, 245th ACS National Meeting, New Orleans, LA, April 2013.

Hamdan, S.; Moore, L.; Lejeune, J.; Das, S.; Gin, D.; Spivak, D.; Warner, I. M.*; “Molecularly Imprinted Polymeric NanoGUMBOS”, PITTCON, Philadelphia, PA, March 2013.

Hamdan, S.; El-Zahab, B.; Das, S.; Warner, I. M.*; “Synthesis and Size-Control of NanoGUMBOS in Aqueous Medium”, 68th Southwest Regional Meeting, Baton Rouge, LA, November 2012.

Hamdan, S.; El-Zahab, B.; Warner, I.M.*; “Synthesis and Size-Control of NanoGUMBOS”, 62nd Southeastern/66th Southwest Regional Meeting, New Orleans, December 2010.

Siraj, N.; Hamdan, S.; Hasan, F.; Das, S.; Regmi, B.; Magut, P.; Alghafly, H.; Galpothdeniya, I.; Speller, N.; McNeel, K.; Warner, I.M.*; “Ionic liquids/GUMBOS for bioanalytical applications”, 69thSouthwest Regional Meeting, Waco, TX, November 2013.

Hamdan, S.; Dumke, J.; El-Zahab, B.; Das, S.; Boldor, D.; Warner, I. M.*; “Size-Control and Characterization of NanoGUMBOS”, Nanotek 2013, Las Vegas, NV, December 2013.

Hamdan, S.; Ho, C.*; “Studies of the Preparations and Use of Sol-Gel for Enzyme Immobilization and Analytical Applications”, PITTCON, Orlando, FL, March 2010.

Hamdan, S.; Ho, C.*; “Immobilization of Fluorophores for Flow Injection Analysis - Chemiluminescence Detection”, SERMACS, Nashville, TN, November, 2008.

PUBLICATIONS

Hamdan, S.; Dumke, J. C.; El-Zahab, B.; Das, S.; Boldor, D.; Warner, I. M. Strategies for Controlled Synthesis of Nanoparticles Derived from a Group of Uniform Materials Based on Organic Salts. *J. Colloid Interface Sci.* **2015***,* 446, 163-169.

Hamdan, S.; Moore, Jr., L.; Le Jeune, J.; Hasan, F.; Carlisle, T.; Bara, J.; Gin, D.; LaFrate, A.; Noble, R. D.; Spivak, D. A.; Warner, I.M. Polymeric Imprinted NanoGUMBOS for Chiral Recognition, in submission.

Dumke, J.C.; Qureshi, A.; Hamdan, S.; El-Zahab, B.; Das, S.; Hayes, D.J.; Boldor, D.; Rupnik, K; Warner, I.M. Photothermal Response of Near-Infrared Absorbing NanoGUMBOS. *App. Spectrosc.* **2014**, 68 (*3*), 340-352.

Galpothdeniya, I.; Das, S.; De Rooy, S.; Regmi, B.; Hamdan, S.; Warner, I. M. Fluorescein-Based Ionic Liquid Sensor for Serum Albumins. *RSC Adv.* **2014**, 4, 17533-17540.

Dumke, J.C.; Qureshi, A.; Hamdan, S.; Rupnik, K.; El-Zahab, B.; Hayes, D.J.; Warner, I.M. In Vitro Studies of Hyperthermal Near-Infrared NanoGUMBOS for Breast Cancer Therapeutics. *Photochem. Photobiol. Sci.* **2014**, 13, 1270-1280.